TR-94-02

CONTROLLING CHAOS

IN

PLASMA FILLED DIODES

P.A.Lindsay
J.Watkins
X.Chen

King's College
222 Strand
London WC2R 2LS UK

F49620-92-J-0219
P 00001

15 May 1992 - 14 November 1993

REPORT DOCUMENTATION PAGE

Form Approved
OMB No. 0704-0188

1. AGENCY USE ONLY (Leave blank)	2. REPORT DATE	3. REPORT TYPE AND DATES COVERED
	14 Jan 94	Final, 15 May 92 - 14 Nov 93

4. TITLE AND SUBTITLE

CONTROLLING CHAOS IN PLASMA FILLED DIODES

5. FUNDING NUMBERS

G
F49620-92-J-0219
P 00001

6. AUTHOR(S)

P.A.Lindsay
J.Watkins
X.Chen

7. PERFORMING ORGANIZATION NAME(S) AND ADDRESS(ES)

King's College London
222 Strand
London WC2R 2LS UK

8. PERFORMING ORGANIZATION REPORT NUMBER

--

9. SPONSORING/MONITORING AGENCY NAME(S) AND ADDRESS(ES)

EOARD
223/231 Old Marylebone Road
London NW1 5TH UK

10. SPONSORING/MONITORING AGENCY REPORT NUMBER

TR-94-02

11. SUPPLEMENTARY NOTES

--

12a. DISTRIBUTION/AVAILABILITY STATEMENT

Approved for public release;
distribution unlimited

12b. DISTRIBUTION CODE

13. ABSTRACT *(Maximum 200 words)*

This report covers the first eighteen months of our investigations. Following a brief introduction the report discusses in some detail the mathematical model of the system, the methods used in solving the corresponding differential equations and the various ways of presentation of the results. The effect of an external load is then discussed in some detail. The report ends with suggestions for future work based on the results obtained so far.

14. SUBJECT TERMS

15. NUMBER OF PAGES

16. PRICE CODE

17. SECURITY CLASSIFICATION OF REPORT	18. SECURITY CLASSIFICATION OF THIS PAGE	19. SECURITY CLASSIFICATION OF ABSTRACT	20. LIMITATION OF ABSTRACT
UNCLASSIFIED	UNCLASSIFIED	UNCLASSIFIED	NONE

CONTENTS

	Summary	4
1.	Introduction	5
2.	Mathematical model	6
3.	Computational details	18
4.	Presentation and discussion of the results	20
5.	The effect of the load	26
6.	Chaos prolegomena	32
7.	The influence of positive ions	38
	Conclusions	44
	References	46
	Captions	47

SUMMARY

This report covers the first eighteen months of our investigations. Following a brief introduction the report discusses in some detail the mathematical model of the system, the methods used in solving the corresponding differential equations and the various ways of presentation of the results. The effect of an external load is then discussed in some detail. The report ends with suggestions for future work based on the results obtained so far.

1. Introduction

The main purpose of this work is to investigate the control of chaos in a plasma-filled diode. A mathematical model of such a system has been considered before [1,2], its main feature being the replacement of a smooth, interelectrode electron cloud by a large number of infinitely thin electron sheets. In the absence of ions similar, continuous systems have been considered in great detail [3], including the effects associated with the granular nature of the electron stream [4]. In the presence of positive ions the system was first considered by J.R.Pierce [5], and then in more detail by others [6,7]. When the electron cloud is discretized, the ions can be treated as a smooth positive background [1], or they can be discretized as well. Drawing on the experience quoted above [4] we are suggesting that the latter is the more appropriate approach to adopt for further investigations.

2. Mathematical model

Let us first of all consider a system which is devoid of positive ions (pure vacuum). The equation of motion for a single sheet of electrons is then given by

$$\rho_{ms}\ddot{x}_1 = \rho_s E_1 \tag{2.1}$$

where x_1 is the position of the sheet, ρ_s and ρ_{ms} are the respective charge and mass surface densities ($\rho_s/\rho_{ms} = -e/m_o$) and E_1 is the average field acting on the sheet,

$$\begin{aligned} E_1 = \bar{E}_1 &= \tfrac{1}{2}(E_I + E_{II}) \\ &= \tfrac{1}{2}\left(-\frac{d-x_1}{d} + \frac{x_1}{d}\right)\frac{\rho_s}{\varepsilon_o} \\ &= -\frac{\rho_s}{\varepsilon_o}\left(\tfrac{1}{2} - \frac{x_1}{d}\right) \end{aligned} \tag{2.2}$$

Here E_I and E_{II} are respectively the fields in the grid/electron-sheet and electron-sheet/anode spaces, the general geometry being that shown in Fig.1. Since the field must change from E_I to E_{II} as we pass through the sheet, the actual field acting on the sheet is the average field $\bar{E}_1$. Substituting (2.2) in (2.1) we find that the single sheet is decelerated when $x_1 < d/2$ and accelerated when $x_1 > d/2$.

In the case of several sheets the average field acting on sheet j is given by

$$\begin{aligned}\bar{E}_j &= E_{II}(\text{all sheets to the left of } j) + E_j + \\ &\quad E_I(\text{all sheets to the right of } j) \\ &= E_{II}(i>j) + E_j + E_I(i<j) \\ &= \frac{\rho_s}{\varepsilon_0}\left[\sum_{i=j+1}^{M}\frac{x_i}{d} + \left(\frac{x_j}{d} - \frac{j}{2}\right) + \sum_{i=1}^{j-1}\frac{x_j - d}{d}\right] \\ &= \frac{\rho_s}{\varepsilon_0}\left[\sum_{i=1}^{M}\frac{x_i}{d} - j + \frac{1}{2}\right]\end{aligned} \tag{2.3}$$

where the sheets are counted from right to left, since sheet 1 would be injected first and would have travelled to the right by the time sheet 2 has been injected, and so on. Here M represents the total number of sheets momentarily in the interelectrode space.

In place of (2.1) we now have the following set of M coupled equations of motion, each representing one of the M electron sheets present in the interelectrode space:

$$\begin{aligned}\rho_{ms}\ddot{x}_1 &= \rho_s\bar{E}_1 \\ &\vdots \\ \rho_{ms}\ddot{x}_j &= \rho_s\bar{E}_j \\ &\vdots \\ \rho_{ms}\ddot{x}_M &= \rho_s\bar{E}_M\end{aligned} \tag{2.4}$$

It is now convenient to introduce the following reduced variables [1] :

$$x' = x/d \quad , \qquad t' = t/t_o \tag{2.5}$$

where d is the separation of the electrodes and t_o is the transit time in the absence of fields of an electron injected with initial velocity $\dot{x}_o = v_o$, i.e. $t_o = d/v_o$. Thus we now have:

$$\frac{dx'}{dt'} = \frac{t_o}{d}\frac{dx}{dt} = \frac{\dot{x}}{v_o}, \qquad \frac{d^2x'}{dt'^2} = \frac{t_o^2}{d}\frac{d^2x}{dt^2} \tag{2.6}$$

In order to introduce the concept of convection current J_c we write

$$\rho_s = \frac{\rho_{s,tot}}{N} = \frac{\rho_o d}{N} = \frac{J_{co}\, d}{v_o N} \tag{2.7}$$

where ρ_s is again the charge surface density of a single sheet, $\rho_{s,tot}$ is the surface density of N sheets and ρ_o is the smoothed-out volume density of N sheets. A typical equation (2.4) can now be written, substituting from (2.3), (2.6) and (2.7):

$$\frac{d^2x'_j}{dt'^2} = \frac{\rho_s}{\rho_{ms}}\,\frac{J_{co}\, t_o^2}{\varepsilon_o v_o N}\left[\sum_{i=1}^{m} x'_i - j + \tfrac{1}{2}\right] \tag{2.8}$$

Note that M may be different from N, since N is a constant and M may vary, being equal to the number of sheets which are present in the interelectrode space at any given time.

In the final step of our derivation of the equations of motion we choose to express the convection current J_{co} as a fraction of the convection current flowing in a similar

space-charge-limited diode $J_{c,scl}$ given by:

$$J_{c,scl} = \frac{2\varepsilon_0}{9}\frac{\rho_{max}}{\rho_s}\frac{v_0^2}{d^2} = \frac{2\varepsilon_0}{9}\frac{\rho_{max}}{\rho_s}\frac{v_0^2}{t_0^2} \qquad (2.9)$$

Substituting (2.9) in (2.8) we finally obtain

$$\frac{d^2x'_j}{dt'^2} = \frac{2\iota}{9N}\left[\sum_{i=1}^{M} x'_i - j + \frac{1}{2}\right] \qquad (2.10)$$

$$\iota = J_{co}/J_{c,scl} \qquad (2.11)$$

as a typical equation of motion for the jth electron sheet [1].

The M equations (2.10) fully describe the motion of M electron sheets, each sheet injected with the same initial velocity $dx'_j/dt' = \dot{x}_o/v_o = 1$ into the interelectrode space. Since the diode is assumed to be short-circuited, the only fields present are those due to the space charge of the sheets themselves. Thus (2.10) represent a computer model of the conditions inside a plane diode, where the cathode has been replaced by a grid, so that the electrons can be injected with a constant velocity v_o which is different from zero [3].

So far we have only considered a short-circuited diode. If a load is connected across the electrodes, we require an additional equation which relates the conditions inside and outside of the diode. Noting the fact that the total current in Fig. 1 must be continuous we can write:

$$I_{tot} = I_{ind} + I_{cap}$$

$$= \frac{A\rho_s}{d} \sum_{i=1}^{M} \dot{x}_i - \frac{\varepsilon_0 A}{d} \dot{V} \qquad (2.12)$$

where V is the potential difference across the load and a suitable expression for the induced current I_{ind} has been derived elsewhere [1]. In the case of a load consisting of a resistor R in series with an inductor L we have

$$V = RI_{tot} + L\dot{I}_{tot} \qquad (2.13)$$

so that, substituting in (2.12) we finally obtain

$$I_{tot} = \frac{\rho_s}{\varepsilon_0} C_v \sum_{i=1}^{M} \dot{x}_i - C_v R\dot{I}_{tot} - C_v L\ddot{I}_{tot} \qquad (2.14)$$

where

$$C_v = \frac{\varepsilon_0 A}{d} \qquad (2.15)$$

expresses the plane geometry of the system. One can also look at it as an irreducible capacitance of the system.

In the presence of the load the equations of motion (2.4) must be adjusted by writing:

$$\ddot{x}_j = \frac{\rho_s}{\rho_{ms}} (\vec{E}_j + E_{load}) = \frac{\rho_s}{\rho_{ms}} \vec{E}_j - \frac{\rho_s}{\rho_{ms}} \frac{V}{d}$$

$$= \frac{\rho_s}{\rho_{ms}} \cdot \frac{\rho_s}{\varepsilon_0} \left[\sum_{i=1}^{M} \frac{x_i}{d} - j + \frac{1}{2} \right] - \frac{\rho_s}{\rho_{ms} d} (RI_{tot} + L\dot{I}_{tot}) \qquad (12.16)$$

Multiplying both sides of (2.14) by $t_o/\rho_s A$ and (2.15) by t^2_o/d we obtain corresponding expressions in terms of the reduced variables (2.5) - (2.7):

$$\frac{d^2 x_i'}{dt'^2} = \frac{2\iota}{9N}\left\{\left[\sum_{i=1}^{M} x'_i - j + \tfrac{1}{2}\right] - T_R I' - T_L \frac{dI'}{dt'}\right\} \tag{2.17}$$

$$T_L \frac{d^2 I'}{dt'^2} + T_R \frac{dI'}{dt'} + I' = \sum_{i=1}^{M} \frac{dx_i'}{dt'} \tag{2.18}$$

Here we have introduced a new reduced variable given by

$$I' = \frac{t_o}{\rho_s A} I_{tot} \tag{2.19}$$

The constants T_R and T_L are defined by writing:

$$\frac{\rho_s}{\rho_{ms}} \cdot \frac{\rho_s}{\varepsilon_o} \cdot \frac{t_o^2}{d} = \frac{\rho_s}{\rho_{ms}} \cdot \frac{J_{so} t_o^2}{\varepsilon_o v_o N} = \frac{2\iota}{9N} \tag{2.20}$$

$$\frac{\rho_s}{\rho_{ms}} \cdot \frac{t_o^2}{d^2} R I_{tot} = \frac{\rho_s t_o^2}{\rho_{ms} d^2} R \frac{\rho_s A}{t_o} I' = \frac{\rho_s}{\rho_{ms}} \cdot \frac{\rho_s}{\varepsilon_o} \cdot \frac{t_o^2}{d} \cdot \frac{\varepsilon_o A}{d} \cdot \frac{R}{t_o} I'$$

$$= \frac{2\iota}{9N} \frac{C_{tot} R}{t_o} I' = \frac{2\iota}{9N} T_R I' \tag{2.21}$$

$$\frac{\rho_s}{\rho_{ms}} \frac{t_o^2}{d^2} L \dot{I}_{tot} = \frac{\rho_s t_o^2}{\rho_{ms} d^2} L \frac{\rho_s A}{t_o^2} \cdot \frac{dI'}{dt'} = \frac{\rho_s}{\rho_{ms}} \cdot \frac{\rho_s}{\varepsilon_o} \cdot \frac{t_o^2}{d} \cdot \frac{\varepsilon_o A}{d} \frac{L}{t_o^2} \frac{dI'}{dt'}$$

$$= \frac{2\iota}{9N} \frac{C_{tot} L}{t_o^2} \frac{dI'}{dt'} = \frac{2\iota}{9N} T_L \frac{dI'}{dt'} \tag{2.22}$$

Since $\rho_s < 0$ in (2.19), it should be noted that I' has an opposite sign to I_{tot}. In the case of Fig. 1 we have $I_{tot} < 0$ and $I' > 0$.

One can see from (2.17), (2.18) that in the presence of a R,L load M+1 coupled second order differential equations are required for the description of the system.

In some cases it is preferable to use the field

$$E' = \frac{d}{2\pi\epsilon_0} E_{load} = \frac{ed}{m_e v_0^2} E_{load} = -\frac{\rho_0 d}{\rho_{mat} v_0^2} E_{load}$$

$$= \frac{\rho_0}{\rho_{mat} v_0^2}(RI_{tot} + L\dot{I}_{tot}) = \frac{\rho_0 t_0^2}{\rho_{mat} d^2}\left(\frac{\rho_0 A}{t_0} RI' + \frac{\rho_0 A}{t_0^2} L\frac{dI'}{dt'}\right)$$

$$= \frac{\rho_0^2 t_0^2}{t_0 \rho_{mat} d}\left(\frac{C_v R}{t_0} I' + \frac{C_v L}{t_0^2}\frac{dI'}{dt'}\right) = \frac{2\alpha}{9N}\left(T_R I' + T_L \frac{dI'}{dt'}\right)$$

$$= E'_R + E'_L \qquad (2.23)$$

where, from (2.23)

$$E'_L = \frac{T_L}{T_R}\frac{dE'_R}{dt'} \qquad (2.24)$$

Substituting for I' in (2.17), (2.18) we now obtain

$$\frac{d^2x'}{dt'^2} = \frac{2\alpha}{9N}\left[\sum_{i=1}^{M} x'_i - j + \tfrac{1}{2}\right] - E'_R - \frac{T_L}{T_R}\frac{dE'_R}{dt'} \qquad (2.25)$$

$$\frac{T_L}{T_R}\frac{d^2E'}{dt'^2} - \frac{dE'}{dt'} - \frac{1}{T_R}E'_R = \frac{2\alpha}{9N}\sum_{i=1}^{M}\frac{dx'_i}{dt'} \qquad (2.26)$$

The evolution of the system is again described by $M+1$ coupled second-order differential equations.

Another load to be considered is in the form of a resistor R and a capacitor C in parallel. In place of (2.12), (2.13 we now have

$$I_{tot} = I_{ind} + I_{cap} = -\frac{A\rho_0}{d}\sum_{i=1}^{M}\dot{x}_i - C_v\dot{V}$$

$$= I_R + I_C = \frac{V}{R} + C\dot{V} \qquad (2.27)$$

where I_R and I_C respectively represent the currents flowing in the two branches of the load. Since the field across the load is given by the usual expression $E_{load} = - V/d$, we obtain from (2.27)

$$E_{load} = - \frac{\rho_s}{\epsilon_o} \frac{\epsilon_o A}{d^2} R \sum_{i=1}^{M} \dot{x}_i + k(C_v + C) \frac{-\dot{V}}{d}$$

$$= - \frac{\rho_s}{\epsilon_o} \frac{C_v R}{\tau_o} \sum_{i=1}^{M} \frac{dx_i'}{dt'} + \frac{R}{\tau_o}(C_v + C) \frac{dE_{load}}{dt'}$$

$$= - \frac{\rho_s}{\epsilon_o} T_R \sum_{i=1}^{M} \frac{dx_i'}{dt'} + (T_R + T_C) \frac{dE_{load}}{dt'} \qquad (2.28)$$

where we have used (2.5), (2.15) and (2.20) - (2.22) for defining x', t', T_R ; in addition we have introduced a new constant given by

$$T_C = RC/\tau_o \qquad (2.29)$$

From (2.23) we can now write for the reduced field

$$E' = - \frac{\rho_s d}{\rho_{ms} v_o^2} E_{load} = \frac{\rho_s^2 t_o^2}{\rho_{ms} d \epsilon_o} T_R \sum_{i=1}^{M} \frac{dx_i'}{dt'} - \frac{\rho_s d}{\rho_{ms} v_o^2}(T_R + T_C) \frac{dE_{load}}{dt'}$$

or

$$E' = \frac{2L}{9N} T_R \sum_{i=1}^{M} \frac{dx_i'}{dt'} - (T_R + T_C) \frac{dE'}{dt'} \qquad (2.30)$$

This equation should be compared to (2.18) which is valid for an R and an L in series. The corresponding equation of motion of the electron sheets is now given by

$$\frac{d^2 x_j'}{dt'^2} = \frac{2\iota}{9N}\left[\sum_{i=1}^{M} x_i' - j + \tfrac{1}{2}\right] - E' \qquad (2.31)$$

This equation is similar to (2.25) except for E' in place of the two terms in E_R'.

Sometimes it is more convenient ro express everything in terms of current. We then have

$$E_{load} = - RI_R/d \qquad (2.32)$$

or

$$E' = - \frac{\rho_s t_o^2}{\rho_{wg} d} E_{load} = \frac{\rho_s t_o^2}{\rho_{wg} d^2} RI_R = \frac{\rho_s t_o^2}{\rho_{wg} d^2} R \frac{\rho_s A}{\tau_o} I_R'$$

$$= \frac{\rho_s t_o^2}{\rho_{wg} d} \frac{\rho_s}{\tau_o} \frac{R}{\tau_o} \frac{t_o A}{d} I_R' = \frac{\rho_s^2 t_o^2}{\rho_{wg} s_o^2 d} \frac{RC_v}{\tau_o} I_R' = \frac{2}{9N} T_R I_R' \qquad (2.33)$$

Thus in terms of current (2.31) and (2.30) acquire the following algebraic form:

$$\frac{d^2 x_j'}{dt'^2} = \frac{2\iota}{9N}\left\{\left[\sum_{i=1}^{M} x_i' - j + \tfrac{1}{2}\right] - T_R I_R'\right\} \qquad (2.34)$$

$$(T_R + T_C)\frac{dI_R'}{dt'} + I_R' = \sum_{i=1}^{M} \frac{dx_i'}{dt'} \qquad (2.35)$$

It should be noted that in the load equations the capacitance C is merely added to C_v, the two being in parallel ($T_R + T_C = R(C_v + C)/\tau_o$).

Let us now consider briefly the initial conditions. It is assumed that initially the diode is free of charge and that no external batteries are present, the energy being delivered to the system by the injection current i. In those circumstances there are no charges on the electrodes until the first electron sheet is injected into the interelectrode space through the left-hand electrode, i.e. the grid. Consequently in the case of (2.17), (2.18) or (2.25), (2.26) the initial boundary conditions are respectively either

$$I' = 0, \frac{dI'}{dt'} = 0 \quad \text{at} \quad t' = 0 \tag{2.36}$$

or

$$E'_R = 0, \frac{dE'_R}{dt'} = 0 \quad \text{at} \quad t' = 0 \tag{2.37}$$

In the case of (2.30), (2.31) or (2.34), (2.35) we again have either

$$E' = 0, \frac{dE'}{dt'} = 0 \quad \text{at} \quad t' = 0 \tag{2.38}$$

or

$$I'_R = 0, \frac{dI'_R}{dt'} = 0 \quad \text{at} \quad t' = 0 \tag{2.39}$$

Finally let us consider an approximate expression for the potential distribution between the electrodes. Since the interelectrode space-charge in our model is represented by a succession of electron charge sheets, the potential function is approximated by a series of straight line segments connecting the potentials of neighbouring sheets.

Expressions for ϕ_I and ϕ_{II} are obtained by integrating the corresponding fields E_I and E_{II} quoted in (2.2); since in our model the fields are constant, the corresponding potential functions must by straight lines sloping downwatds between the grid and point i in Fig. 1, and upwards between i and the anode. For example:

$$\phi_I = -\int_0^x E_I\,dx = \frac{\rho_s}{\epsilon_0}\frac{d-x_i}{d}\,x < 0 \qquad (2.40)$$

$$\phi_{II} = -\int_d^x E_{II}\,dx = -\frac{\rho_s}{\epsilon_0}\frac{x_i}{d}\,(x-d) < 0 \qquad (2.41)$$

since $\rho_s < 0$. In the presence of many sheets we find that for sheet j we have [1]:

$$\begin{aligned}\phi_j &= \sum_{i=j+1}^{M}\phi_{TIi} + \sum_{i=1}^{j}\phi_{Ii} + \phi_0 \\ &= \frac{\rho_s}{\epsilon_0 d}\left[\sum_{i=j+1}^{M} x_i(d-x_j) + \sum_{i=1}^{j} x_j(d-x_i)\right] + \phi_0 \\ &= \frac{\rho_s}{\epsilon_0 d}\left[x_j\left(jd - \sum_{i=1}^{M} x_i\right) + d\sum_{i=j+1}^{M} x_i\right] + \phi_0 \qquad (2.42)\end{aligned}$$

In the presence of a load (2.29) has an additional terms given by $V_j = -E_{load}x_j$. Dividing both sides by

$$\phi_0 = -\frac{\rho_{s0}}{\rho_s}\frac{v_0^2}{2} = -\frac{9d^2}{4\epsilon_0}\frac{J_{scl}}{v_0} \qquad (2.43)$$

which is another form of (2.9) and then using (2.7)

we finally obtain

$$\phi'_j = \frac{\phi_j}{\phi_0} = \frac{J_{ic}/\epsilon_0 v_0 N}{-9d^2 J_{ic1}/4\epsilon_0 v_0}\left[x_j\left(jd - \sum_{i=1}^{m} x_i\right) + d\sum_{i=j+1}^{m} x_i\right] - \frac{E_{imp}d}{\phi_0}x_j + 1$$

$$= -\frac{4\epsilon}{9N}\left[x'_j\left(j - \sum_{i=1}^{m} x'_i\right) + \sum_{i=j+1}^{m} x'_i\right] - 2E'x'_j + 1 \qquad (2.44)$$

An approximation to the potential function ϕ' is obtained by connecting all the points ϕ'_j with straight line segments.

It should be noted that (2.17), (2.18) and also (2.25), (2.26) are linear; however the boundary conditions of the system are expressed in terms of (2.31) which is nonlinear, so that the inherent nonlinearity of the system is suitably expressed in this fashion.

3. Computational details

Two different methods have been used for the solution of equations (2.17), (2.18) and (2.25), (2.26) or (2.30), (2.31) and (2.34), (2.35).

The first method is based on the use of backward and forward differences. As is customary in such cases each second order differential equation is first converted into two first order differential equations and the corresponding derivatives are then expressed in terms of the finite differences, using second order approximation. Thus, for example, we obtain for the equations of motion of the j-th electron sheet:

$$\dot{x}_{k+1} = \left\{ \frac{3}{2} \ddot{x}_k - \frac{1}{2} \ddot{x}_{k-1} \right\} \Delta t + \dot{x}_k \qquad (3.1)$$

and

$$x_{k+1} = \left\{ \dot{x}_k + \left(\frac{2}{3} \ddot{x}_k - \frac{1}{6} \ddot{x}_{k-1} \right) \Delta t \right\} \Delta t + x_k \qquad (3.2)$$

This method has been initially developed by Birdsall and Bridges [1] for the solution of equations describing the conditions in a short-circuited diode. We have extended it to cover the case of a diode with a partly reactive load connected across its electrodes.

The second method of solving the $M + 1$ coupled differential equations is based on a fourth-order Runge-Kutta subroutine of proven reliability. This method is particularly convenient when the number of equations is large, say greater than 20; it is also very fast.

The following methods have been used for testing the accuracy of our results. In the absence of a load, i.e. when the diode was short-circuited, we would compare our numerical results with those obtained analytically. In most cases the agreement was excellent (of the order of 0.01%) provided the injection current $\nu < 8$; at $\nu \geq 8$ a virtual cathode appears and the sheet model develops oscillations.

For purely resistive loads we were able to use Birdsall's and Runge-Kutta subroutines and then compare the results; as a rule we would reject any results that would differ by more than 0.1%. In the case of more complicated loads containing reactive components we could only use the Runge-Kutta subroutine; we would then test the numerical accuracy of the results by systematically reducing the time integration interval until we were satisfied that the accuracy was better than 0.1%. This simple procedure can be quite effective in practice, provided it is used sensibly.

4. Presentation and discussion of the results

There are several ways of presenting the results of our calculations and we will discuss them in turn.

(A) Sheet position

The simplest way of presenting our results is to plot the position of all the sheets of charge, as shown in Figs. 2 a-d for four different values of the injection current density $\iota = J_{co}/J_{scl}$. The position of the sheets is shown along the horizontal x'-axis, the vertical axis being used for indicating their potential relative to the entrance grid situated at $x' = 0$. Since in this case the diode is short-circuited, the reduced potential of both electrodes is the same and equal to $\phi' = 1$. The whole picture has been obtained for a single instant of time, well after the transient due to a gradual injection process has died out. The values of the current density ι have been chosen so as to cover the three areas of interest shown in Fig. 3, i.e. stable, hysteresis and oscillatory (unstable) regions. It is to be noted that in the last two cases, Figs. 2 c & d, there exists a marked tendency for the sheets to cluster near the injection electrode, their potential becoming negative in many cases.

(B) Interelectrode potential profile

Another simple presentation of the results is that shown in Figs. 4 a,b , where we have plotted the reduced potential of each sheet ϕ' against its position along the x' axis, all values being obtained for a single instant

of time and after the transient has died out. Thus the B-type presentation is very similar to the A-type presentation, although now the potential curve is much easier to visualize. We have also used this example to show the difference in the potential distribution between a short-circuited diode, Fig. 4 a and that with a simple resistive load defined by $T_R = C_v R/t_o = 0.1$ connected across its electrodes, Fig. 4 b. We can see that in the latter case the anode is at a lower potential than the grid, the potential difference $V = RI_{tot}$ being generated by the current flowing through the resistive load R, as shown in Fig.1. Both results have been obtained for the same current density $\iota = 6$.

The main weakness of the simple presentations of the type A and B is that they are valid for a single instant in time only, i.e. they do not tell us anything about the development of the system with time. In order to overcome this we must use other methods of presentation.

(C) Trajectories

Since the system is 1D, one can gain information about its evolution by plotting $x' = x/d$ against $t' = t/t_o$. Figs. 5 a and b show the corresponding trajectories for $\iota = 4.0$ (short-circuited diode) and $\iota = 9.0$ (diode with a R,L load). In the first case, Fig. 5 a corresponds to a stable potential distribution, the charge sheets move smoothly between the electrodes, The second case, Fig. 5 b, corresponds to the other extreme where, due to the large values of ι and T_L we have quite violent changes in the sheet trajectories, leading to large amplitude oscillations.

Since the position of each charge sheet is noted at fixed time intervals and then indicated by a dot, the density of the dots is inversely proportional to the velocity of travel of the sheets.

(D) Depth of potential minimum versus time

Strictly speaking there is no potential minimum in our case; all we have at our disposal is a charge sheet which is at a potential that is lower than the potential of all the other sheets. Figs. 6 a and b show the value of such a potential as a function of time respectively for two different values of the injection current density ι. We find that for $\iota = 4.0$, Fig. 6 a, the lowest potential, after a brief transient, settles down to a constant value. In the case of $\iota = 9.0$, Fig. 6 b, the lowest potential oscillates in a somewhat uneven or 'chaotic' fashion. These oscillations have a clear character of 'relaxation' oscillations, their upward movement being much faster than their downward movement, as can be seen by the density of dots. Closer investigation of drawings such as Figs. 2 c & d indicate that the oscillations occur because the charge sheets first bunch near the grid and are then jettisoned at approximately equal intervals.

(E) Position of potential minumum versus time

Another presentation of the system is that of the position of the potential minimum against time. However this presentation suffers from an inherent weakness in the form of a built-in discontinuity, since in our model there is no such thing as a true minimum, but only the position

of a sheet temporarily at the lowest potential. Thus at odd moments there is a sudden and discontinuous jump from one sheet to the other. Figs. 7 a and b clearly show the jerky movement of the potential 'minimum' with time. In Fig. 7 a the movement is so fast that we only get a blur in the form of a thick horizontal line, but in Fig. 7 b the jumps are quite noticeable, especially on the downward strokes.

(F) Field across the load versus time

In the presence of the load it is often convenient to plot the field E' across the load against time, as shown in Fig. 8. Since this is possible only when the load is present, we have chosen $\ell = 9.0$, $T_R = 0.1$ as an example. This should be compared with Fig. 6 b where V_{min} is plotted against time for a short-circuited diode and ℓ also equal to 9.0. In the case of Fig. 8 the field E' does not change sign, once the transient has died out.

Since our system is 1D in character, the $(x', \dot{x}')$ phase space is a 2D plane and the phase trajectories of the system are 3D curves with the t'-axis at right angles to the $(x', \dot{x}')$-plane. If we then 'strobe' the trajectories, i.e. note the values of x', $\dot{x}'$ at regular time intervals and plot them in the $(x', \dot{x}')$-plane, we obtain what is usually referred to as a Poincaré section of the system. Let us consider such a presentation but at the same time alter it somewhat by taking

x'_{min}, $\dot{x}'_{min}$ instead of x', $\dot{x}'$.

(G) Velocity of x'_{min} versus its position

The velocity of the potential minimum $\dot{x}'_{min}$ against its position is shown for two cases respectively in Figs. 9 a and b. In Fig. 9 a we have $\iota = 4.0$ and a short-circuited diode and in Fig. 9 b we have $\iota = 9.0$ and a load in the form of $T_R = 0.1$, $T_L = 1.0$. Naturally this is another presentation of the results respectively shown in Figs. 7 a and b. As is usual with other Poincaré sections the presentation of the results is more revealing and possibly easier to interpret, since we now have information about both x'_{min} and $\dot{x}'_{min}$. In Fig. 9 a the velocity of the potential minimum clearly settles to a constant value $\dot{x}'_{min} = \dot{x}_{min}/v_o = 0.83$ (note that in fact this is the velocity of a given sheet), its position oscillating in a narrow range near the middle, $x'_{min} = x_{min}/d \approx 0.5$. In the case of Fig. 9 b the Poincaré section reveals marked variations both in the position x'_{min} and in the velocity $\dot{x}'_{min}$. Regrettably both presentations suffer from the artificial discontinuities caused by jumps from one charge sheet to the other which are inherent in our definition of x'_{min} and $\dot{x}'_{min}$.

(H) Potential minimum versus the field

One more presentation of the results proved to be of interest. Instead of plotting V_{min} against time, it is probably better in the presence of a load to plot V_{min} against E'. This type of presentation is quite

smooth, i.e. it does not suffer from artificial discontinuities, as can be seen from Fig. 10 which is plotted for $\nu = 9.0$, $T_R = 0.1$, $T_L = 1.0$. Fig. 10 should be compared with Figs. 7 b and 9 b which are plotted for similar values of the relevant parameters. Both the periodicity of the system and the relaxation character of the oscillations indicated by lack of mirror symmetry are clearly shown in the drawing.

5. The effect of the load

The majot objective of these investigations is to determine the effect of the load on the behaviour of a plasma-filled diode, in particular its possible role in the control of chaos. So far we have developed a technique of investigations by creating a suitable mathematical model of the system and evovlving various forms of presentation of the results. We now wish to describe the effect of the load on the stability of operation of the system in the absence of positive ions and then make suggestions concerning possible influence of positive charges.

The mathematical model described in Section 2 includes an external load which is in the form of a resistor and an inductor in series or a resistor and a capacitor in parallel, Fig. 1, the irreducible capacitance of the tube being connected in parallel with the load, the source of power being in the form of a constant current ν injected through the grid.

In our case the simplest load takes the form of a pure resistor R, as has been briefly discussed elsewhere [1]. In Fig. 11 a we have a table of results summarizing our investigations. We find that for low values of T_R there are no oscillations until the current $\nu \geq 3.0$. This is consistent with the results obtained analytically when the corpuscular nature

of the electron stream has been ignored (hydrodynamic approximation) [8]; we then find from curve a in Fig. 7 of ref. 8 that in a short-circuited diode ($T_R = 0$, $\phi_a' = 1.0$) the virtual cathode appears also when $\iota \geq 8.0$, i.e. for the same values of the current as those leading to oscillations in the numerical case. This fact had already been noted by others [1]. However this simple relationship is no longer valid for larger values of T_R. For example at $T_R = 8.0$ and $\iota = 4.0$ the system becomes unstable and begins to oscillate, bringing the anode voltage down to a mean value of $\phi_a' = 0.8$, although in ref. 8 for $\iota = 4.0$ the virtual cathode does not set in until $\phi_a' = 0.35$. Clearly even a simple resistive load, which is absent in ref. 8, has a profound effect on the behaviour of the system, probably by intriducing an element of feedback in addition to that already present in the system and associated with the space charge acting as a medium facilitating communication between the two electrodes (see also ref. 7). As we shall see shortly the effect of the load becomes more wide ranging when reactive components are included. Figs. 11 b - d show typical oscillations for three different values of T_R, namely $T_R = 0.01$, 0.1 and 0.8 and for a single value of the injection current $\iota = 9.0$. The oscillations are rather irregular, their amplitude and shape varying in a random fashion; also, as mentioned before, they have the character of relaxation rather than harmonic oscillations, their rise associated with sheet dumping at the grid (see Figs.11 c and d) being much faster than their downward stroke, which

is associated with a slower build-up of the interelectrode space charge. This is clearly indicated by the density of dots, the system being 'strobed' at equal time intervals. It should be noted that the amplitude of oscillations increases by a factor of ~ 3 as T_R varies between 0.01 and 0.8; so does the frequency of oscillations, but only by some 10%. The corresponding frequency spectra of the oscillations are shown in Figs. 11 e - g. We find that, because of their relaxation character, the oscillations are rich in harmonics; also they become progressively 'cleaner' as T_R increases, their chaotic or more accurately random character being more pronounced at lower values of T_R. It should be added that the two figures in brackets respectively refer to the DC level and the amplitude of the fundamental component, the amplitude being normalized to unity in the drawings.

Let us now consider a load which has a reactive component in the form of an inductor L in series with a resistor R, as shown in Fig. 1, the results of the computations now being collected in a table shown in Fig. 12 a. We find that for $L = 4.0$, i.e. in the stable range of operation (see Fig. 3), the addition of an inductor to a purely resistive load of $T_R = 0.1$ does not cause instabilities. The situation is quite different however for larger values of the injection current, such as $L = 9.0$. Now, as we know, the oscillations are likely to be present even in a short-circuited diode and the

addition of a purely resistive load increases their amplitude, as shown in Figs. 11 b - d. The addition of an inductor further emphasizes the effect, provided T_L is sufficiently large; this can be clearly seen by comparing Figs. 11 c and 12 d, the effect of T_R probably being stronger, Figs. 11 d and 12 d. A weak inductor, $T_L = 0.001$, has a negligible effect on the amplitude and shape of the wave, as can be seen from Figs. 11 c and 12 b (note different scales). However for $T_L = 0.1$ and 1.0, Figs. 12 c and d, there is a considerable growth in the amplitude of oscillations, finally reaching a factor of ~ 3. At the same time the oscillations again become 'cleaner', i.e. more regular, although they still retain their relaxation character. This is particularly noticeable in frequency spectra, Figs. 12 e - g, which clearly show the 'cleaning up' process; at the same time the relaxation character of the oscillations is further confirmed by the presence of harmonics, Fig. 12 g, apart from which the spectrum is remarkably 'clean'. There is some suspiscion here that we may be dealing with a resonance phenomenon, bearing in mind the presence of R, L of the load and the inherent capacitance C_v of the tube. In our opinion this point merits further investigation, especially since some preliminary computations revealed very high amplitudes of 'clean' oscillations for vanishingly small T_R and moderate values of T_L.

In our third and last example the load is in the form of a resistor R and a capacitor C in parallel, as shown in Fig. 1. In fact this is equivalent to a purely resistive load with an abnormally large capacitance assigned to the tube and given by $C_v + C$ instead of just C_v. However, as can be seen from (2.31), (2.31) and (2.34), (2.35) this analogy is not complete, since T_R does not always appear in the combination $(T_R + T_C) = R(C_v + C)/t_o$. The results of our computations are collected in a table and shown in Fog. 13 a. We now find that in this case the oscillations only occur for $\omega = 9.0$, Figs. 13 b - d. The three sets of results, $T_R = 0.1$ and three values of $T_C = 0.001$, 0.1 and 1.0, are very similar and they hardly differ from those for $T_R = 0.1$, $T_L = T_C = 0$ shown in Fig. 11 c. This further supports our conjecture that the load capacitance C is merely added to that of the tube C_v, no resonance phenomena being possible in this configuration. Comparing Figs. 11 f and 13 f we find that there is no noticeable change in the frequency of oscillations due to the addition of C, although the frequeney spectrum is slightly 'cleaner' in the presence of C. This is even more noticeable when we compare Figs. 11 f and 13 g where, in the latter case, $T_C = 1.0$. One would assume that the R,C combination acts here as a filter.

Finally it is worth noting the effect of various types of load on the intermediate, or hysteresis range of values of the injection current ι, Fig. 3. We have already mentioned the fact that in the case of a purely resistive load oscillations may occur even for injection currents as low as $\iota = 4.0$, provided that T_R is sufficiently large, in our case $T_R = 0.8$, Fig. 11 a. The same applies to the intermediate range of injection currents, say $\iota = 6.0$, where hysteresis occurs in the case of a short-circuited diode, Fig. 3. In the presence of a relatively large inductance, $T_R = 0.1$, $T_L = 1.0$, we find from Fig. 12 a that although no oscillations occur for $\iota = 4.0$, they are excited at $\iota = 6.0$; however this only happens after a realtively lengthy transient, as if the system could not quite decide what to do, Fig. 14. At the same time the hysteresis effect clearly shown in Fig. 3 disappears, the system following the lower branch of the curve in both directions. In the case of a capacitance C in parallel with R no oscillations are excited at $\iota = 6.0$, $T_R = 0.1$ and $T_C = 1.0$, as is shown in Fig. 13 a.

6. Chaos prolegomena

In the discussion of chaos it is always important to define precisely the system and the corresponding phase space and its Poincaré sections. In our case the electrodes, the space-charge which in general would comprise negative electrons and positive ions and the load together represent our system. Since we have energy losses in the system, both at the electrodes where the kinetic energy of the charged particles is being converted into heat and in the load, where the flow of current generates the usual heat losses in the resistive component of the load, the system is clearly non-Hamiltonian and we should expect the appearance of strange attractors if and when the system becomes chaotic.

At this stage of our investigations we assume that the electrodes are infinite planes which are parallel to each other, so that the envisaged system is 1D in character, the corresponding phase space being constructed from the position and velocity variables x and $\dot{x}$. The difficulty arises in deciding which x and which $\dot{x}$, or possibly some other more suitable parameters should be used in the representation of our system.

The simplest possible model of our system is that of a single sheet of electrons traversing the interelectrode space. The corresponding equation of motion for a short-circuited diode has been derived elsewhere [1] and in the notation of Section 2 is given by the following expression

$$\frac{d^2x'}{dt'^2} = \frac{\rho_s^2 t_o^2}{\epsilon_o \rho_{ms} d}(x'-\tfrac{1}{2}) = m'^2(x'-\tfrac{1}{2}) \qquad (5.1)$$

which is similar to (2.10) for $N = M = 1$ and $m'^2 = 24/9$. The solutions of (5.1) are given by

$$x' = \tfrac{1}{2}(1 - \cosh m't') + \frac{1}{m'}\sinh m't' \qquad (5.2)$$

$$\frac{dx'}{dt'} = -\tfrac{1}{2}m' \sinh m't' + \cosh m't' \qquad (5.3)$$

A set of the corresponding phase trajectories, each for a different value of the parameter $m' = 24/9$ and thus related to the injection current density ϵ, are shown in Fig. 14 a. We find that there are only two possibilities: either the sheet reaches the anode ($m' < 2$) or it returns to the cathode ($m' > 2$), a singular case being given by $m' = 2$, it takes an infinite time for the sheet to reach the centre of the interelectrode space. If we now strobe the phase trajectory at equal time intervals $\Delta t'$, we obtain what could be called somewhat grandeloquently a 'Poincaré section' of the system. Our problem in this simple case is that the system is aperiodic and therefore

there is no preferred value of $\Delta t'$, so that the whole point of plotting a Poincaré section is virtually lost.

Let us now consider a more realistic case when we have some twenty sheets injected, M of them remaining in the interelectrode space at any given time. The corresponding 'Poincaré sections' for $\epsilon = 4.0$ and zero load are shown in Figs. 14 b and c, respectively with and without the transient, the system being strobed at $\Delta t' = 0.01$, which is the same as the integration interval. We can see from Fig. 14 c that the phase space trajectory is similar to any of the trajectories shown in Fig. 14 a for $m' < 2$, the system remaining stable throughout. The effect of the transient is clearly shown in Fig. 14 b - it simply amounts to an upward swing before the trajectories settle to a value $dx'/dt' = 1$ at the anode, as they ought to. The situation is radically different for $\epsilon = 9.0$, $T_R = 0.1$, $T_L = 1.0$, when there are well established oscillations, Fig. 12 d. The corresponding phase space trajectories, again strobed at $\Delta t' = 0.01$, are shown in Figs. 14 d and e, respectively with and without the transient. We can clearly see from Fig. 14 e that some sheets land on the anode and other sheets return to the cathode, frequently after some considerable hesitation in the vicinity of $x' = 1/3$. This is very much in agreement with the time trajectories shown in Fig. 5 b but, as we well know, in total disagreement with the simple hydrodynamic model [8]. Clearly the 'either,or' situation with a singular solution for $m' = 2$ and shown in Fig. 14 a also no longer applies.

When the system becomes unstable and begins to oscillate it is often more revealing to use a phase space described in Section 4H and comprising the E field across the load and the value of the potential minimum V_{min}. In Fig. 15 a are shown the corresponding phase trajectories for $\iota = 9.0$, $T_R = 0.1$ and $T_L = 1.0$, which are the same values of parameters as those chosen for the systems shown in Figs. 10, 12 d and 14 d, e. In this case we have a relatively 'clean' set of oscillations and the plots of Figs. 10 and 15 a, the latter including a transient, confirm that. Since we now have a well defined period of ascillations given by $\Delta t' = 2.3$, a more representative Poincaré section in shown in Figs. 15 b and c, respectively for two different phase values, the system now being strobed once during each cycle.

Finally in Figs. 15 d - f are plotted phase space trajectories for $\iota = 9.0$, $T_R = 0.1$ where, as can be seen from Fig. 11 c, the oscillations are particularly 'dirty'. We now find that the corresponding phase space trajectories exhibit similar characteristics, Fig. 15 d being strobed at $\Delta t' = 0.01$ (integration interval) and Figs. 15 e and f at $\Delta t' = 2.1$, which is the approximate period of oscillations. Although this is still not a behaviour which could be described as being 'chaotic', it certainly is much more irregular than that shown in Figs. 15 a - c.

In our search for a convincing example of chaos in the absence of positive ions we have investigated the effect of very high injection currents in the case of a short-circuited diode. In Figs. 16 a - e we have plotted $\dot{x}'_{min}$ against x'_{min} respectively for ι = 9, 12, 15, 18 and 23. We note that initially during the transient the pattern is full of discontinuities or jumps and then it settles down to a rather fuzzy eye-shaped curve reminiscent of Fig. 9 b and representing relaxation oscillations. As the value of the injection current ι increases we find that first a gap appears in the closed curve indicating that some combinations of x'_{min}, $\dot{x}'_{min}$ are no longer possible. This gap tends to grow, the fuzzy eye-shaped pattern shrinking more and more, until at ι = 18 and 23 we are left with a fairly shapeless distribution of points in what, in effect, is a Poincaré section. At the same time the transient also becomes very scattered. Although the pattern has become very irregular, before we can call it chaotic we still have to find a hierarchy of bifurcations. We know from the literature [3] that in a short-circuited diode there is at least one 'bifurcation' point at ι = 8; for $\iota < 8$ there are two solutions of the corresponding hydrodynamic equation, i.e. (6.1) with $\bar{\alpha}$ = 0, one stable and one unstable [10] and that at ι = 8 the two solutions coalesce. For $\iota \geq 8$ there is a sudden discontinuity in the current reaching the anode, Fig. 3.

if we follow the hydrodynamic model and in the numerical calculations the system breaks out into oscillations. Whether this finally leads to a proper chaotic behaviour as ν increases even further requires additional investogations.

7. The influence of positive ions

So far we have only considered the conditions on a vacuum diode, i.e. when the space charge is solely due to the negative charge of the electrons. However our main task is to consider the conditions in a plasma filled diode, i.e. in a system where the space charge is due to the negatice charge of the electrons and the corresponding positive charge of ions, the initial ratio of the two being left to our choise. The idea of deliberately adding positive ions was probably first suggested by J,R,Pierce [5] and at the time it was simply intended to increase the perveance of the system, so that more current could be drawn from the cathode. We now know that the situation is much more complicated, the system being prone to all sorts of instabilities and oscillations, including chaotic behaviour [7] .

The simplest way of taking into account the effect of positive ions is to assume that they form an immobile backdrop against which the movement of electrons takes place. The assumption of immobility is based on the fact that respective masses of ions and electrons usually differ by at least three orders of magnitude. If we then assume that both electrons and ions form perfectly smooth space-charge clouds, the corresponding differential equation

$$\frac{d^2\phi}{dx^2} = \frac{-J_0}{\varepsilon_0\sqrt{\frac{2e}{m_e}}}\left(\frac{1}{\sqrt{\phi}} - \frac{\bar{a}}{\sqrt{\phi_0}}\right), \quad J_0 < 0 \qquad (7.1)$$

can be solved analytically [6]. Here J_o is the injection current density and $\phi_o = m_e v_o^2/2e$ expresses the initial electron velocity v_o of the injected electrons. Since $\bar{\alpha} = n_{io}/n_{eo}$ expresses the contribution due to positive ions, their absence is indicated by $\bar{\alpha} = 0$; (6.1) then reverts to its familiar form valid for a vacuum diode [8]. The main difference between vacuum and plasma-filled diodes is that, as we can see from (6.1), in the absence of positive ions $d^2\phi/dx^2$ must remain positive, whereas in their presence the second derivative may change sign, for example when for sufficiently large ϕ the electron density drops below that of the ions.

In the computational model of our system the electron cloud is expressed by a series of infinitely thin 2D sheets of charge; for a single sheet the presence of immobile positive ions is then represented by a correcting factor $f = 1 - \bar{\alpha}$ in (2.2), so that for $\bar{\alpha} = 1$ a single sheet would experience no forces and would travel with a constant velocity from one electrode to the other. Mathematically this can be expressed by writing in place of (2.2) [1] :

$$E_1 = \bar{E}_1 = \frac{\rho_s}{\epsilon_o} f\left(\frac{x_1}{d} - \frac{1}{2}\right) \qquad (7.2)$$

In the presence of several sheets the situation is more complex since in place of (2.3) we now have:

$$\bar{E}_j = E_{II}(\text{all sheets to the left of } j) + E_j + E_i(\text{all sheets to the right of } j)$$

$$= E_{II}(i > j) + E_j + E_I(i < j)$$

$$= -\frac{\rho_0}{\varepsilon_0}\left[\sum_{i=j+1}^{M}\frac{x_i}{d} + (1-\bar{\alpha}N)\left(\frac{x_j}{d} - \frac{1}{2}\right) + \sum_{i=1}^{j-1}\frac{x_i - d}{d}\right]$$

$$= -\frac{\rho_0}{\varepsilon_0}\left\{\left[\sum_{i=1}^{M}\frac{x_i}{d} - j + \frac{1}{2}\right] - \bar{\alpha}N\left(\frac{x_j}{d} - \frac{1}{2}\right)\right\} \qquad (7.3)$$

bearing in mind that $\rho_{io} = -\bar{\alpha}\rho_{eo} = -\bar{\alpha}N\rho/d$. In the absence of positive ions $\bar{\alpha} = 0$ and (7.3) reduces to (2.3).

Turning to the equations of motion we now find, repeating the algebra contained in (2.4) - (2.9) that (2.10) now acquires a more general form

$$\frac{d^2x'_j}{dt'^2} = \frac{2}{9N}\left\{\left[\sum_{i=1}^{M} x'_i - j + \frac{1}{2}\right] - \bar{\alpha}N(x'_j - \frac{1}{2})\right\} \qquad (7.4)$$

Consequently in the presence of immobile positive ions all the expressions derived previously and quoted as (2.17), (2.25), (2.31) and (2.34) are still valid as long as we substitute everywhere the RHS of (7.4) for the corresponding shorter expressions in the square brackets. One can look at the new expressions as computational models of (7.1) when a suitable load is connected across the electrodes.

In order to obtain an expression for the new potential distribution in the presence of immobile positive ions we have to calculate first of all the additional potential distribution due to the ions. We find from (6.3) that the field at x due to the ions alone is given by

$$E_{III} = -\frac{\rho_s}{\varepsilon_0}\bar{\alpha}N\left(\frac{x}{d} - \tfrac{1}{2}\right) \tag{7.5}$$

Since $\rho_s < 0$ the field $E_{III} < 0$ for $0 \leq x < \frac{1}{2}d$ and $E_{III} > 0$ for $\frac{1}{2}d < x \leq d$. Integrating (7.5) we now obtain:

$$\phi_{III} = -\int_0^{x_j} E_{III}\,dx = \frac{\rho_s}{\varepsilon_0}\bar{\alpha}N\left[\frac{x^2}{2d} - \tfrac{1}{2}x\right]_0^{x_j}$$

$$= \frac{\rho_s}{2\varepsilon_0}\bar{\alpha}N x_j\left(\frac{x_j}{d} - 1\right) \tag{7.6}$$

where $\phi_{III} = 0$ at $x_j = 0$ and $x_j = d$, the function being a parabola with its maximum at $x_j = \frac{1}{2}d$, as was to be expected. Adding (7.6) to (2.42) we now obtain:

$$\phi_j = \frac{\rho_s}{\varepsilon_0 d}\left[x_j\left(jd - \sum_{i=1}^{M} x_i\right) + d\sum_{i=j+1}^{M} x_i + \tfrac{1}{2}\bar{\alpha}Nx_j(x_j - d)\right] + \phi_0 \tag{7.7}$$

Dividing both sides by (2.43) and adding the effect of a load

$$\phi_j' = -\frac{4c}{9N}\left[x_j'\left(j - \sum_{i=1}^{M} x_i'\right) + \sum_{i=j+1}^{M} x_i' + \tfrac{1}{2}\bar{\alpha}Nx_j'(x_j' - 1)\right] - 2E'x_j' + 1 \tag{7.8}$$

It should be noted that since $x_j' \leq 1$ by definition, the additional term associated with the positive ions has as opposite sign to the preceding terms associated with the electron cloud.

In order to confirm the equivalence of (7.1) and (7.4), we decided to consider a simple case of a short-circuited diode with $\bar{a}$ = 1 and operating at two different values of the injection current ι, viz. $\sqrt{\iota}$ = 5.82 and 8.00. As was to be expected in the presence of positive ions the relative values of the injection current density are much higher. The results of our computations are shown respectively in Figs. 17 a and b. As before a hydrodynamic equation of the type (7.1) provides us with both stable and unstable solutions, however a numerical solution of (7.4) invariably leads to stable configurations only, provided we are outside the range of oscillatory solutions. Thus in Fig. 3 or ref. 7 we have a plot of stable and unstable solutions of (7.1) for $\bar{a}$ = 1, the first bifurcation point occurring at α/π = 1, which corresponds to our $\sqrt{2\iota}/3\pi$ = 1 or $\sqrt{\iota}$ = 6.6643. To the left of this point we have stable solutions for E_o = 0, which corresponds to a constant potential distribution shown in Fig. 17 a, whereas to the right of the bifurcation point we have stable solutions for $E_o \neq 0$, as is shown in Fig. 17 b, the E_o = 0 solutions then being unstable; it is worth noting that the maximum of the potential function is very close to its analytical value of 1.7325. Having established at least to some extent a formal agreement between the results obtained with the help of (7.1) and (7.4) we did not persue this line of investigations any further for reasons which are discussed more fully in the following paragraph.

In our opinion the above numerical model of a plasma-filled diode suffers from two weaknesses. First of all the assumption of infinitely heavy (immobile) positive ions is unwelcome since in a way it introduces singularities into the governing equations of motion. However what is possibly even more worrying is the fact that although the electron cloud has been discretized by being converted into a number of charge sheets, the corresponding cloud of positive ions has not. We know from other considerations [10] that this is a dangerous path to follow. We are therefore suggesting in a new proposal that the work should be continued by discretizing both clouds of charge. Since the discretization of the electron cloud not only emphasizes the corpuscular nature of electrons but also leads to new phenomena such as oscillations which could not have been predicted analytically using a perfectly smooth model of the cloud, it is to be expected that the discretization of the positive ion cloud may well lead to similar new phenomena which could not be predicted at present. This would be of particular relevance in the analysis and control of chaos in a plasma-filled diode.

CONCLUSIONS

In the first period of our investigations we have been able to establish suitable numerical models describing the conditions inside a plane diode with and without positive ions. Having developed suitable computer codes we have been able to investigate in some detail the effect of load in a system containing an electron cloud represented by a number of charge wheets. We have then derived suitable expressions and developed appropriate codes for a system comprising electron sheets and an immobile cloud of positive ions. We have also made suggestions for a further development of this particular aspect of our investogations. Finally in Section 6 we have discussed the basics of chaos as applied to our particular system

We have now reached a stage in our investigations when further extension of our work should be considered. There are three obvious routes we can follow in order to obtain a clearer and more complete picture of the behaviour of our system, in particular bearing chaos and its control in mind.

1. The most obvious is the addition of a resonant circuit in place of R, L in series or R, C in parallel. This would require the raising of the euqations of motion from the second to the thord order, a process which sould not create any special computational difficulties. Since we know that chaos can be controlled

by injection of a small signal of well defined frequency, the presence of a load in the form of a resonant circuit may be of significance.

2. We are well placed in view of our earlier work [4] to investigate the effect of initial velocity spread of the injected electrons. This has been briefly investigated before [1] and we know that a velocity spread can wipe out oscillations altogether and replace them with noise. Again this type of investigation would be of relevance to the problem of chaos control.

3. The most interesting extension of our work would be in the direction of discretization of plasma. So far two approaches have been used in the treatment of plasma. In the case of our numerical model positive ions have acted as an immovable charged background, the electron cloud being in the form of charged sheets. In practice this amounts to the introduction of a correction factor in (7.2) given by $f = 1 - \bar{\alpha}$ for a single electron sheet and a more complex expression in the case of several sheets, (7.4). The other approach, based on hydrodynamics and frequently used in analytical investigations, assumes a smooth space-charge of either sign [5-7]. In the last paragraph of Section 6 we have indicated in some detail the reasons why in our opinion both the electron cloud and the cloud of positive ions should be discretized. This would recognize the corpuscular nature of positive charges, a step, judging by our past experience [4], of considerable practical importance in the modelling of interaction processes.

REFERENCES

1. C.K.Birdsall and W.B.Bridges, 'Electron Dynamics of Diode Regions', Academice Press 1966, New York.

2. C.K.Birdsall and A.B.Langdon, 'Plasma Physics via Computer Simulation' Adam Hilger, New York 1991.

3. K.R.Spangenberg, 'Vacuum Tubes', McGraw-Hill, New York 1948; pp. 248-265.

4. V.Petridis and P.A.Lindsay, New formulation of noise in collision-free systems. III, Int. J. Electronics 38 (1975) 293-329.

   P.A.Lindsay and T.W.Chong, The influence of a constant magnetic field on electron cloud in equilibrium, II. Space-charge fluctuations, Int. J. Electronics 52 (1982) 525-544.

5. J.R.Pierce, Limiting stable current in electron beams in the presence of ions, J. Appl. Phys. 15 (1944) 721-726; Possible fluctuations in electron streams due to ions, ibid. 19 (1948) 231-236; Note on stability of electron flow in the presence of positive ions, ibid. 21 (1950) 1063.

6. V.M.Smirnov, Instability of nonlinear stationary potential oscillations in electron-ion beams, Soviet Phys. JETP 23 (1966) 668-672.

   V.D.Shapiro and V.I.Shevchenko, Contribution to the nonlinear theory of instability of an electron beam in a system with electrodes, Soviet Phys. JETP 25 (1967) 92-97.

7. B.B.Godfrey, Oscillatory nonlinear electron flow in a Pierce diode, Phys. Fluids 30 (1987) 1553-1560.

8. C.E.Fay, A.L.Samuel and W.Shockley, On the theory of space charge between parallel plane electrodes, BSTJ 17 (1938) 49-79.

9. C.F.F.Karney, Stochastic ion heating by lower hybrid wave, Phys. Fluids 21 (1978) 1584-1599.

   S.Kuhn, Linear longitudinal oscillations in collisionless plasma diodes this sheaths. I. Method, Phys. Fluids 27 (1984) 1821-1833; II. Application to an extended Pierce-type problem, ibid. 27 (1984) 1834-1851.

10. R.J.Lomax, Unstable electron flow in a diode, Proc.IEE C 108 (1960) 119-121.

CAPTIONS

1. The model of the diode.
2. Position and potential of individual sheets: (a) ι = 4.0; (b) ι = 6.0; (c) ι = 8.0; (d) ι = 9.0.
3. The anode current ι_a as a function of the injection current ι for a short-circuited diode.
4. Interelectrode potential distribution: (a) ι = 6.0, S.C.; (b) ι = 6.0, T_R = 0.1.
5. Electron trajectories: (a) ι = 4.0, S.C.; (b) ι = 9.0, T_R = 0.1, T_L = 1.0.
6. Potential minimum against time: (a) ι = 4.0, S.C.; (b) ι = 9.0, S.C.
7. Position of the potential minimum against time: (a) ι = 4.0, S.C.; (b) ι = 9.0, T_R = 0.1, T_L = 1.0.
8. The field E' against time: ι = 9.0, T_R = 0.1.
9. Velocity of the potential minimum against its position: (a) ι = 4.0, S.C.; (b) ι = 9.0, T_R = 0.1, T_L = 1.0.
10. Potential minimum against the field: ι = 9.0, T_R = 0.1, T_L = 1.0.
11. System performance for different values of ι and T_R: (a) Table of results; potential minimum against time for ι = 9.0: (b) T_R = 0.01, (c) T_R = 0.1, (d) T_R = 0.8; frequency spectrum for ι = 9.0: (e) T_R = 0.01, (f) T_R = 0.1, (g) T_R = 0.8.

12. System performance for $T_R = 0.1$ and different values of ι and T_L.

(a) Table of results; potential minimum against time, $\iota = 9.0$:

(b) $T_L = 0.001$, (c) $T_L = 0.1$, (d) $T_L = 1.0$;

frequency spectrum, $\iota = 9.0$:

(e) $T_L = 0.001$, (f) $T_L = 0.1$, (g) $T_L = 1.0$.

13. System preformance for $T_R = 0.1$ and different values of ι and T_C.

(a) Table of results; potential minimum against time, $\iota = 9.0$:

(b) $T_C = 0.001$, (c) $T_C = 0.1$, (d) $T_C = 1.0$;

frequency spectrum, $\iota = 9.0$:

(e) $T_C = 0.001$, (f) $T_C = 0.1$, (g) $T_C = 1.0$.

14. Phase-space trajectories: $\dot{x}'$ against x':

(a) for a single sheet, S.C.; for many sheets:

(b) $\iota = 4.0$, S.C., (c) the same, transient removed;

(d) $\iota = 9.0$, $T_R = 0.1$, $T_L = 1.0$, (e) the same, transient removed.

15. Phase-space trajectories: potential minimum against field:

(a) $\iota = 9.0$, $T_R = 0.1$, $T_L = 1.0$, $\Delta t' = 0.01$;

(b) the same, $\Delta t' = 2.3$; (c) the same, $\Delta t' = 2.3$, different phase; (d) $\iota = 9.0$, $T_R = 0.1$, $\Delta t' = 0.01$, (e) the same, $\Delta t' = 2.1$, (f) the same, $\Delta t' = 2.1$, different phase.

16. Poincaré sections: $\dot{x}'_{min}$ against x'_{min}

(a) $\iota = 9.0$, (b) $\iota = 12.0$, (c) $\iota = 15.0$, (d) $\iota = 18.0$, (e) $\iota = 23.0$.

17. Potential distribution, s.c., $\bar{\alpha} = 1$:

(a) $\iota = 28.33$, (b) $\iota = 64.09$.

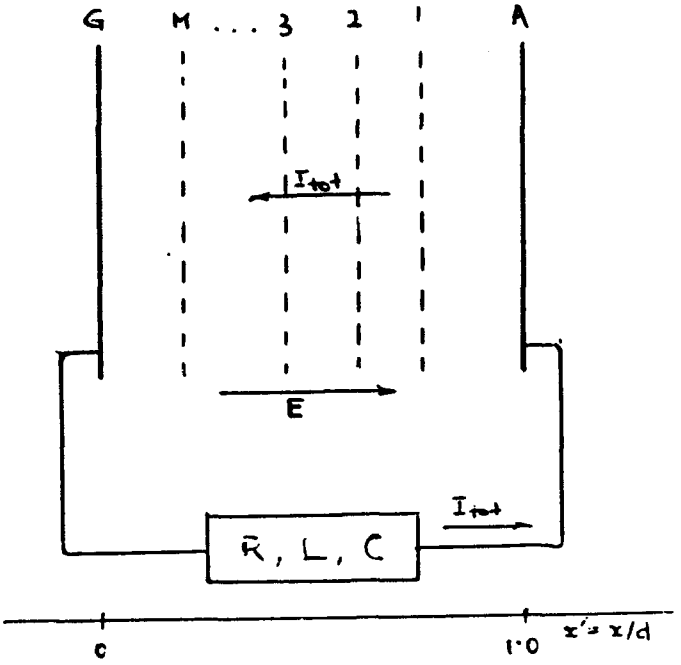

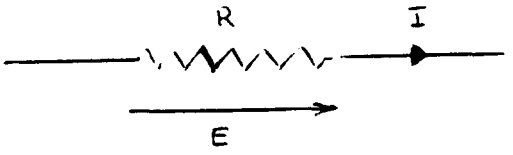

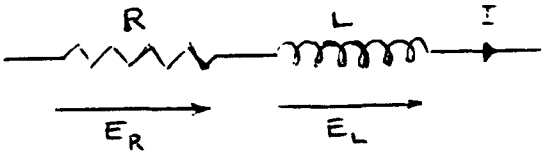

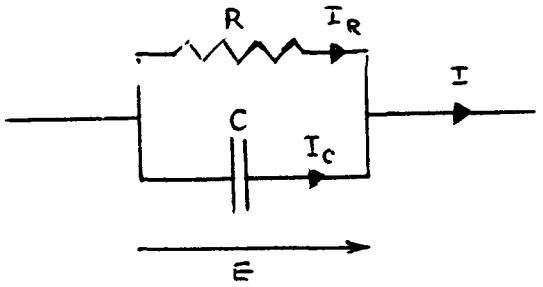

Fig. 1

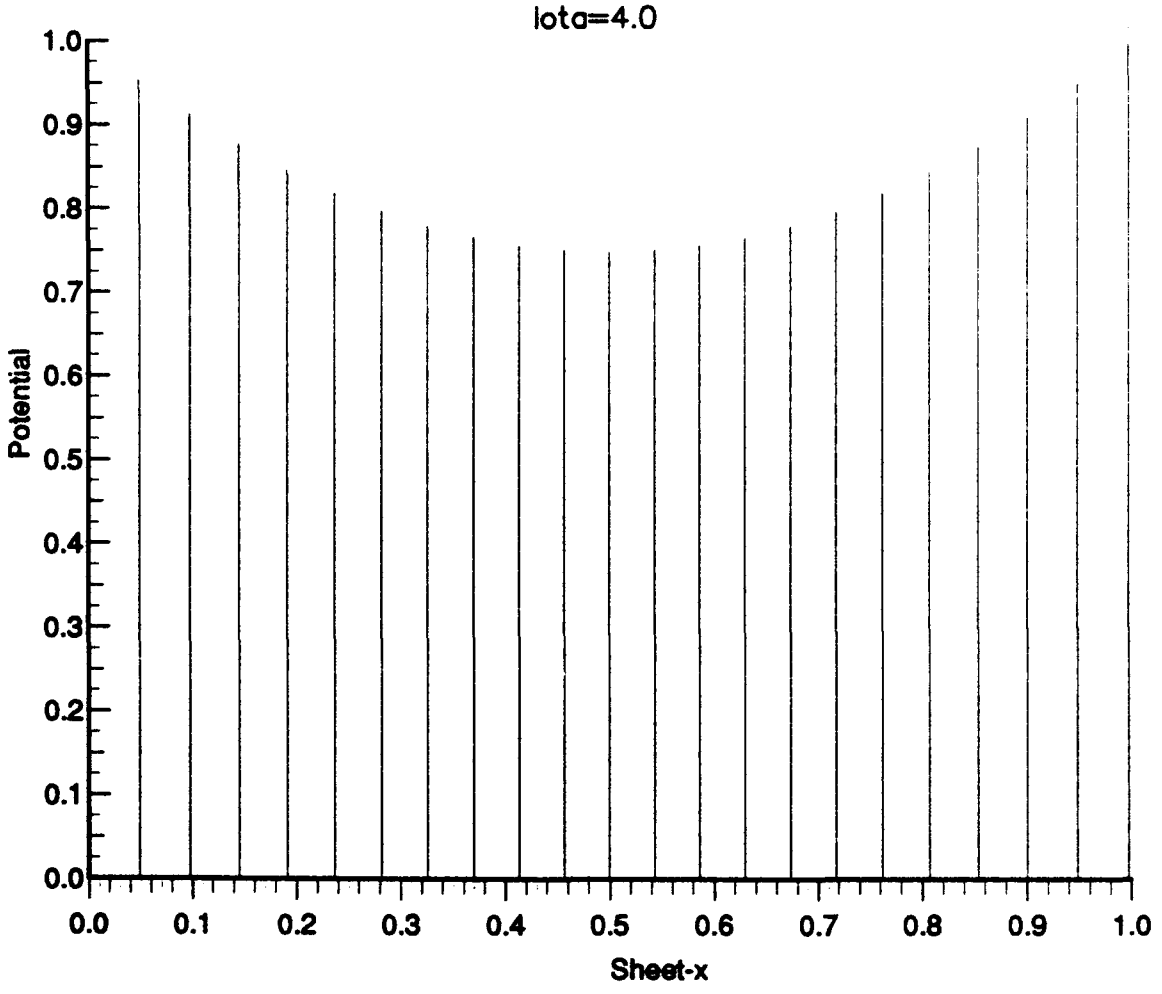
lota=4.0
Potential
1.0
0.9
0.8
0.7
0.6
0.5
0.4
0.3
0.2
0.1
0.0
0.0
0.1
0.2
0.3
0.4
0.5
0.6
0.7
0.8
0.9
1.0
Sheet-x

Fig. 2 a

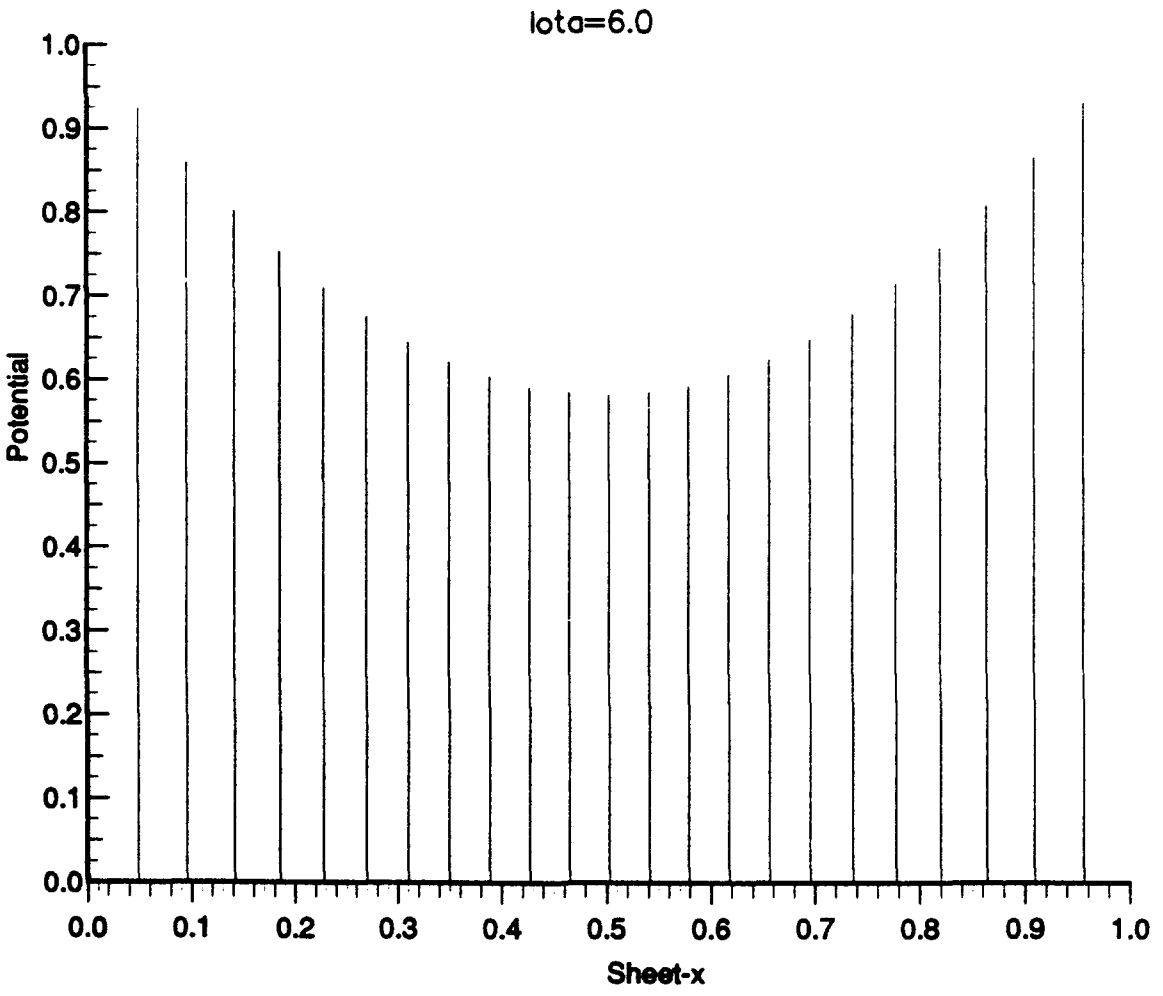
lota=6.0
Potential
1.0
0.9
0.8
0.7
0.6
0.5
0.4
0.3
0.2
0.1
0.0
0.0
0.1
0.2
0.3
0.4
0.5
0.6
0.7
0.8
0.9
1.0
Sheet-x

Fig. 2 b

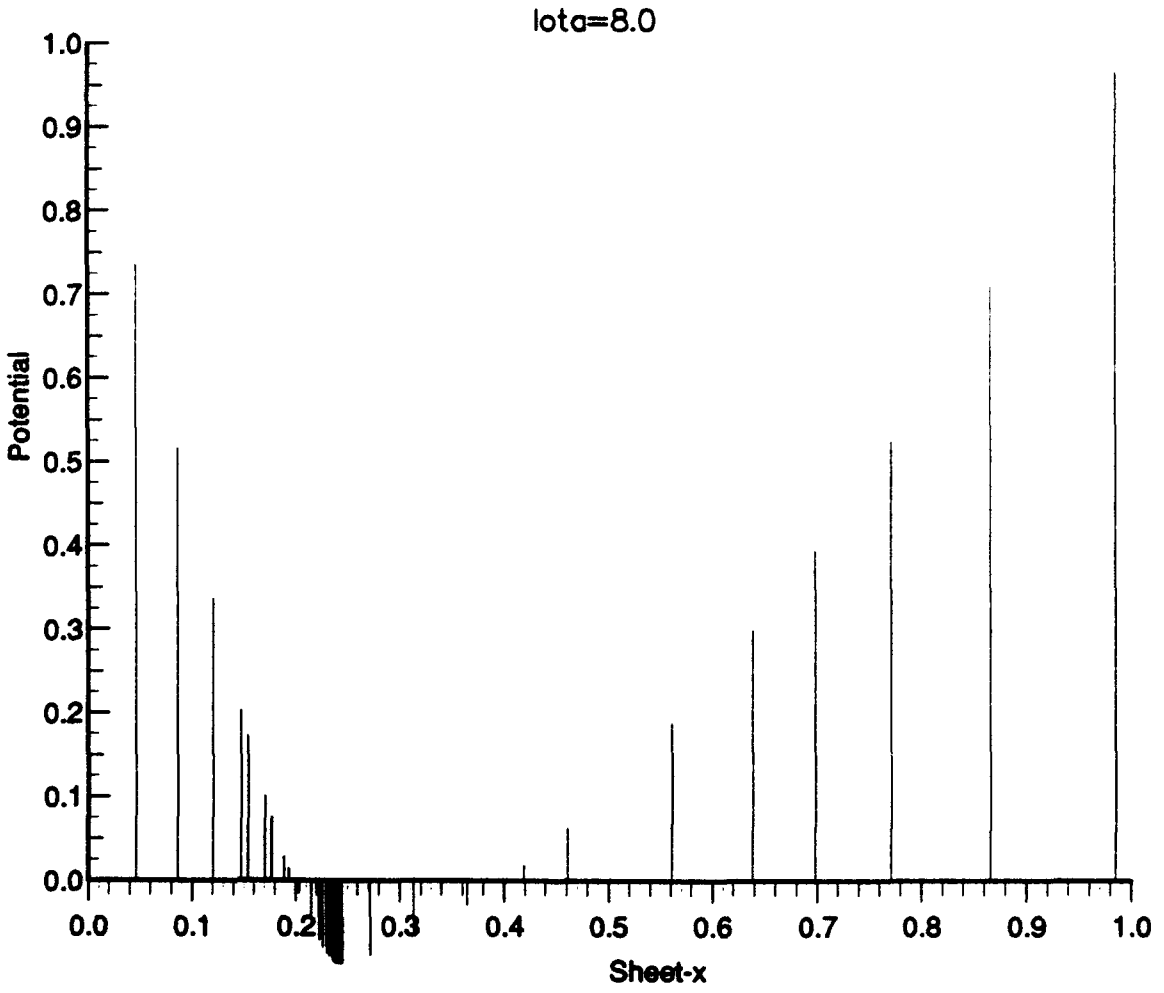
lota=8.0
Potential
Sheet-x
1.0
0.9
0.8
0.7
0.6
0.5
0.4
0.3
0.2
0.1
0.0
0.0
0.1
0.2
0.3
0.4
0.5
0.6
0.7
0.8
0.9
1.0

Fig. 2 c

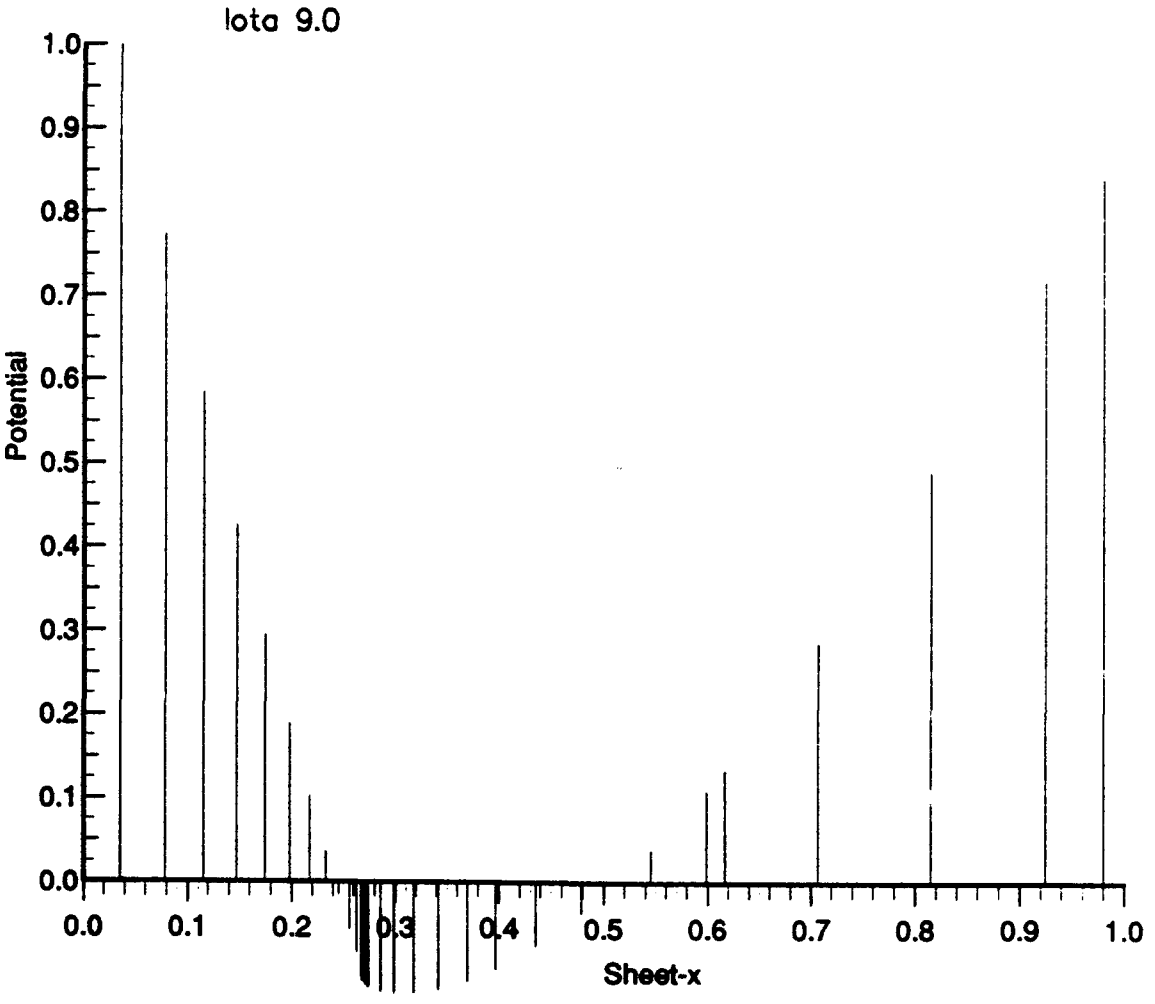
Iota 9.0
Potential
1.0
0.9
0.8
0.7
0.6
0.5
0.4
0.3
0.2
0.1
0.0
0.0
0.1
0.2
0.3
0.4
0.5
0.6
0.7
0.8
0.9
1.0
Sheet-x

Fig. 2 d

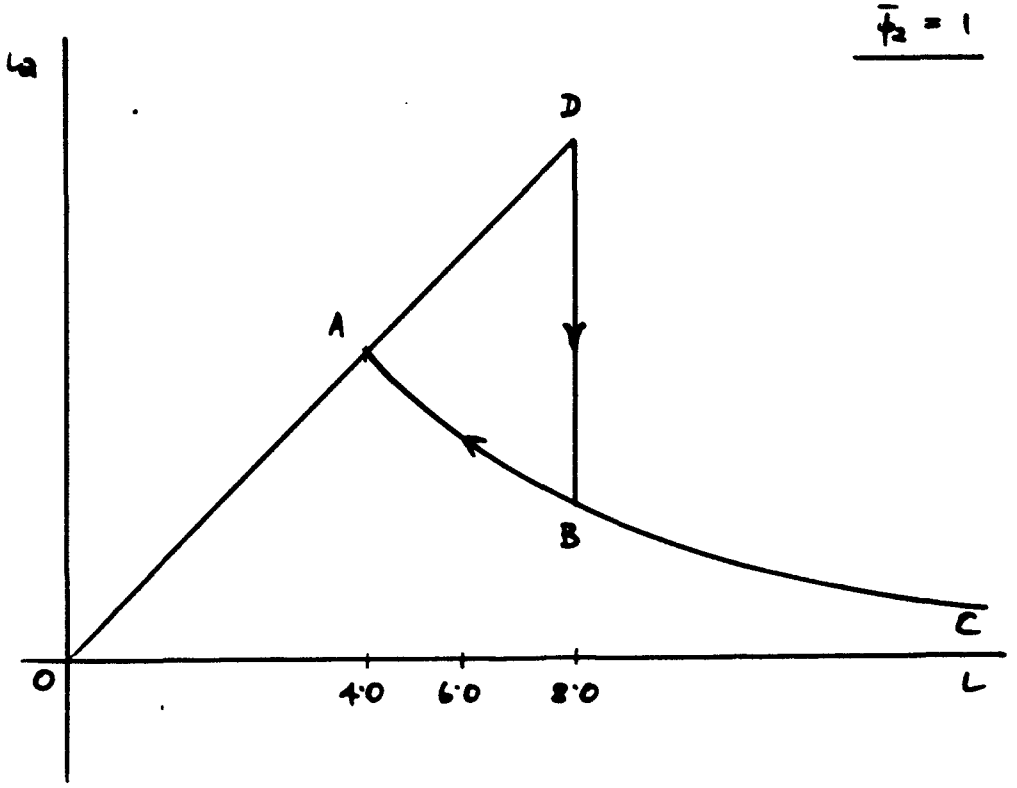

OA - minimum near the centre, no oscillations

AB - minimum near the centre when there are no oscillations; for T_L 1.0 oscillations develop and the hysteresis loop disappears

BC - minimum near the entrance electrode (grid); relaxation oscillations (fast rise, slow fall) are invariably present

Fig. 3

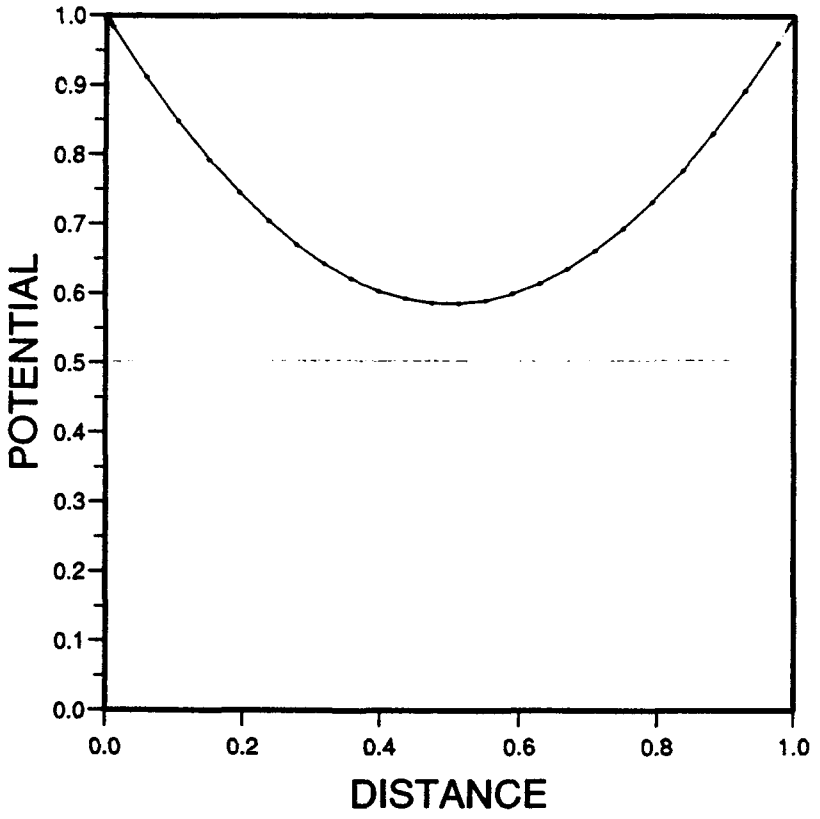
1.0
0.9
0.8
0.7
0.6
0.5
0.4
0.3
0.2
0.1
0.0
POTENTIAL
0.0
0.2
0.4
0.6
0.8
1.0
DISTANCE

Fig. 4 a

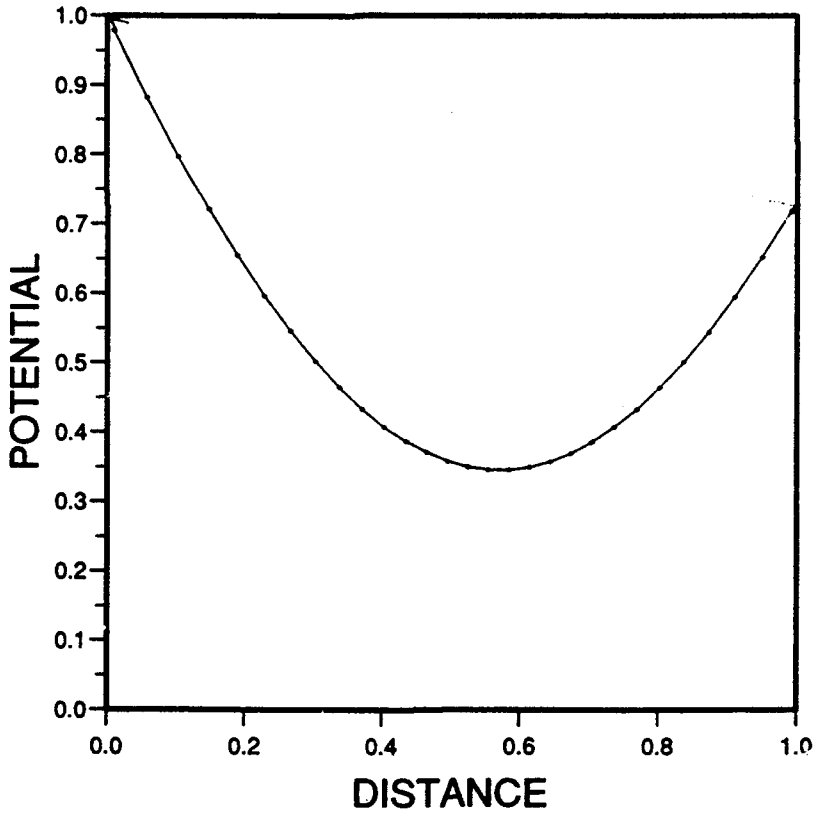
POTENTIAL
1.0
0.9
0.8
0.7
0.6
0.5
0.4
0.3
0.2
0.1
0.0
0.0
0.2
0.4
0.6
0.8
1.0
DISTANCE

Fig. 4 b

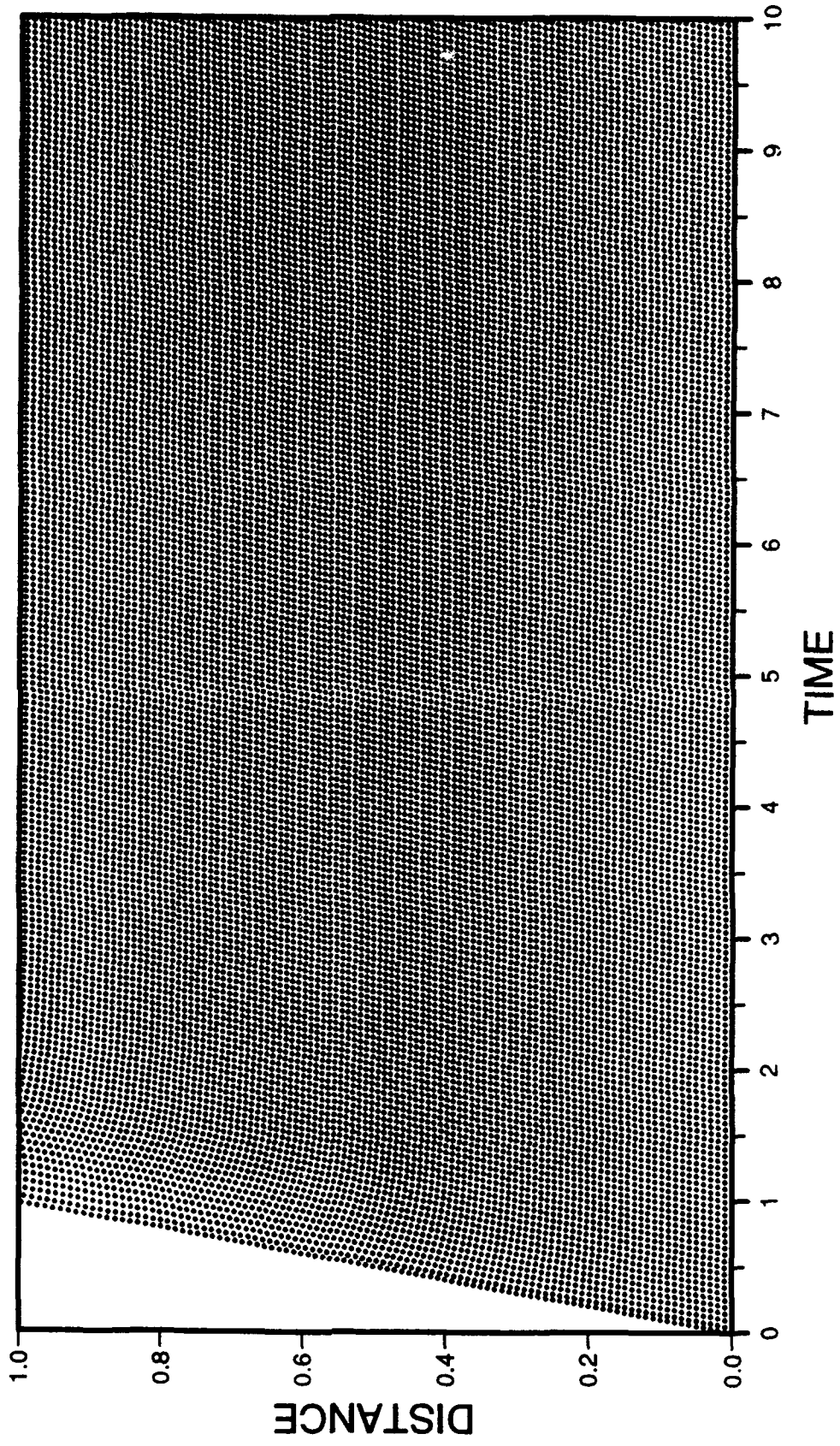

ι =4. (S.C.)

Fig. 5 a

$\iota = 9.\ \tau_R = 0.1\ \tau_L = 1.0$

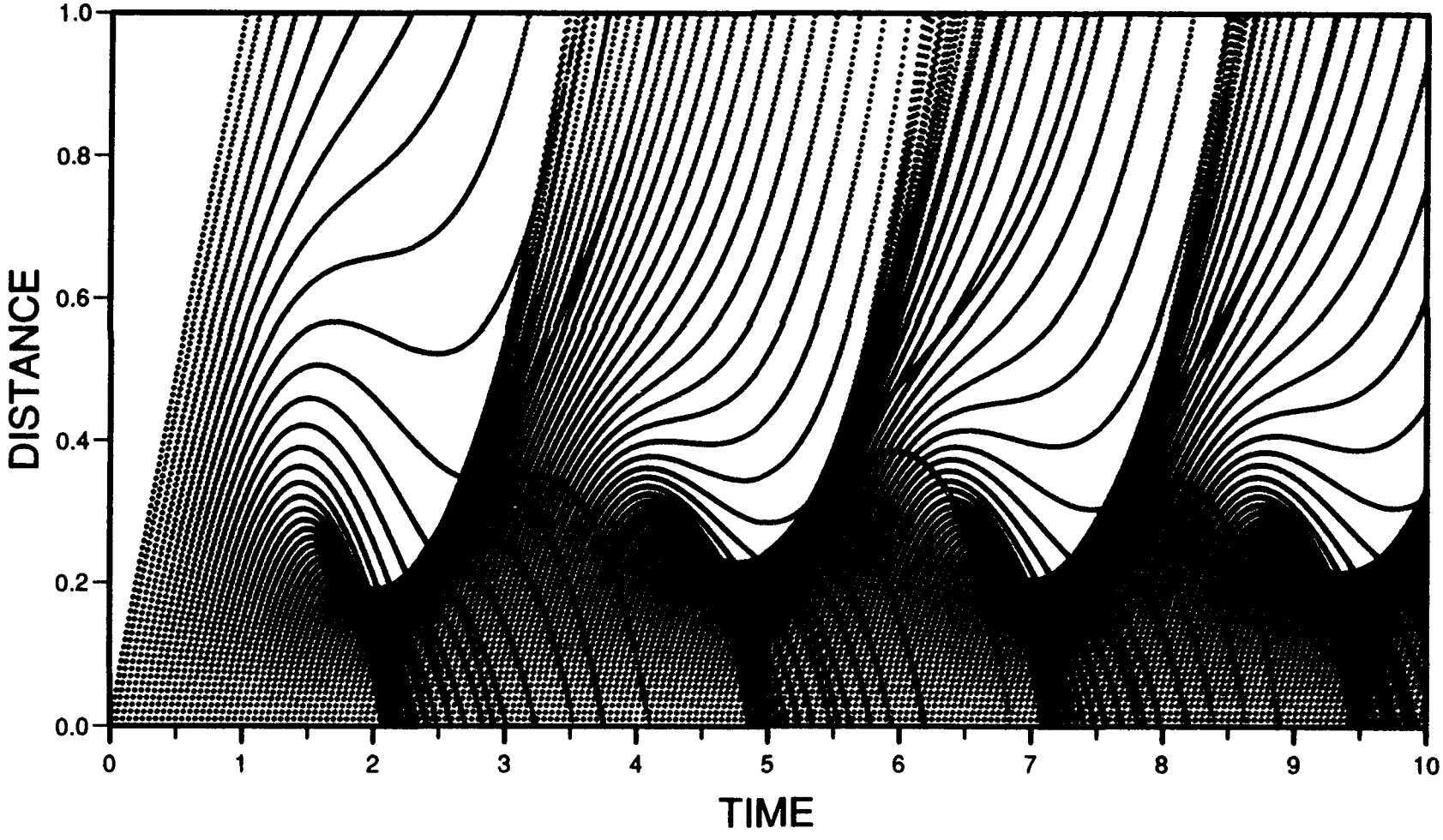

Fig. 5 b

ζ=4. (S.C.)

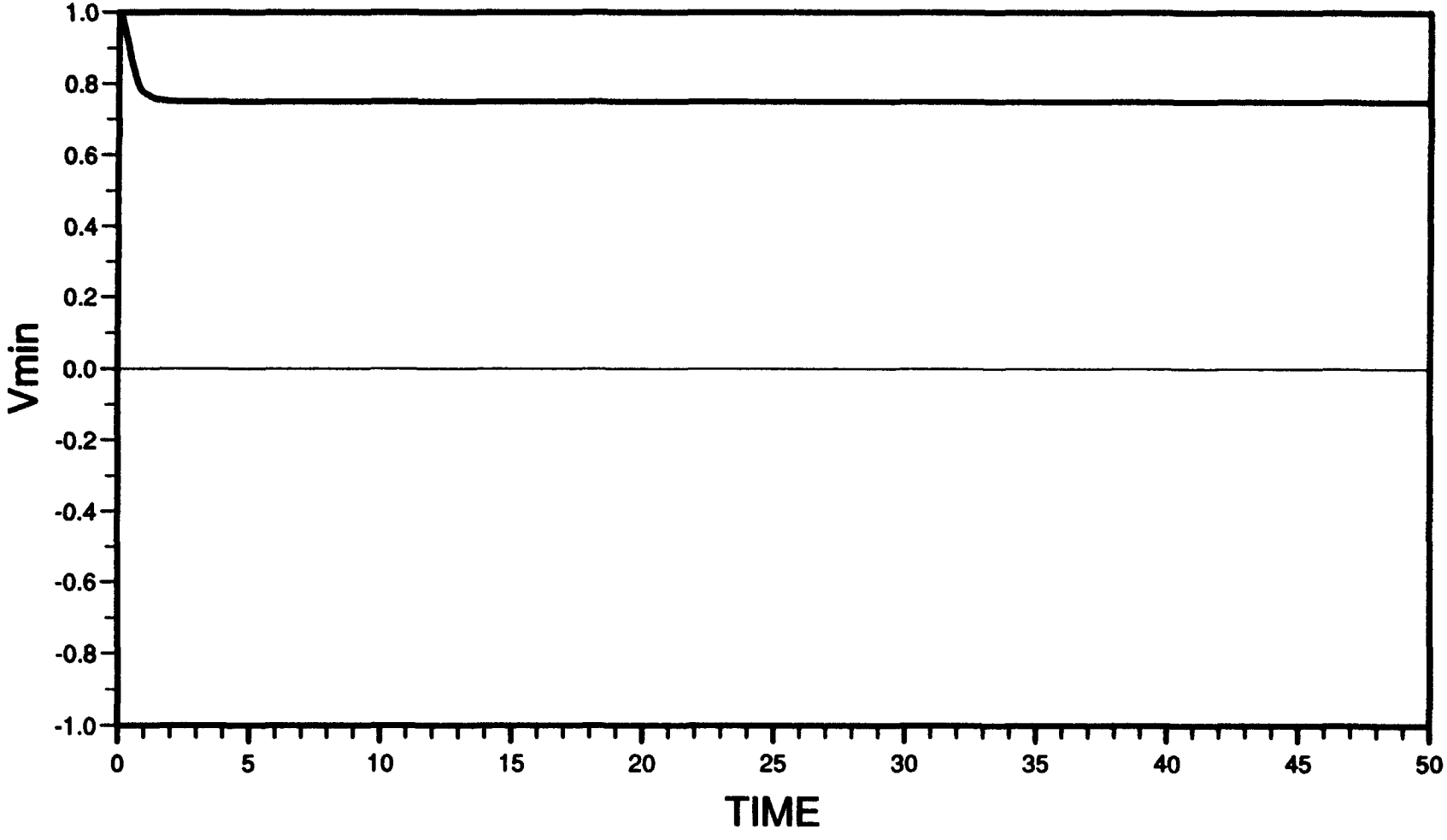
1.0
0.8
0.6
0.4
0.2
0.0
-0.2
-0.4
-0.6
-0.8
-1.0
Vmin
0
5
10
15
20
25
30
35
40
45
50
TIME

Fig. 9 a

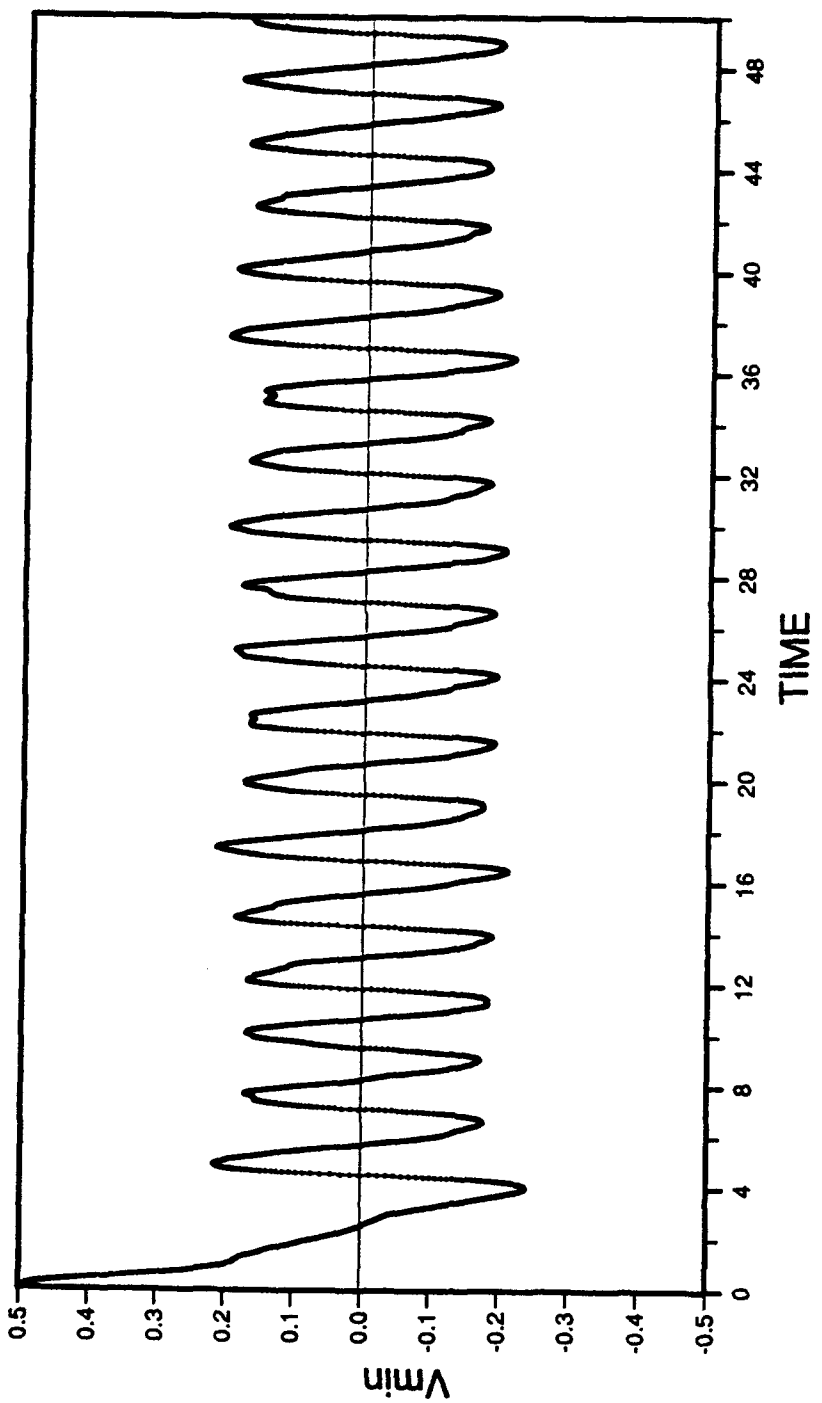

ϵ =9. (S.C.)

Fig. 6 b

L =4. (S.C.)

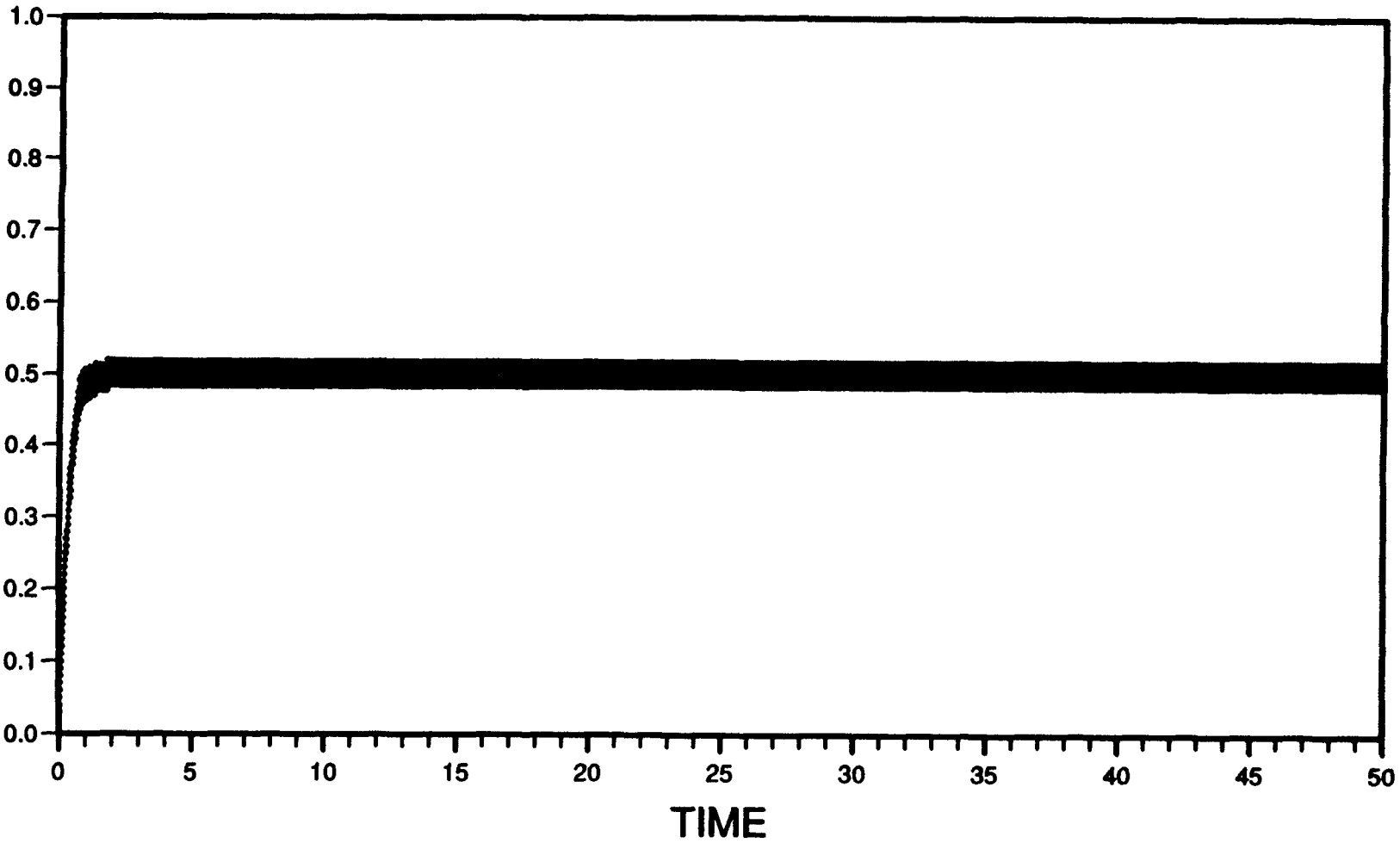
1.0
0.9
0.8
0.7
0.6
0.5
0.4
0.3
0.2
0.1
0.0
Xmin
0
5
10
15
20
25
30
35
40
45
50
TIME

Fig. 7 a

ι =9. T_R =0.1 T_L =1.0

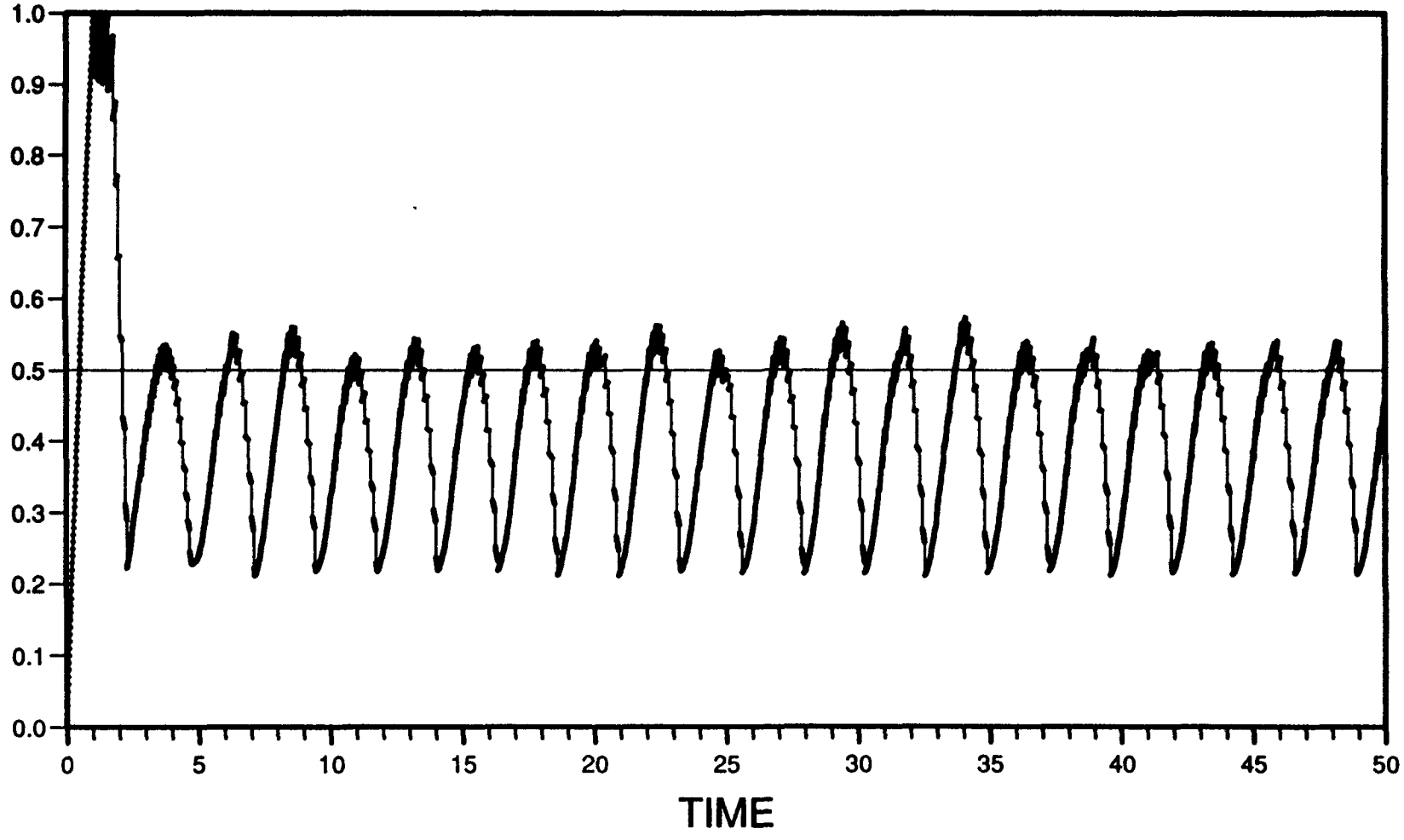

Fig. 7 b

$\iota = 9.\ T_R = 0.1$

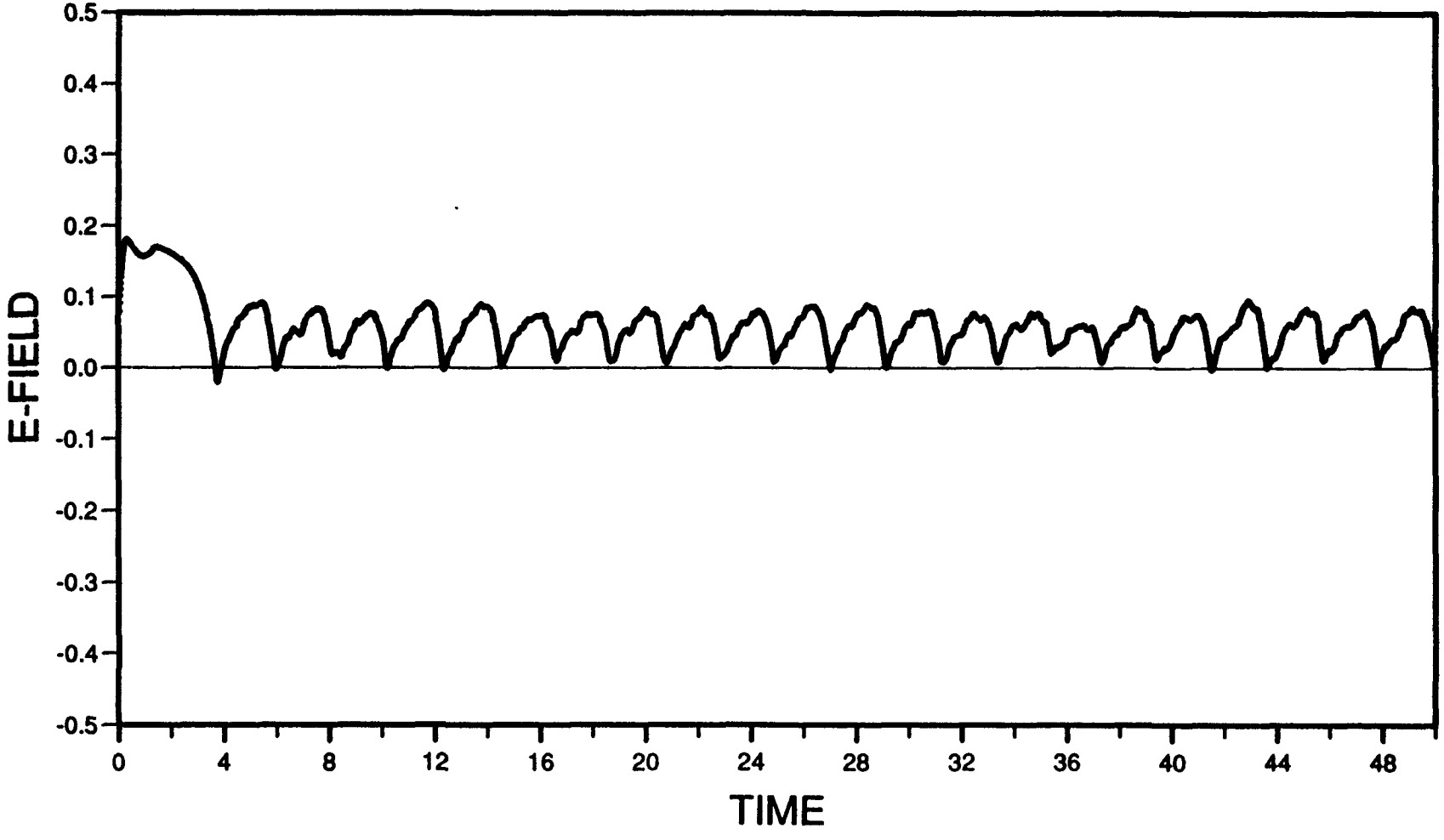

Fig. 3

ι =4. (S.C.)

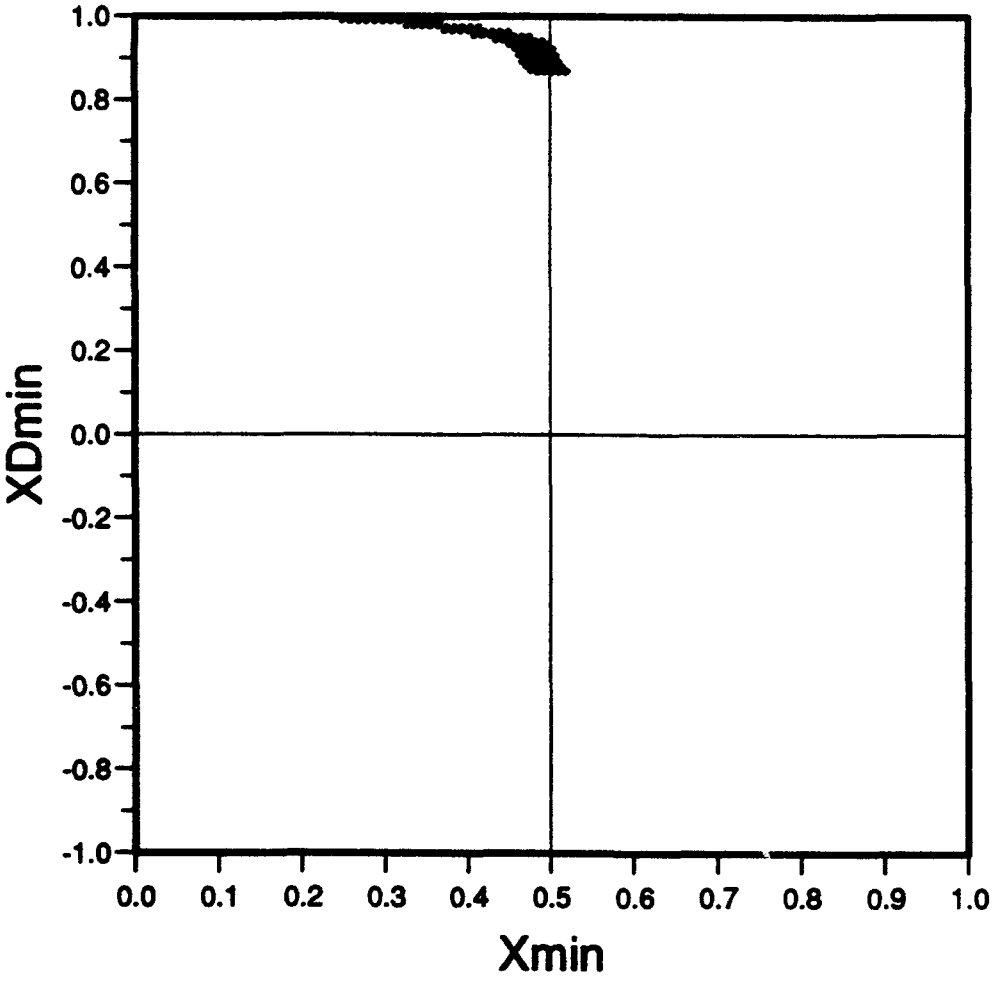

Fig. 9 a

ι =9. T_R =0.1 T_L =1.0

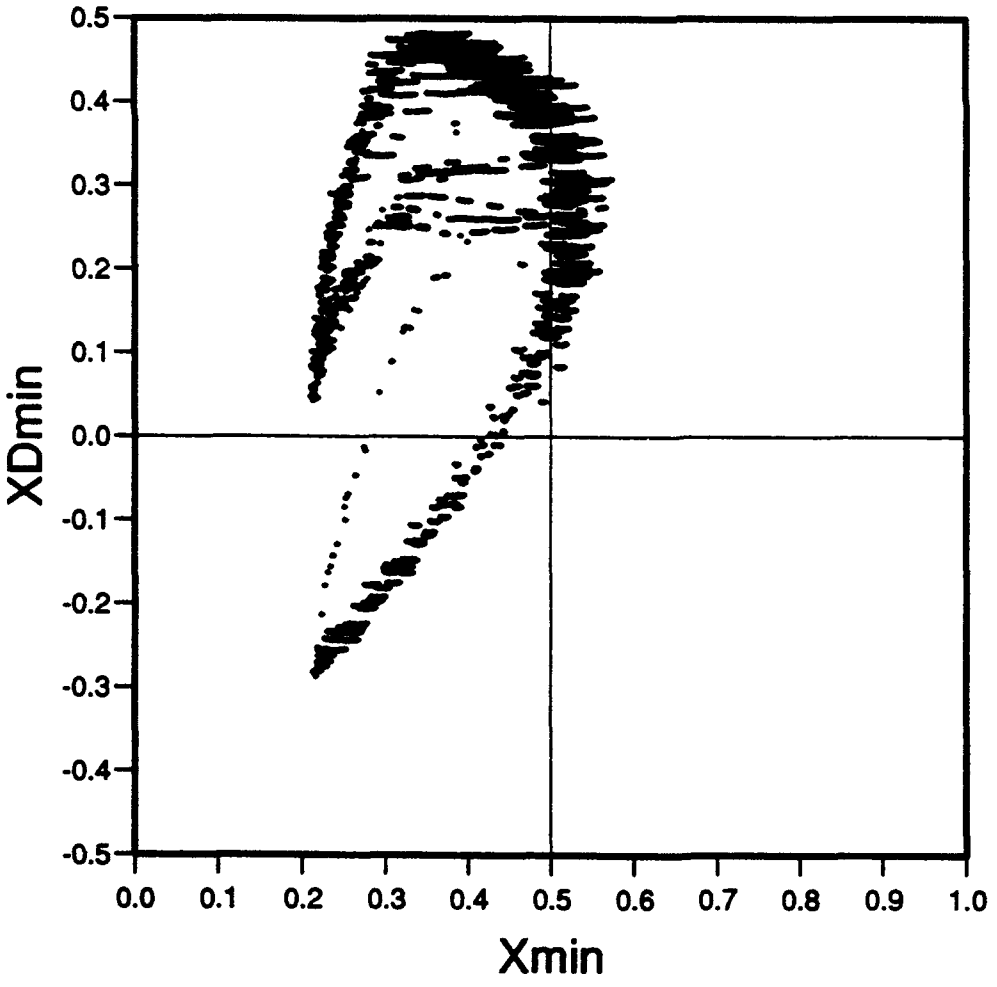

Fig. 9 b

L =9. T_R =0.1 T_L =1.0

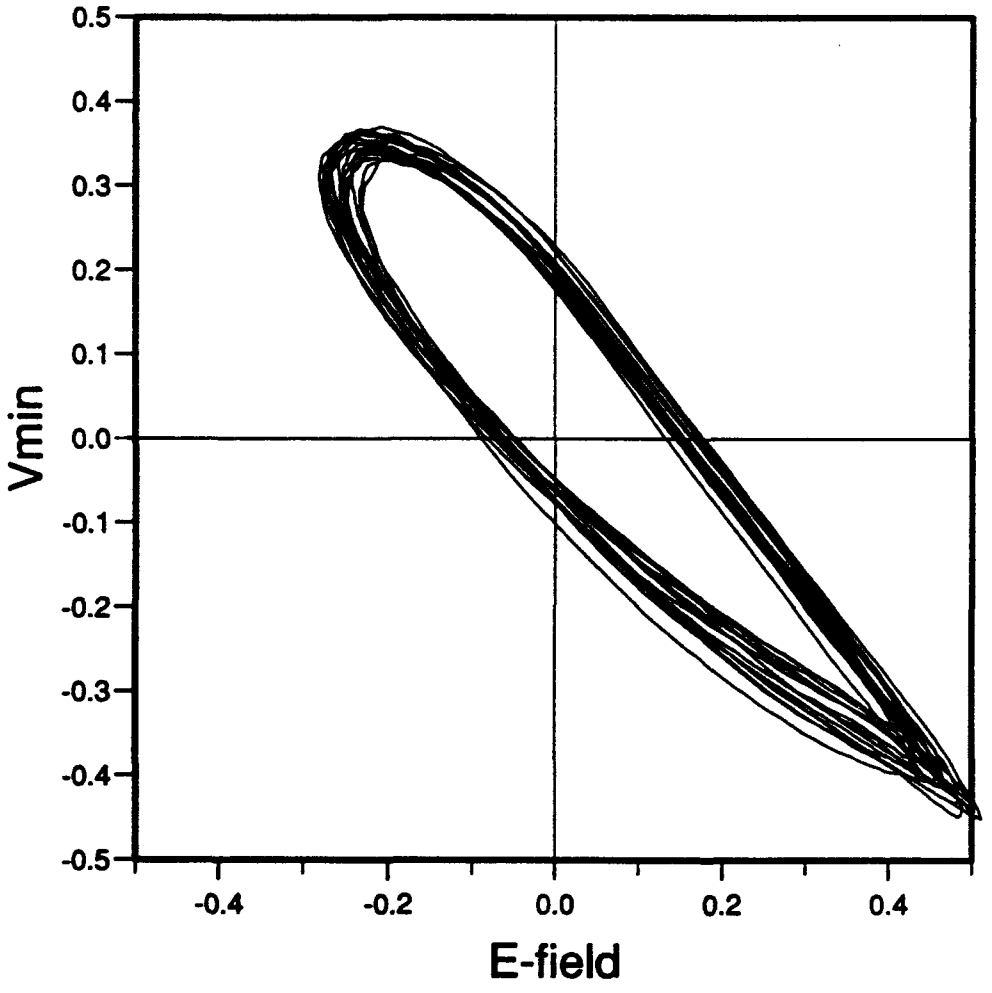

Fig. 10

$T_L = T_C = 0$

T_R \ L	4.0	6.0	9.0
0.01	ST	ST	OSC
0.1	ST	ST	OSC
0.8	OSC	OSC	OSC

ST - stable, no oscillations

OSC - oscillations present

Fig. 11 a

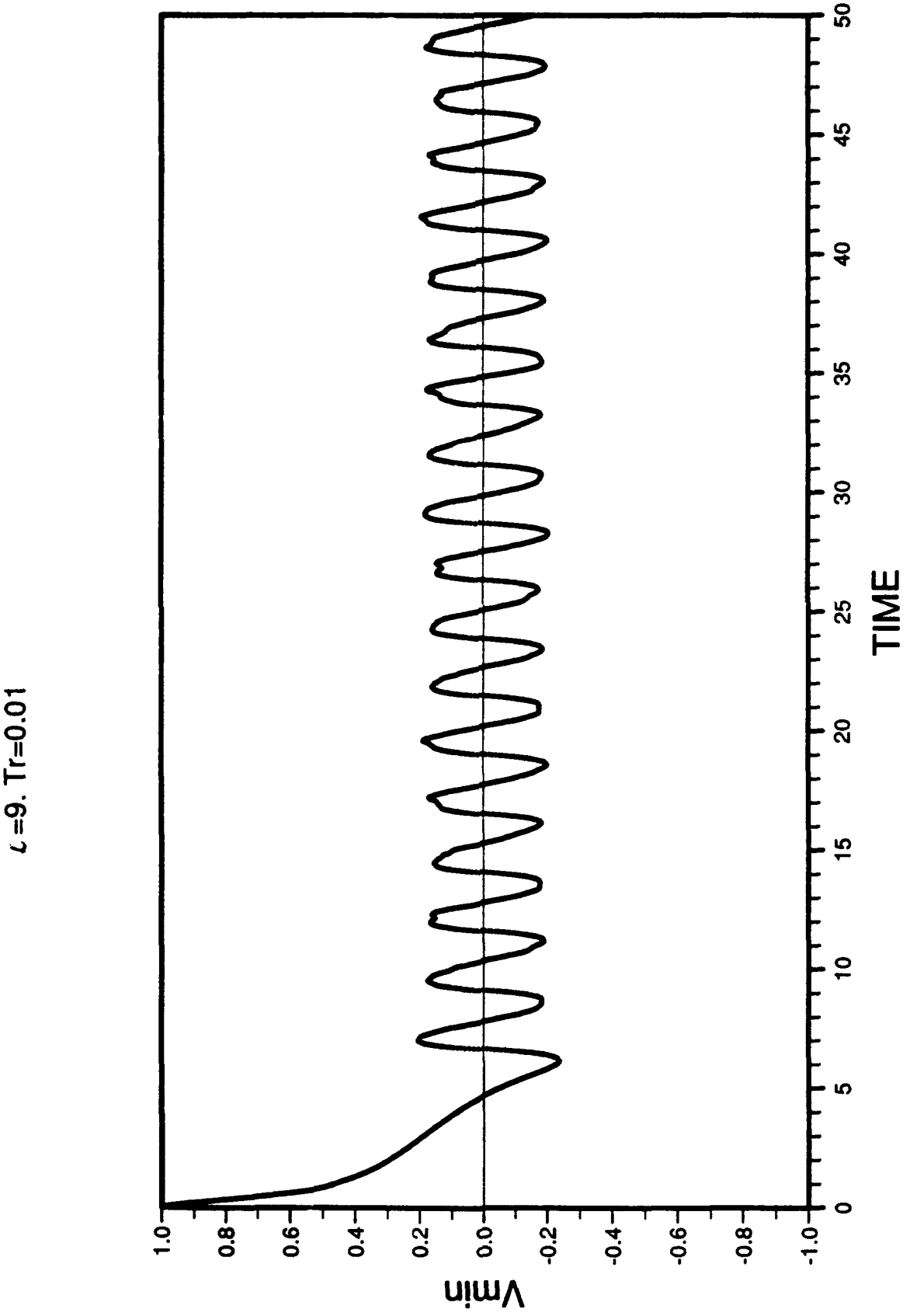
ζ=9. Tr=0.01
Vmin
TIME
1.0
0.8
0.6
0.4
0.2
0.0
-0.2
-0.4
-0.6
-0.8
-1.0
0
5
10
15
20
25
30
35
40
45
50

Fig. 11 b

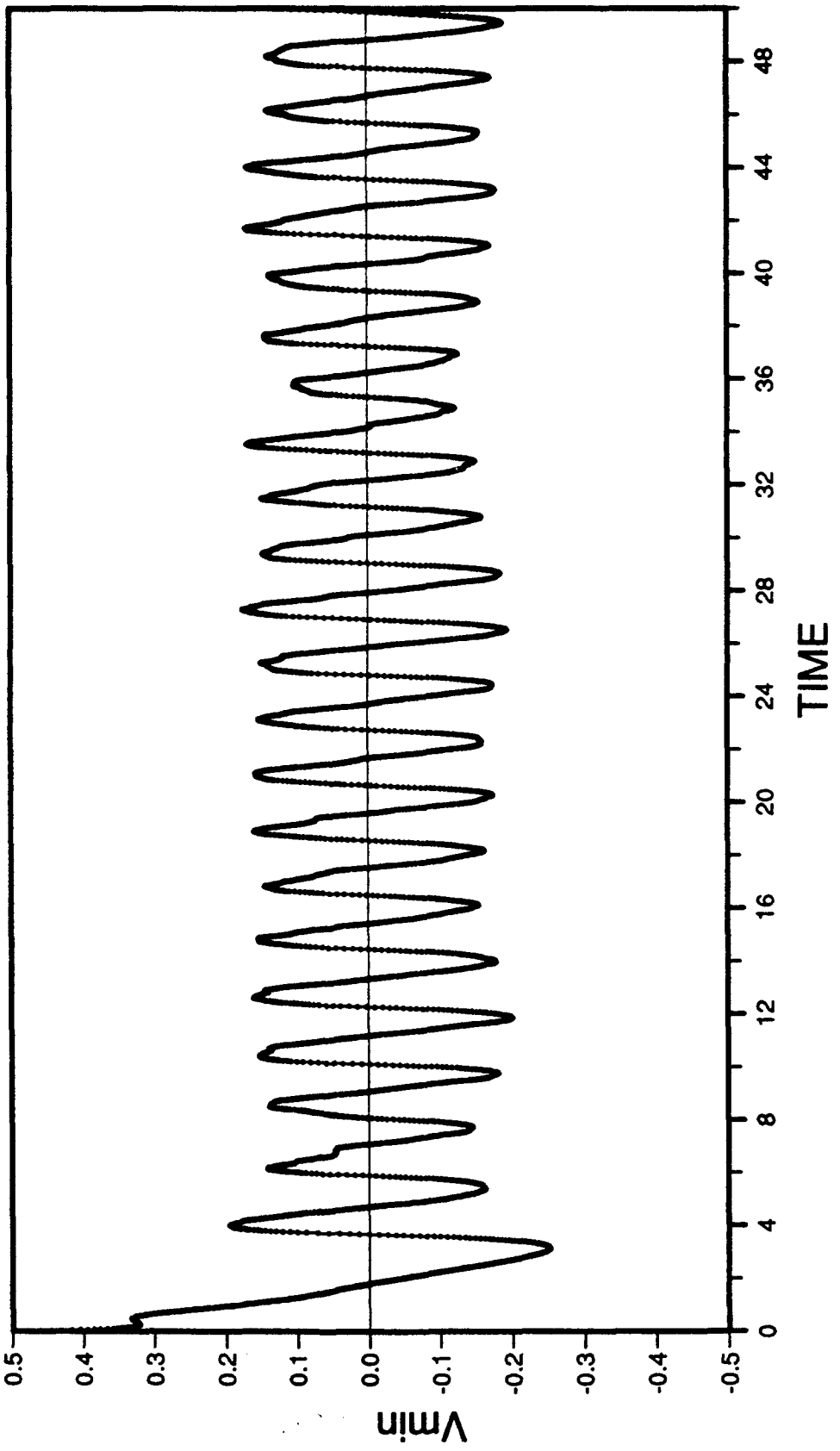

$\iota = 9\ T_R = 0.1$

Fig. 11 c

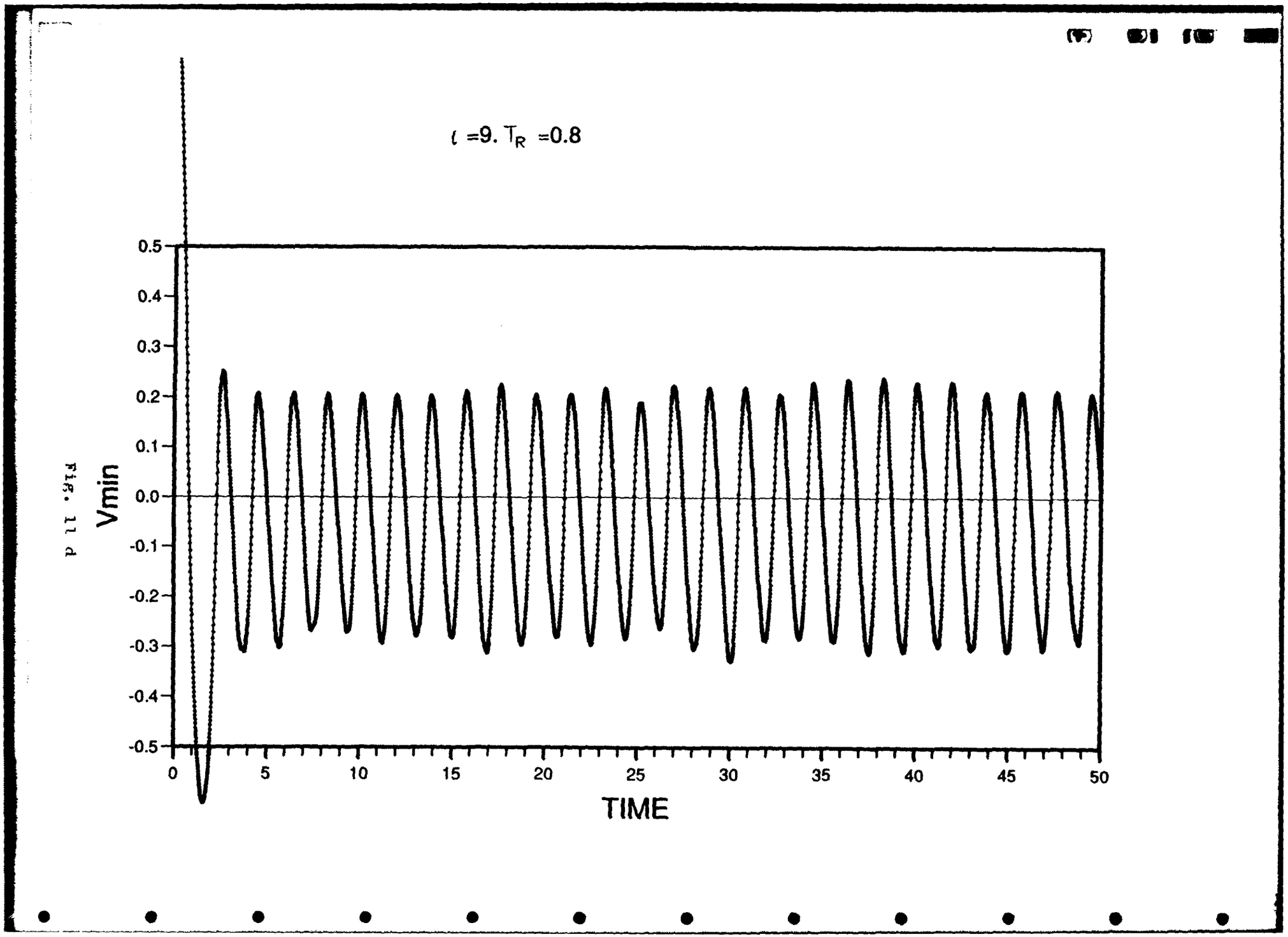
ι =9. T_R =0.8
0.5
0.4
0.3
0.2
0.1
0.0
-0.1
-0.2
-0.3
-0.4
-0.5
Vmin
0
5
10
15
20
25
30
35
40
45
50
TIME

Fig. 11 d

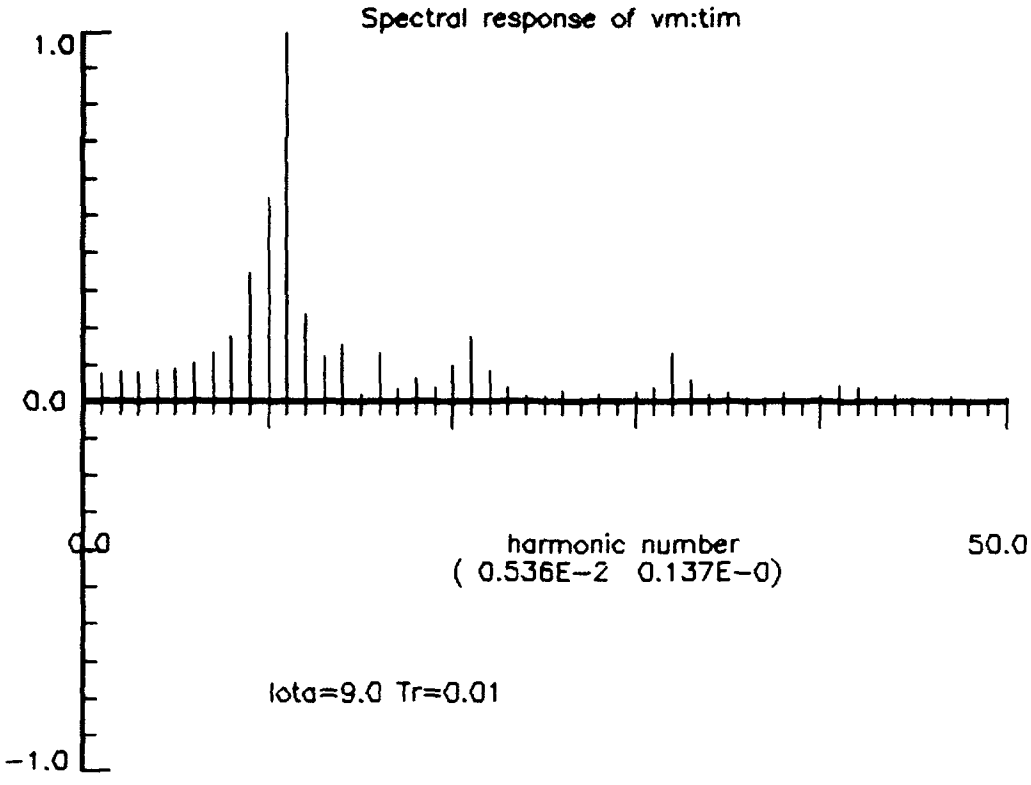
Spectral response of vm:tim
1.0
0.0
-1.0
0.0
harmonic number
50.0
(0.536E-2 0.137E-0)
Iota=9.0 Tr=0.01

Fig. 11 e

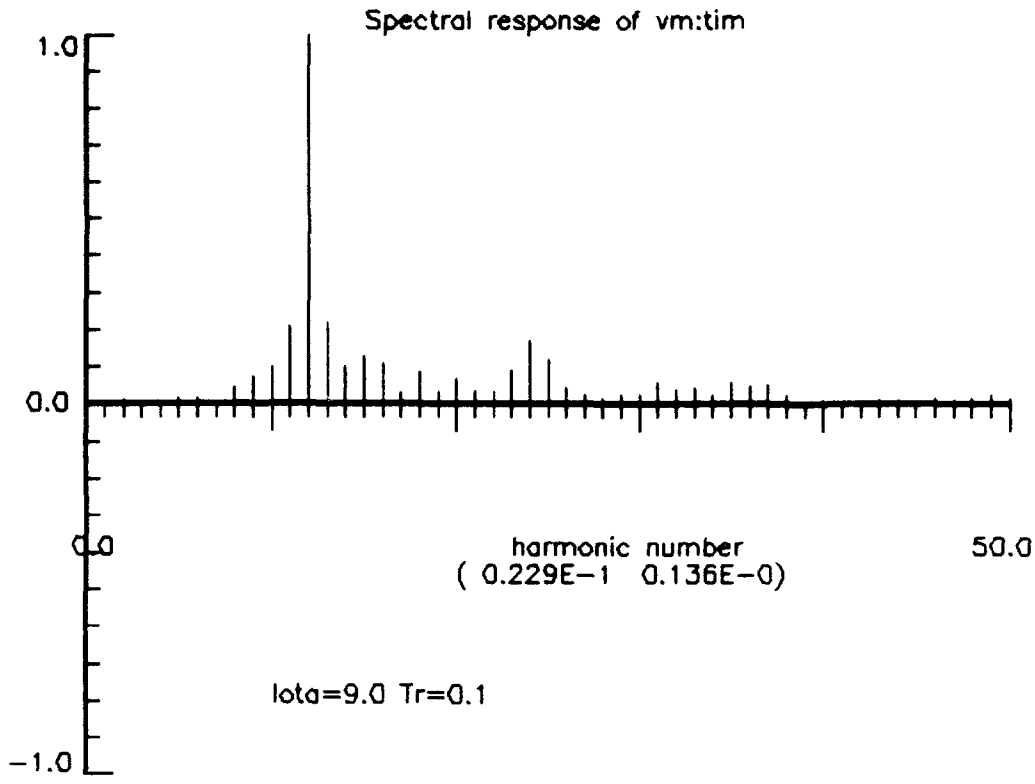
Spectral response of vm:tim
1.0
0.0
-1.0
0.0
harmonic number
50.0
(0.229E-1 0.136E-0)
Iota=9.0 Tr=0.1

Fig. 11 f

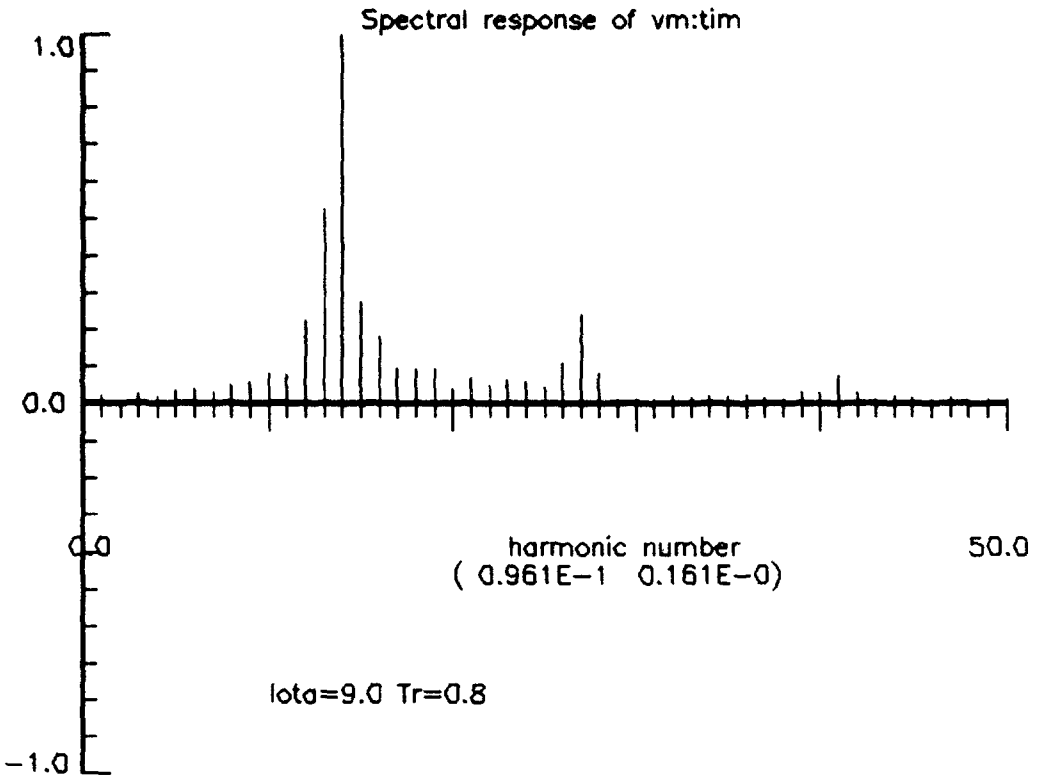
Spectral response of vm:tim
1.0
0.0
-1.0
0.0
harmonic number
50.0
(0.961E-1 0.161E-0)
Iota=9.0 Tr=0.8

Fig. 11 g

$T_R = 0.1,\ T_C = 0$

T_L \ L	4.0	6.0	9.0
0.001	ST	ST	OSC
0.1	ST	ST	OSC
1.0	ST	OSC	OSC

ST - stable, no oscillations

OSC - oscillations present

Fig. 12 a

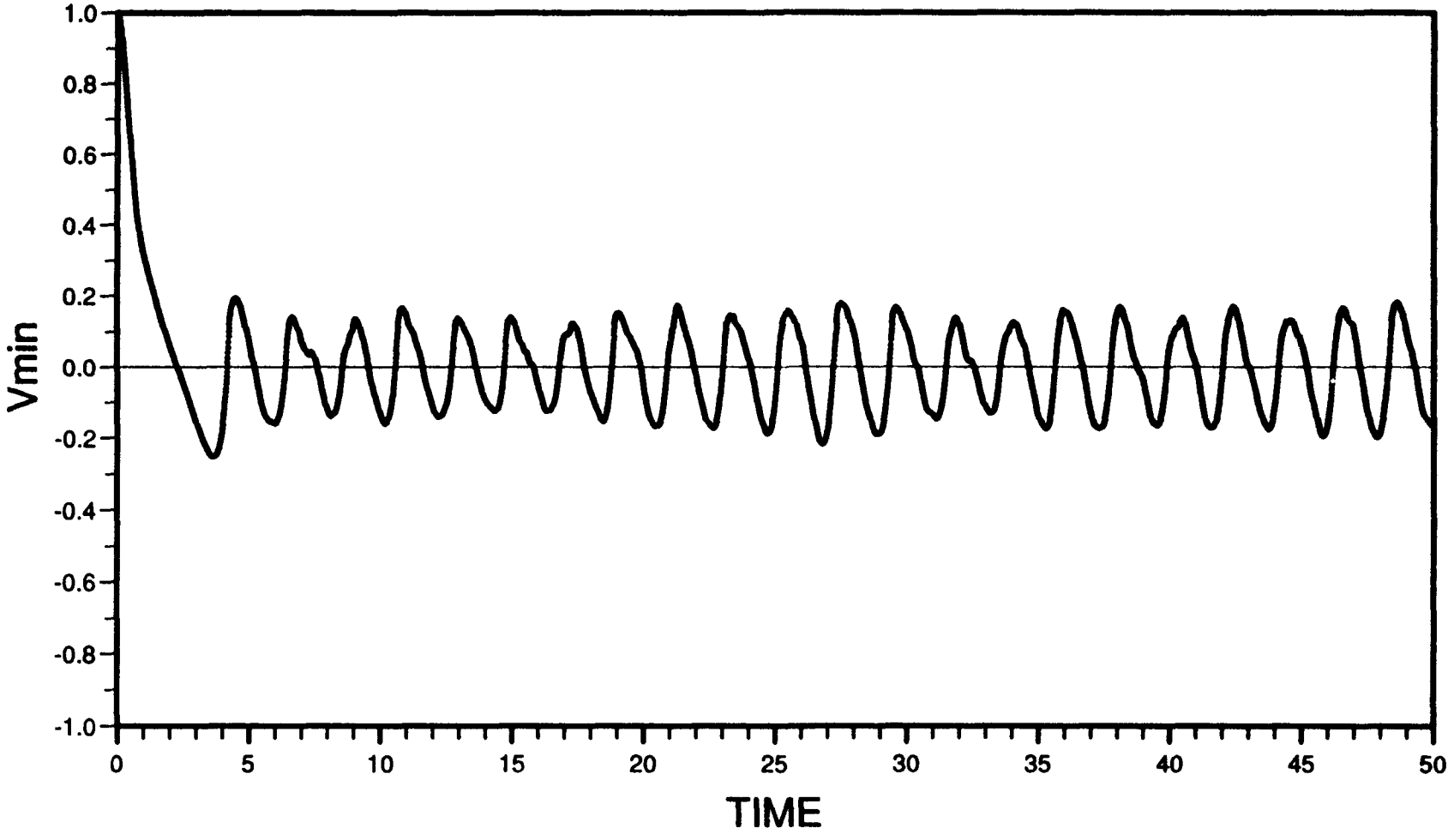
ι =9. Tr=0.1 Tl=0.001
Vmin
1.0
0.8
0.6
0.4
0.2
0.0
-0.2
-0.4
-0.6
-0.8
-1.0
0
5
10
15
20
25
30
35
40
45
50
TIME

Fig. 12 b

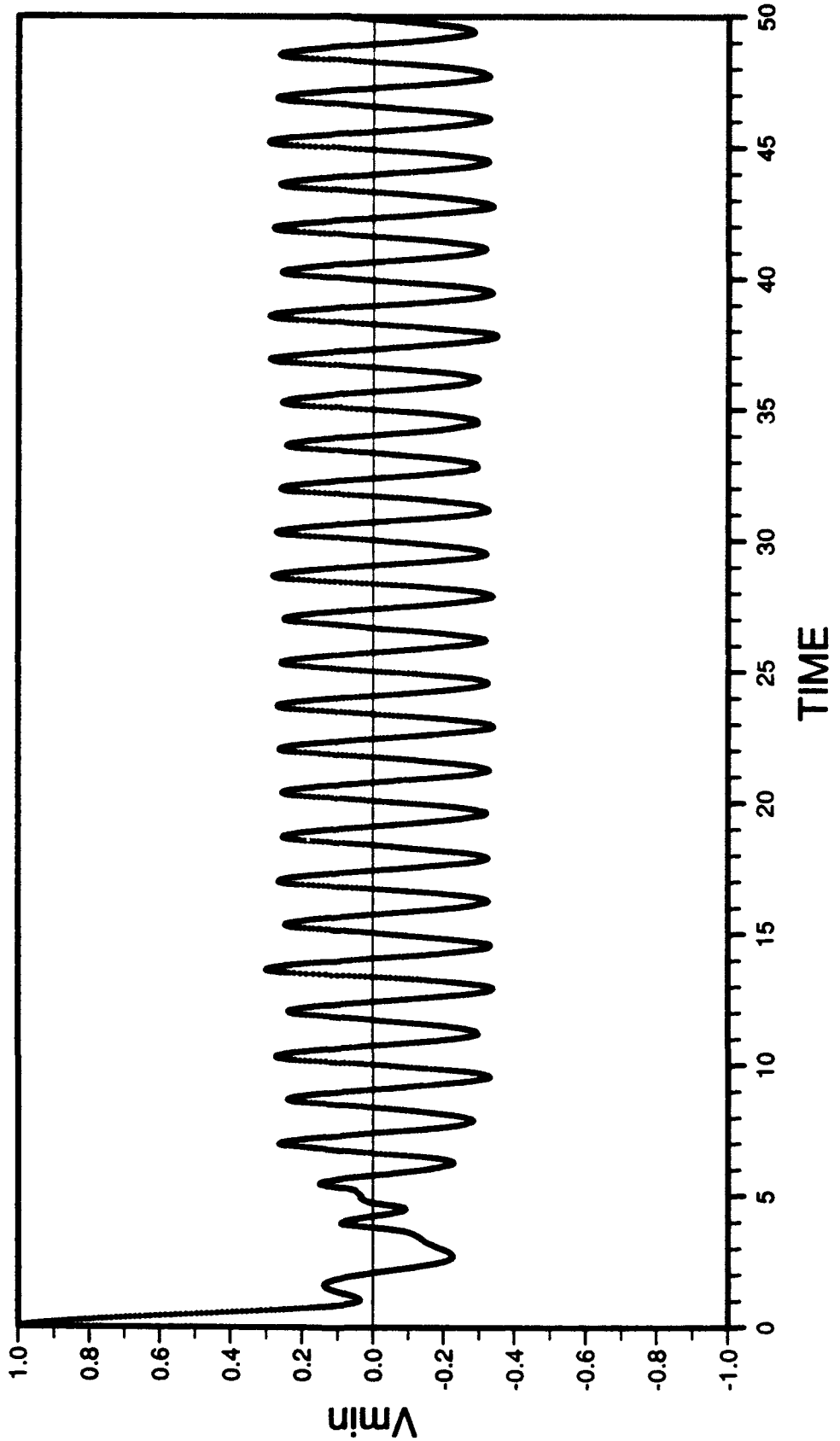
ι =9. Tr=0.1 Tl=0.1
Vmin
TIME
1.0
0.8
0.6
0.4
0.2
0.0
-0.2
-0.4
-0.6
-0.8
-1.0
0
5
10
15
20
25
30
35
40
45
50

Fig. 12 c

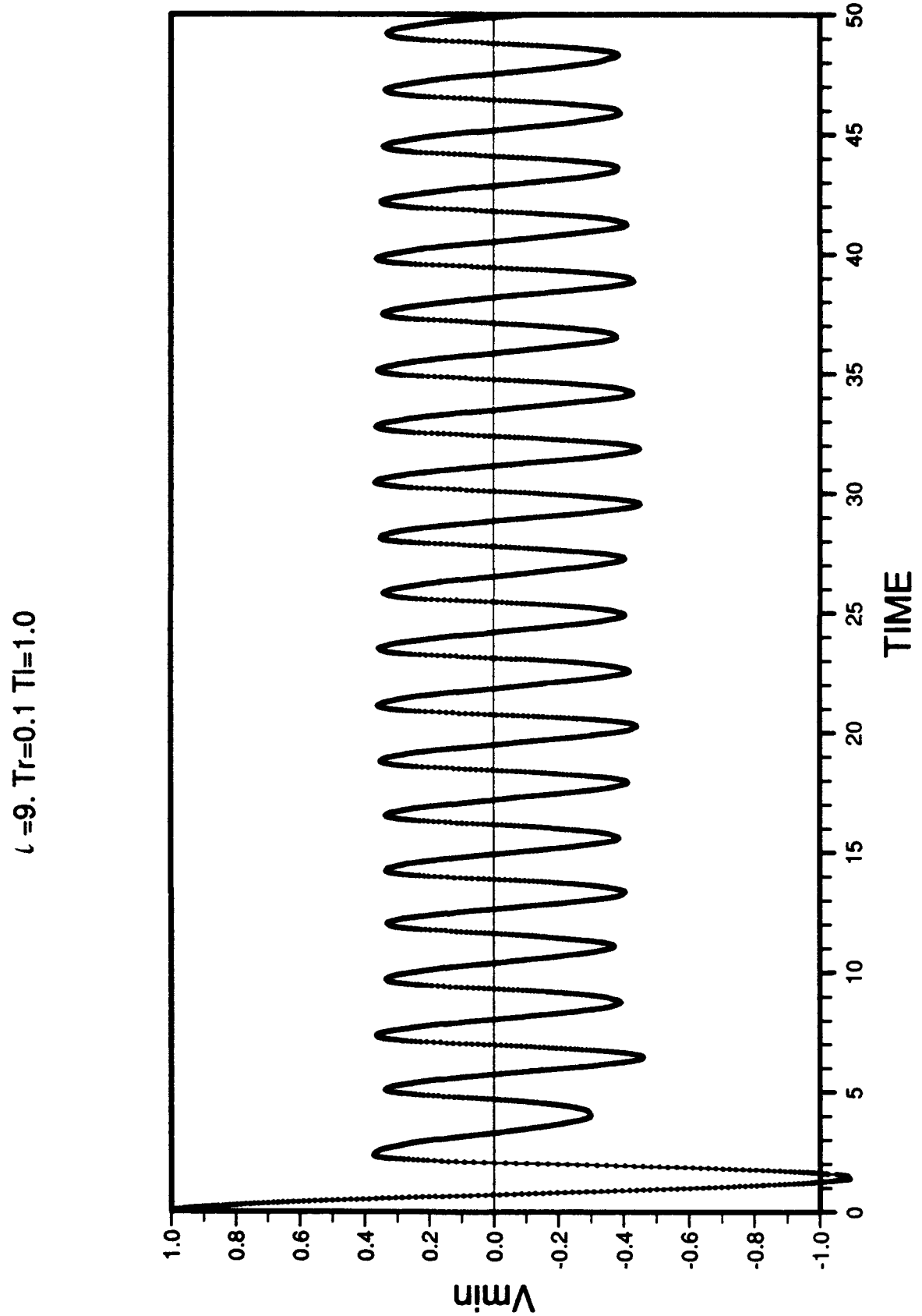
ζ =9. Tr=0.1 Tl=1.0
Vmin
TIME
1.0
0.8
0.6
0.4
0.2
0.0
-0.2
-0.4
-0.6
-0.8
-1.0
0
5
10
15
20
25
30
35
40
45
50

Fig. 12 d

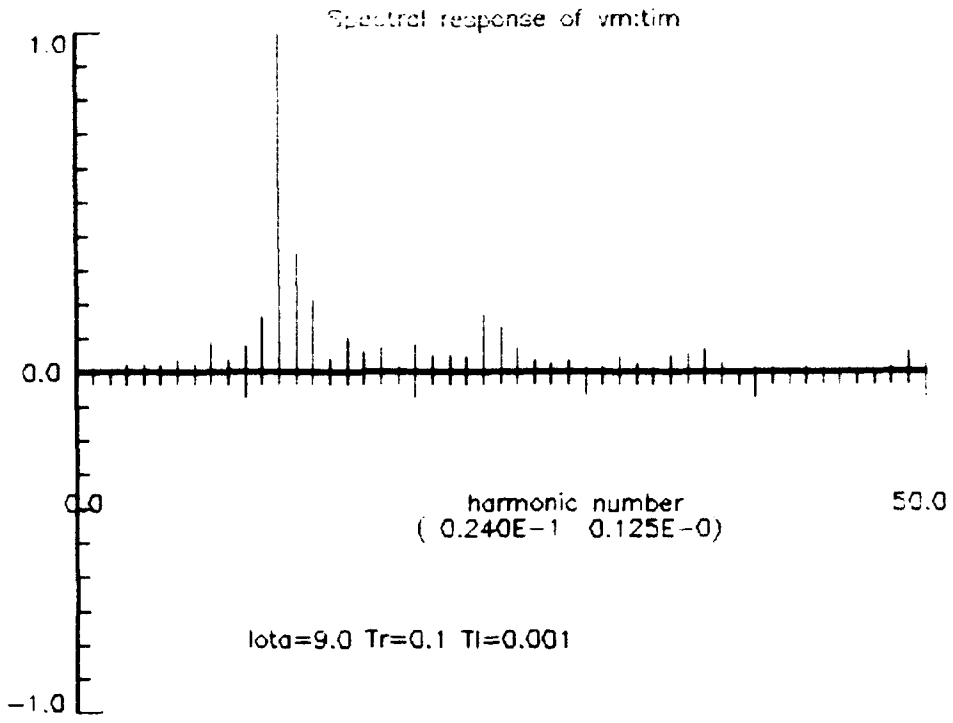
Spectral response of vm:tim
1.0
0.0
-1.0
0.0
harmonic number
(0.240E-1 0.125E-0)
50.0
Iota=9.0 Tr=0.1 TI=0.001

Fig. 12 e

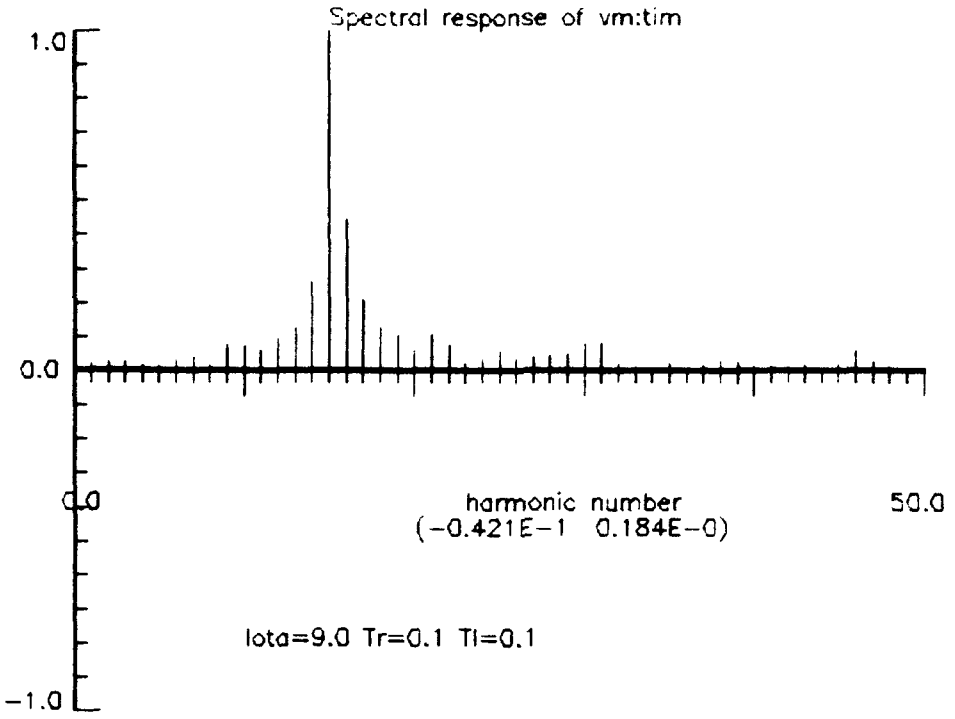
Spectral response of vm:tim
1.0
0.0
-1.0
0.0
harmonic number
50.0
(-0.421E-1 0.184E-0)
Iota=9.0 Tr=0.1 Ti=0.1

Fig. 12 f

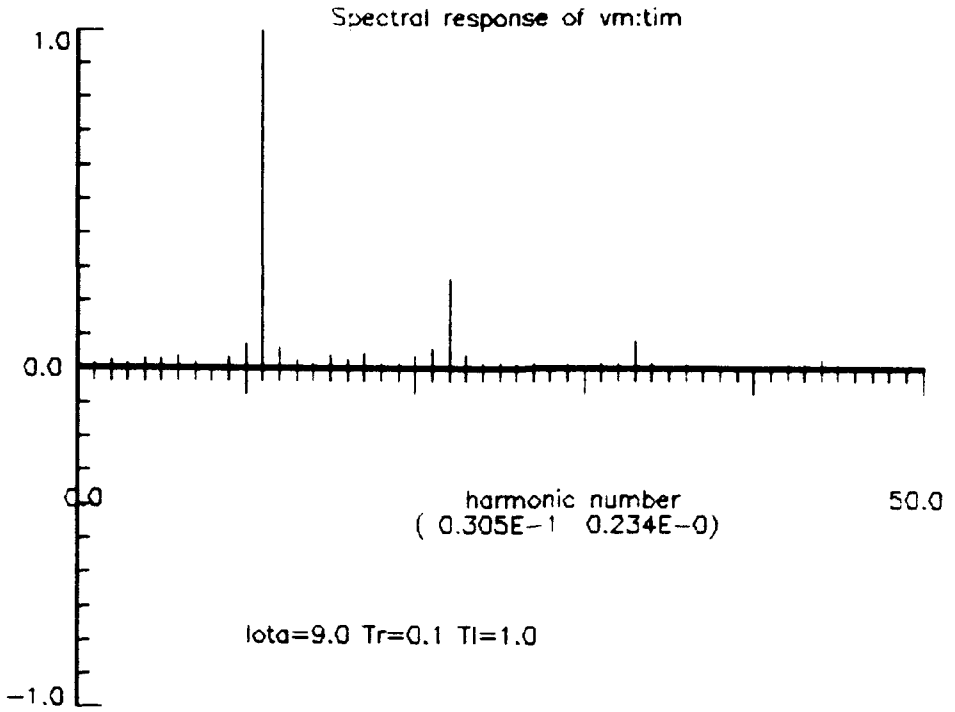
Spectral response of vm:tim
1.0
0.0
-1.0
0.0
harmonic number
(0.305E-1 0.234E-0)
50.0
Iota=9.0 Tr=0.1 TI=1.0

Fig. 12 g

$T_R = 0.1,\ T_L = 0$

T_C \ L	4.0	6.0	9.0
0.001	ST	ST	OSC
0.1	ST	ST	OSC
1.0	ST	ST	OSC

ST - stable, bo oscillations

OSC - oscillations present

Fig. 13 a

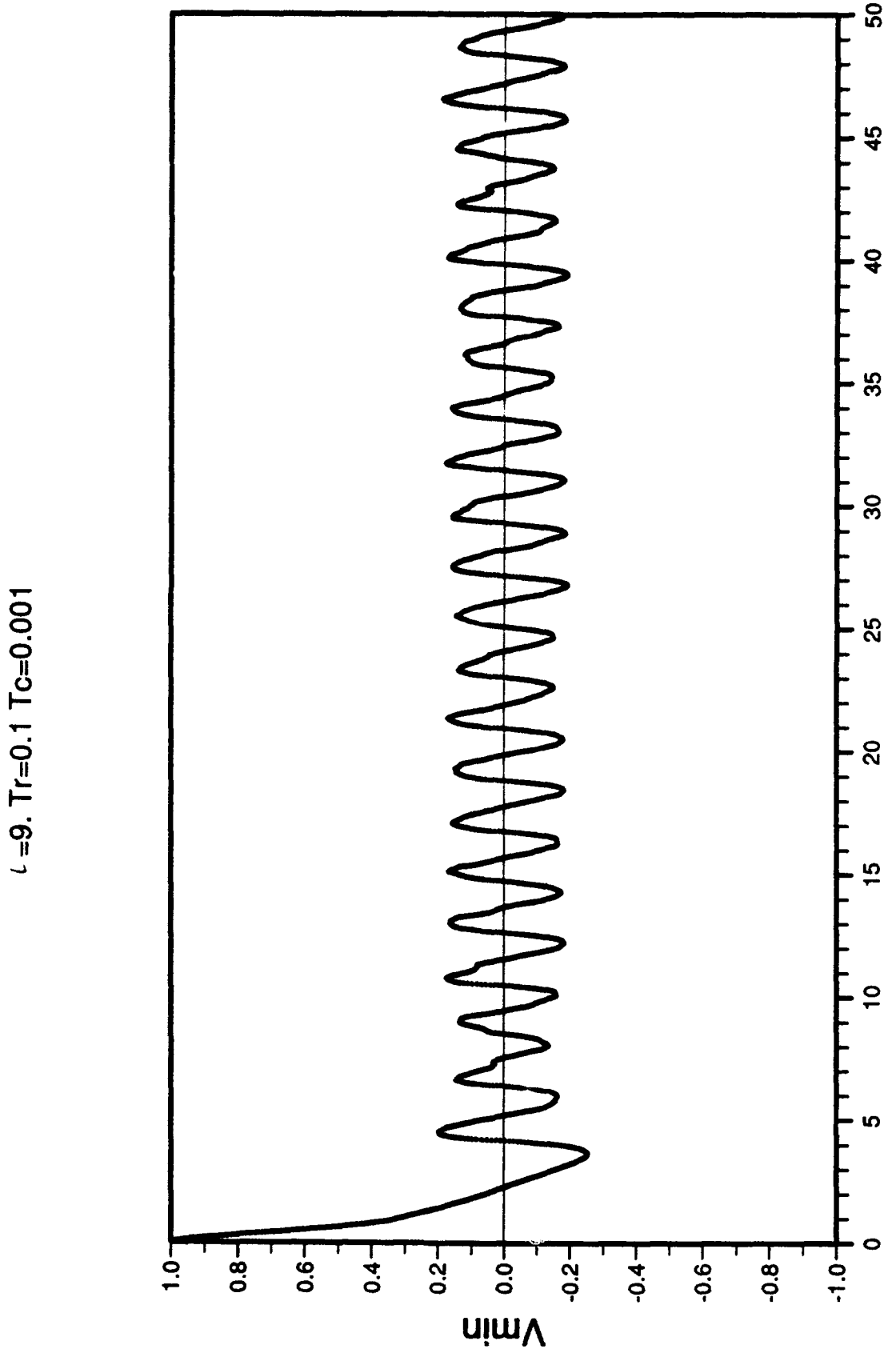
ι =9. Tr=0.1 Tc=0.001
Vmin
TIME
1.0
0.8
0.6
0.4
0.2
0.0
-0.2
-0.4
-0.6
-0.8
-1.0
0
5
10
15
20
25
30
35
40
45
50

Fig. 13 b

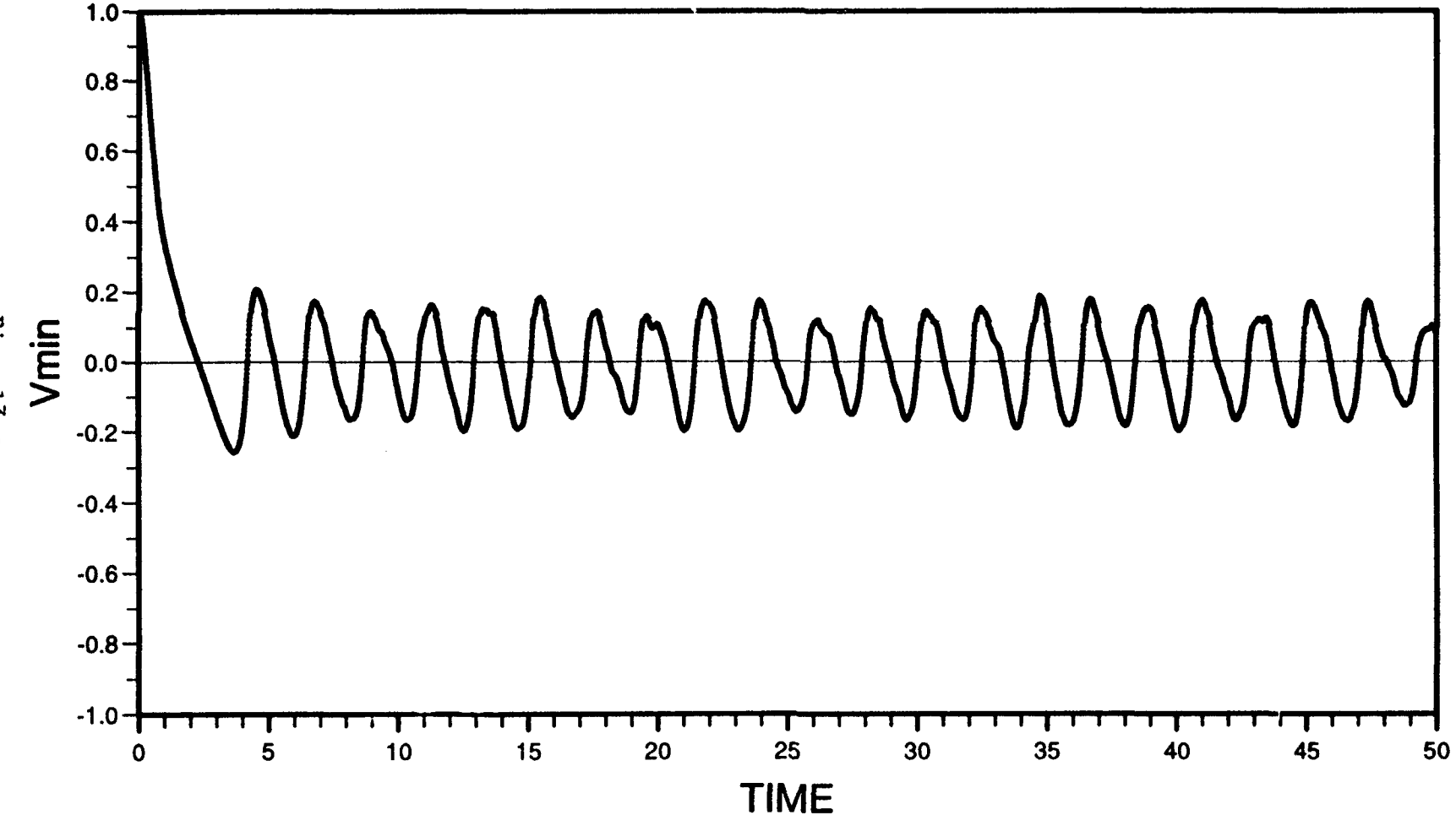
ι =9. Tr=0.1 Tc=0.1
1.0
0.8
0.6
0.4
0.2
0.0
-0.2
-0.4
-0.6
-0.8
-1.0
Vmin
0
5
10
15
20
25
30
35
40
45
50
TIME

Fig. 13 c

ι =9. Tr=0.1 Tc=1.0

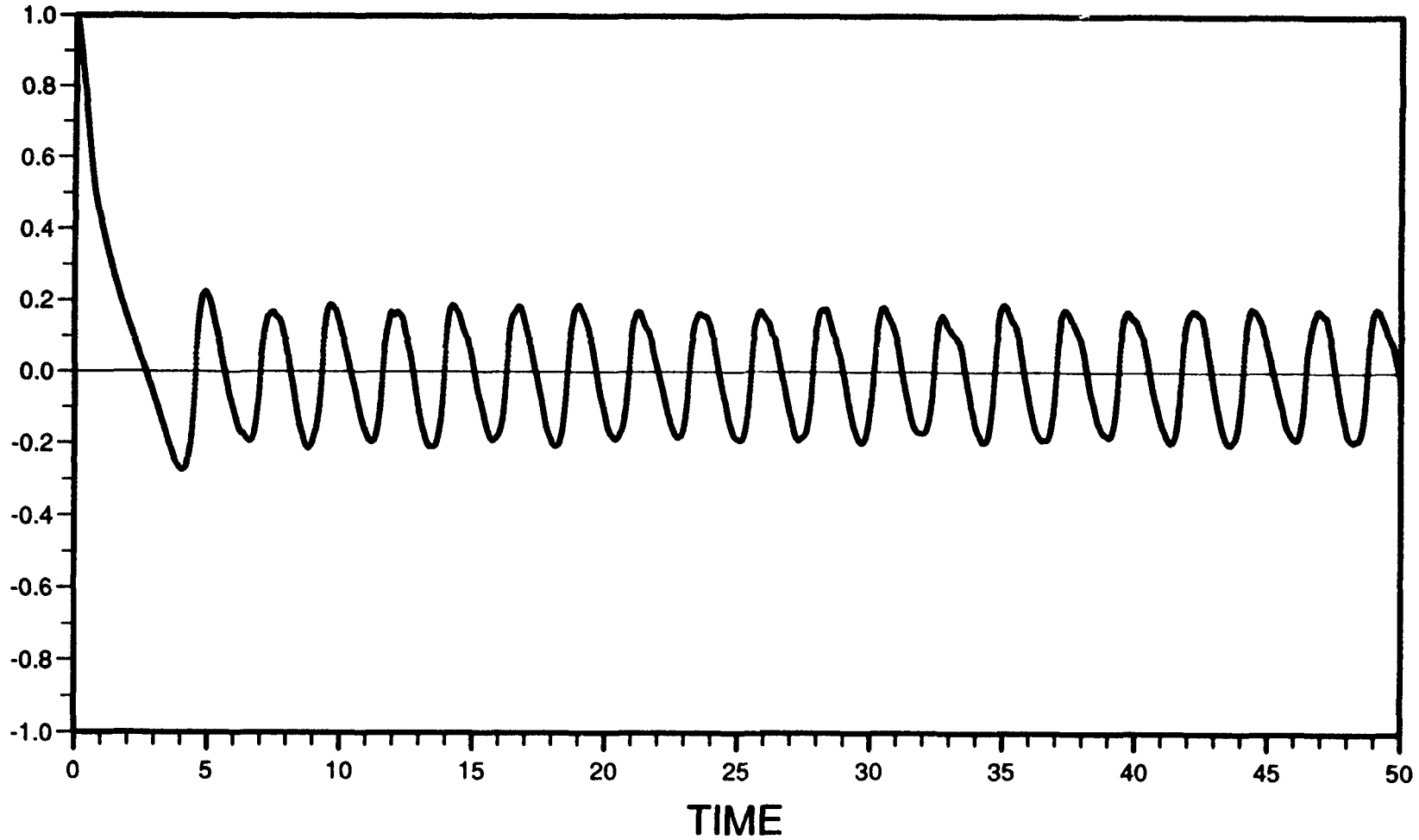

Fig. 13 d

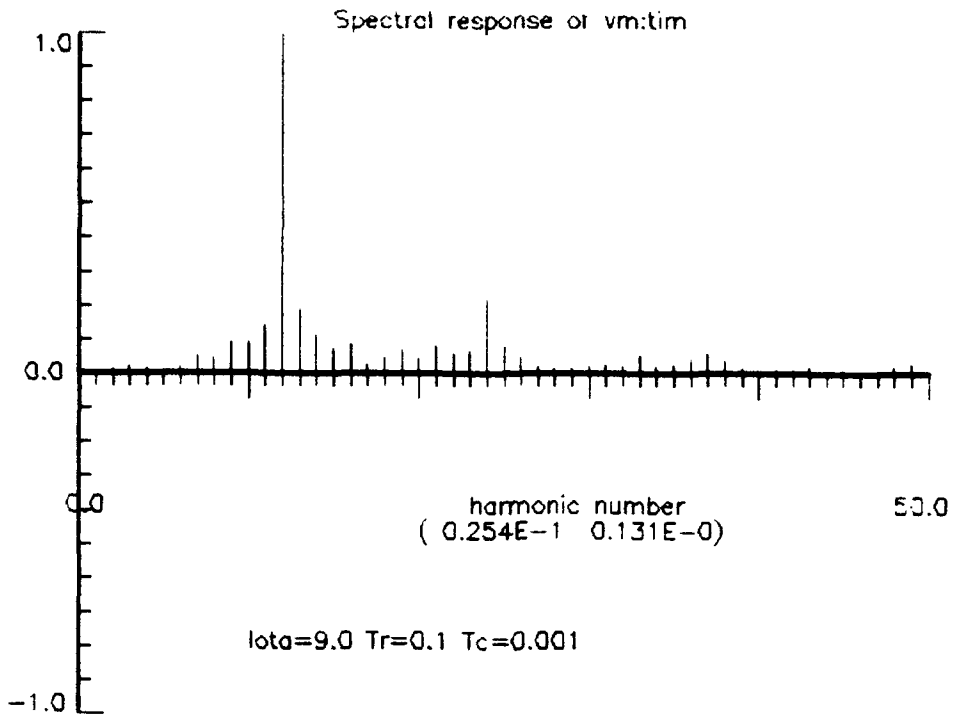
Spectral response of vm:tim
1.0
0.0
-1.0
0.0
harmonic number
(0.254E-1 0.131E-0)
50.0
Iota=9.0 Tr=0.1 Tc=0.001

Fig. 13 e

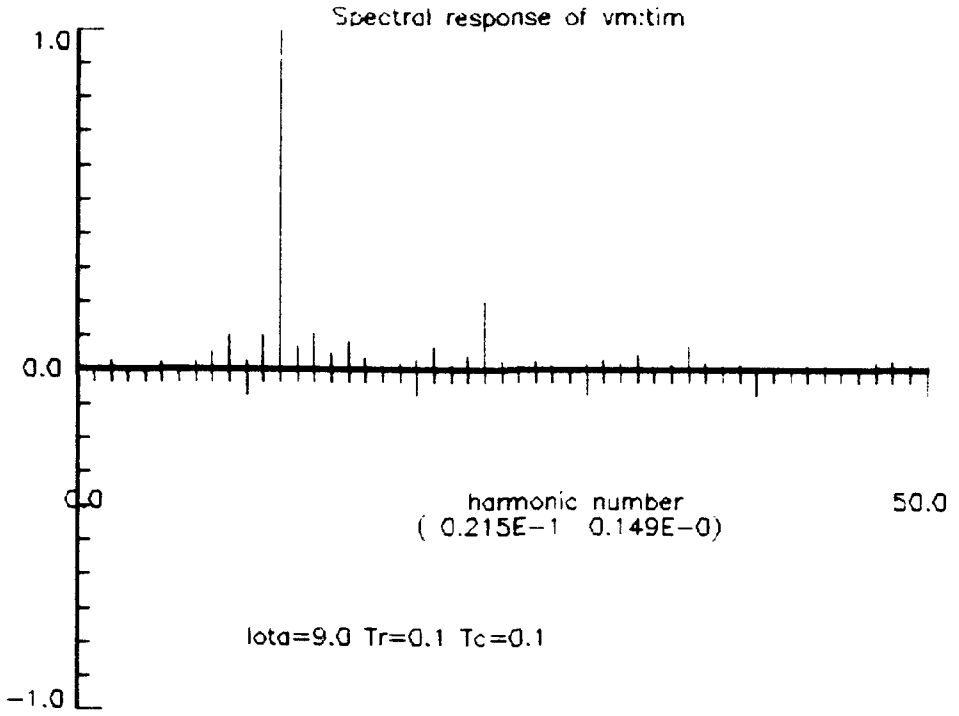
Spectral response of vm:tim
1.0
0.0
-1.0
0.0
harmonic number
50.0
(0.215E-1 0.149E-0)
Iota=9.0 Tr=0.1 Tc=0.1

Fig. 13 f

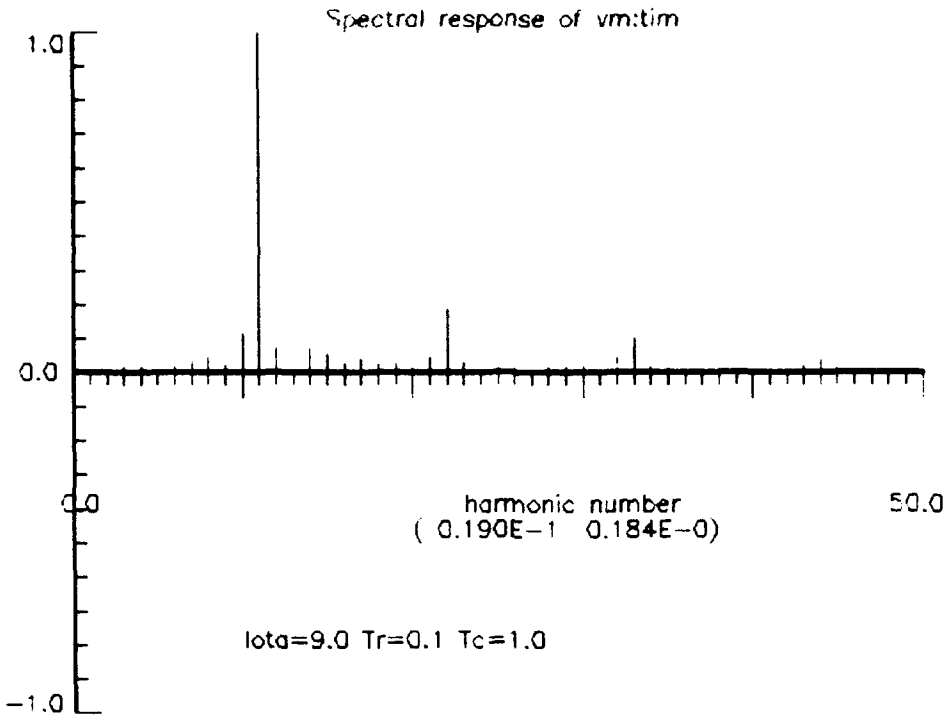
Spectral response of vm:tim
1.0
0.0
-1.0
0.0
50.0
harmonic number
(0.190E-1 0.184E-0)
Iota=9.0 Tr=0.1 Tc=1.0

Fig. 13 g

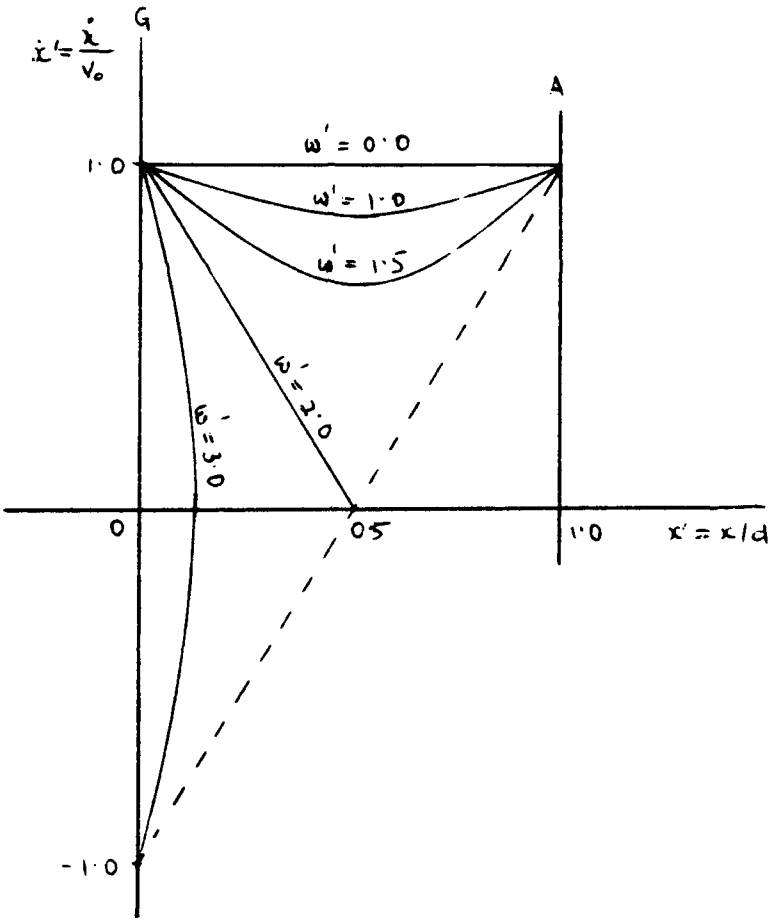
G
$\dot{x}' = \frac{\dot{x}}{V_0}$
A
$\omega' = 0.0$
1.0
$\omega' = 1.0$
$\omega' = 1.5$
$\omega' = 2.0$
$\omega' = 3.0$
0
05
1.0
$x' = x/d$
-1.0

Fig. 14 a

t =4. S.C.

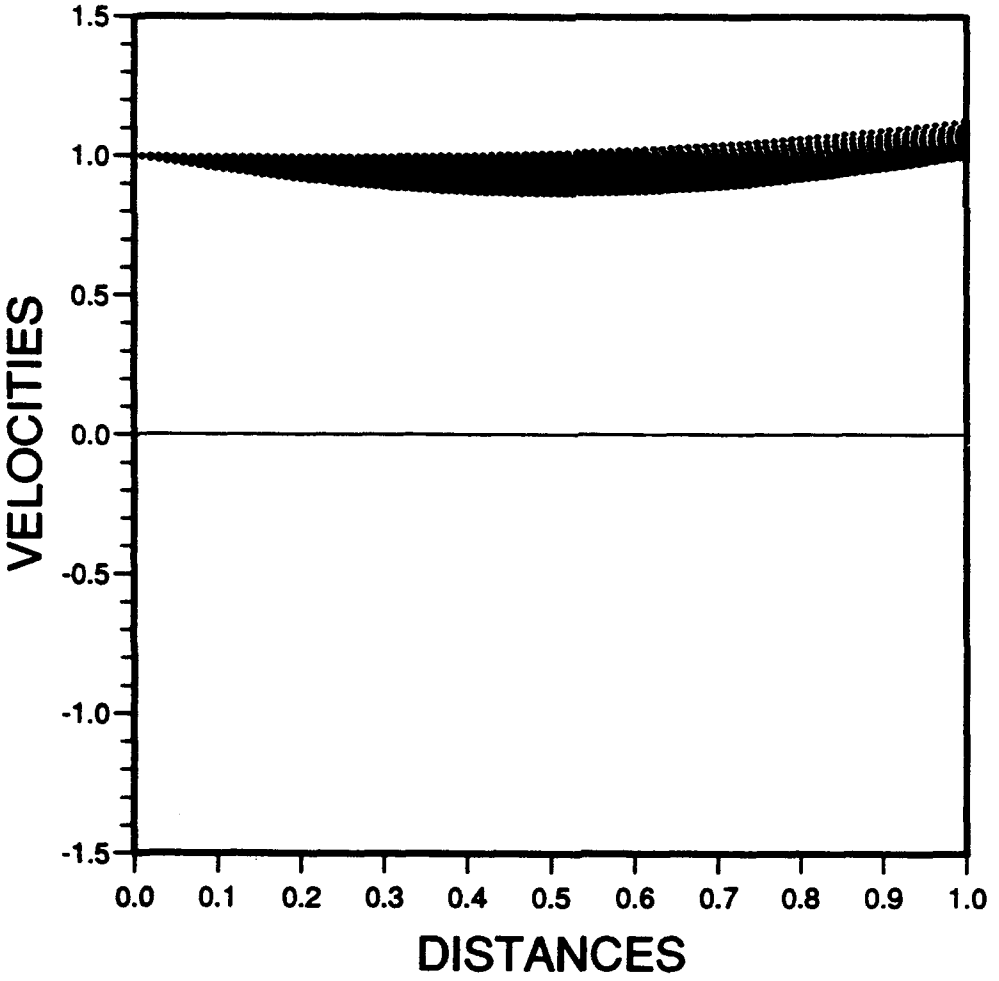
1.5
1.0
0.5
0.0
-0.5
-1.0
-1.5
VELOCITIES
0.0
0.1
0.2
0.3
0.4
0.5
0.6
0.7
0.8
0.9
1.0
DISTANCES

Fig. 14 b

ι =4. S.C.

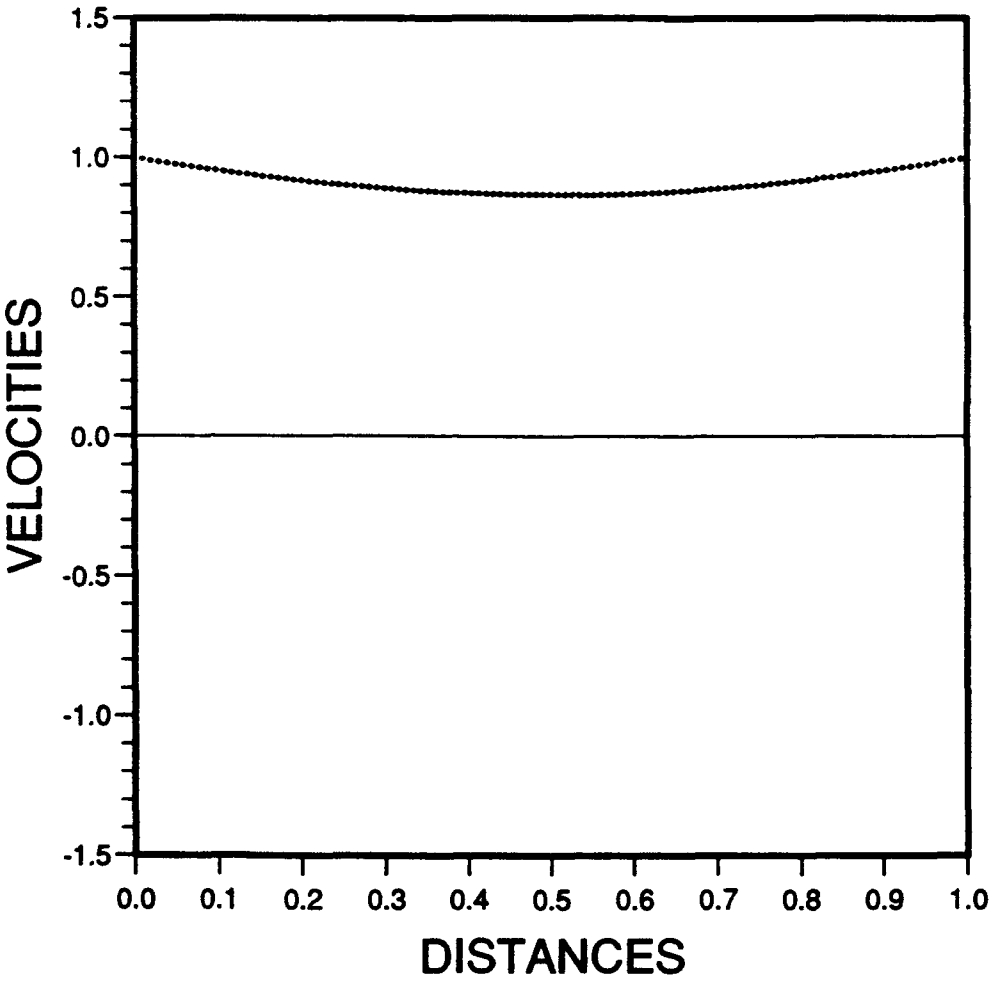
1.5
1.0
0.5
0.0
-0.5
-1.0
-1.5
VELOCITIES
0.0
0.1
0.2
0.3
0.4
0.5
0.6
0.7
0.8
0.9
1.0
DISTANCES

Fig. 14 c

ι=9. Tr=0.1 Tl=1.0

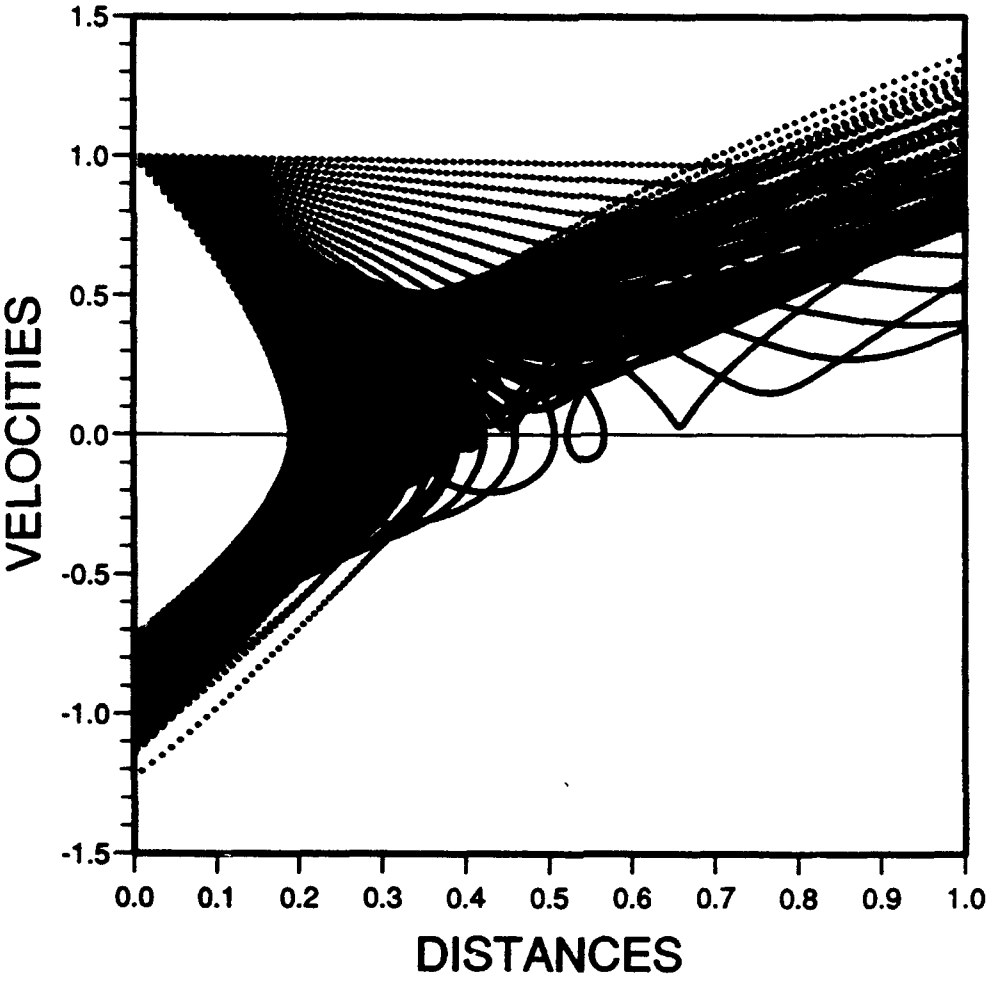

Fig. 14 d

ζ =9. Tr=0.1 Tl=1.0

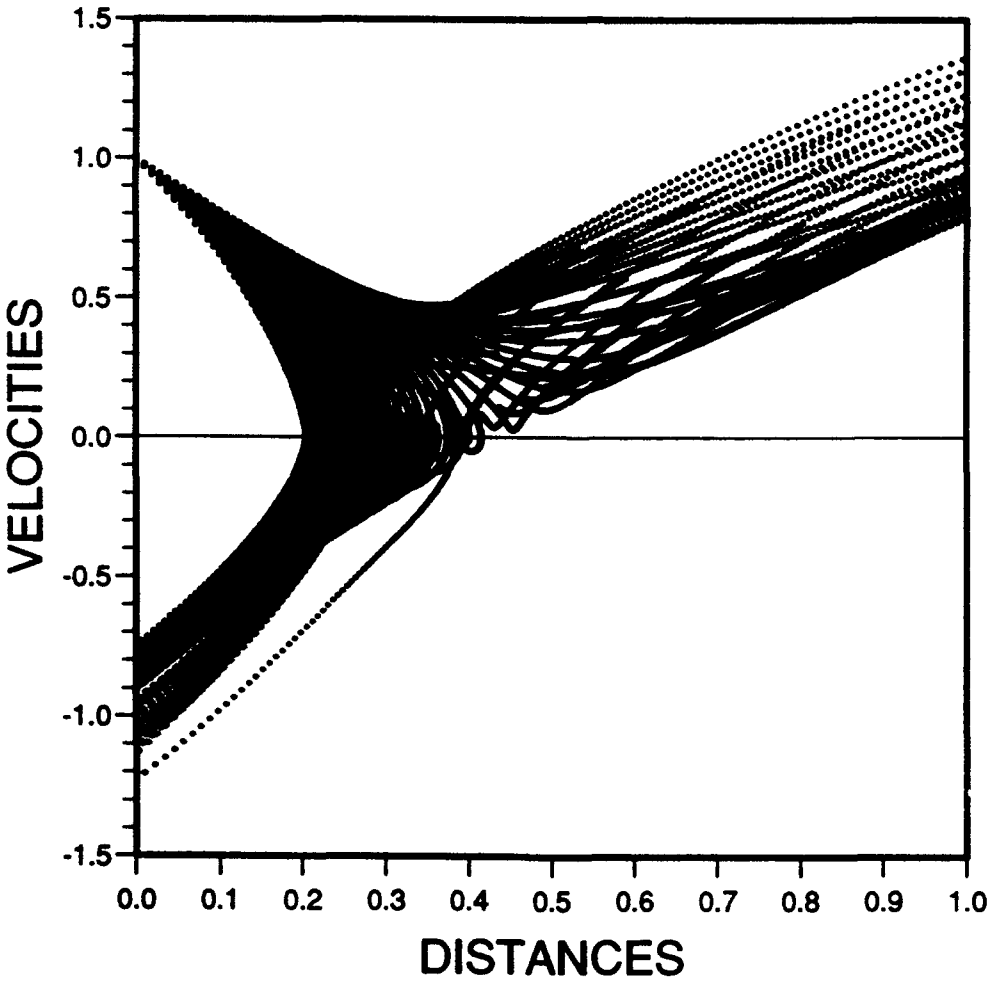

Fig. 14 e

ι=9. Tr=0.1 Tl=1.0

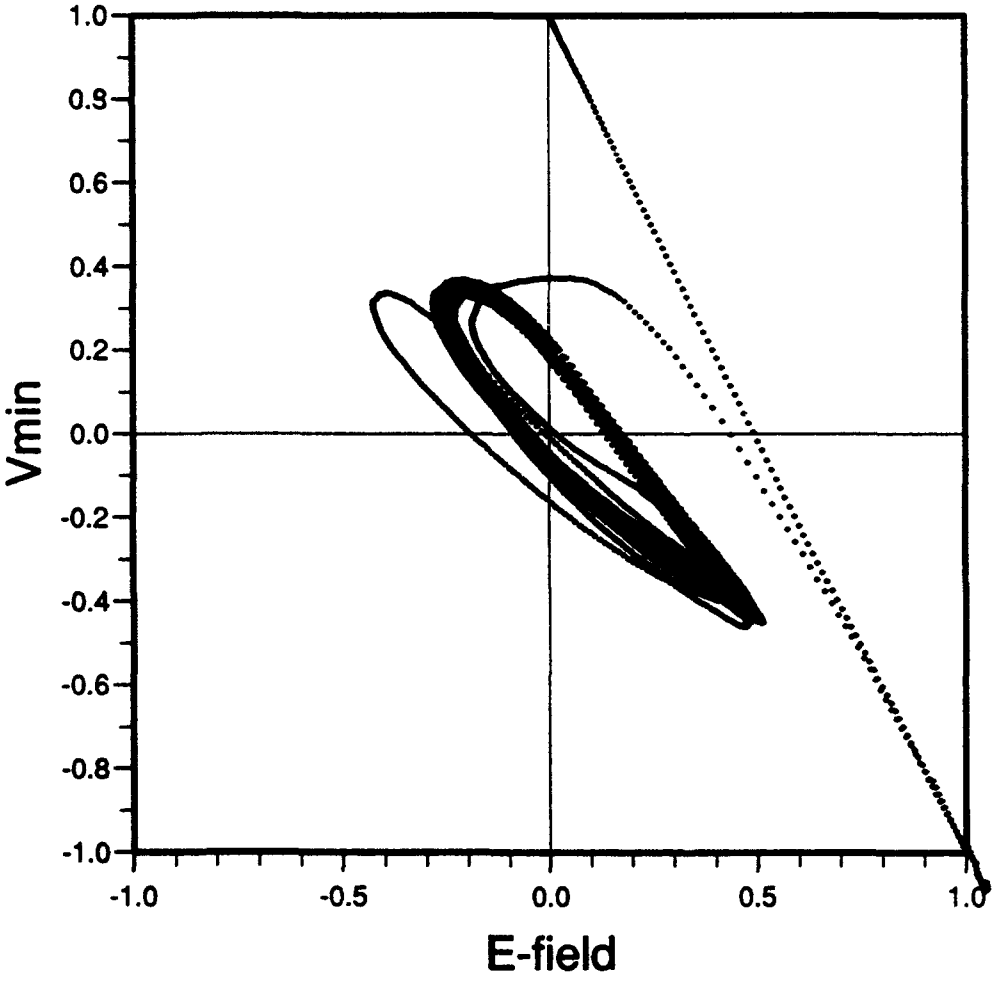

Fig. 15 a

ι=9. Tr=0.1 Tl=1.0

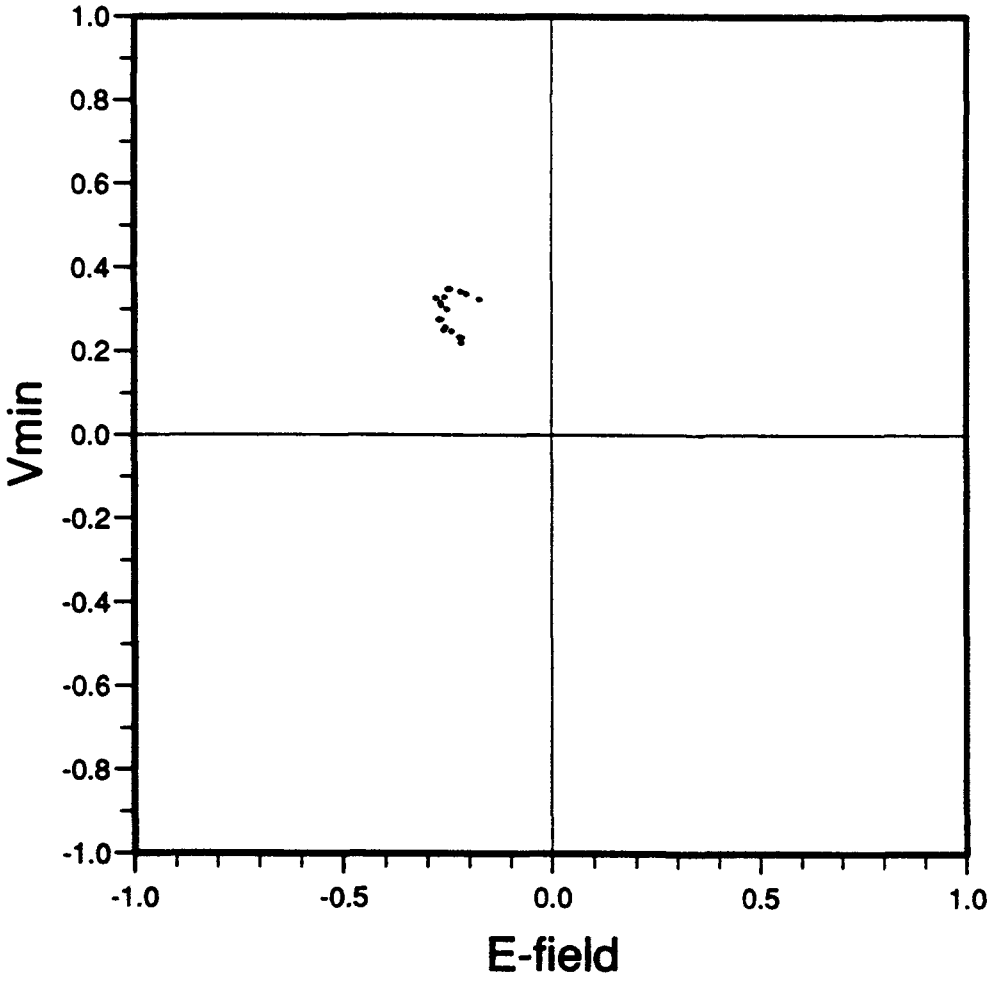

Fig. 15 b

ι=9. Tr=0.1 Tl=1.0

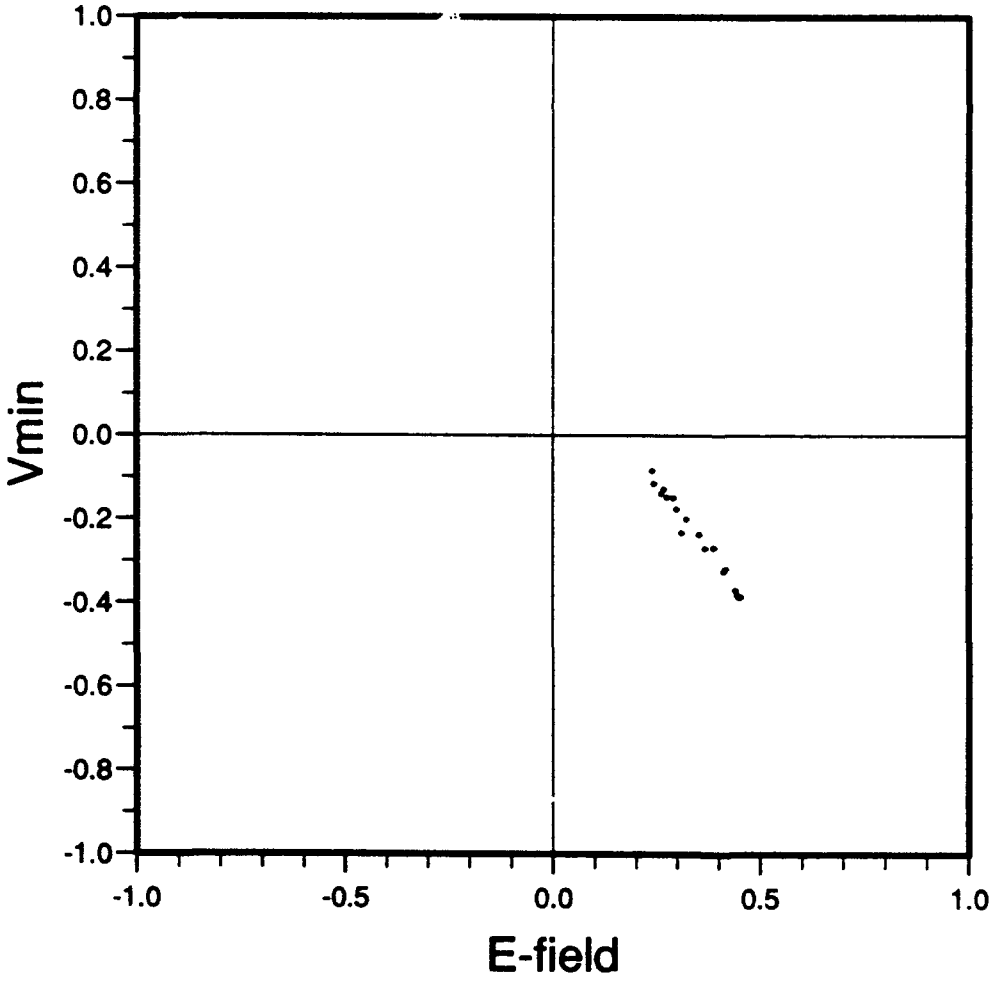

Fig. 15 c

ι =9. Tr=0.1

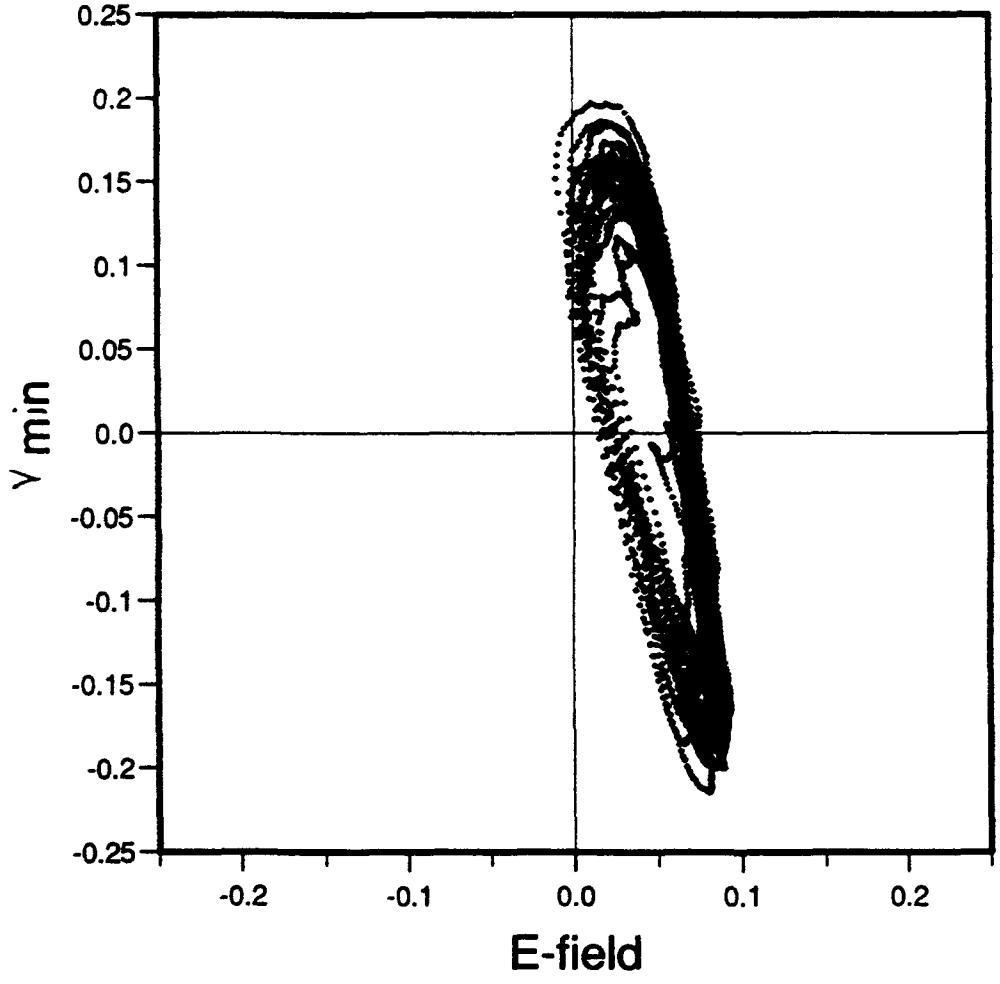

Fig. 15 d

ι =9. Tr=0.1

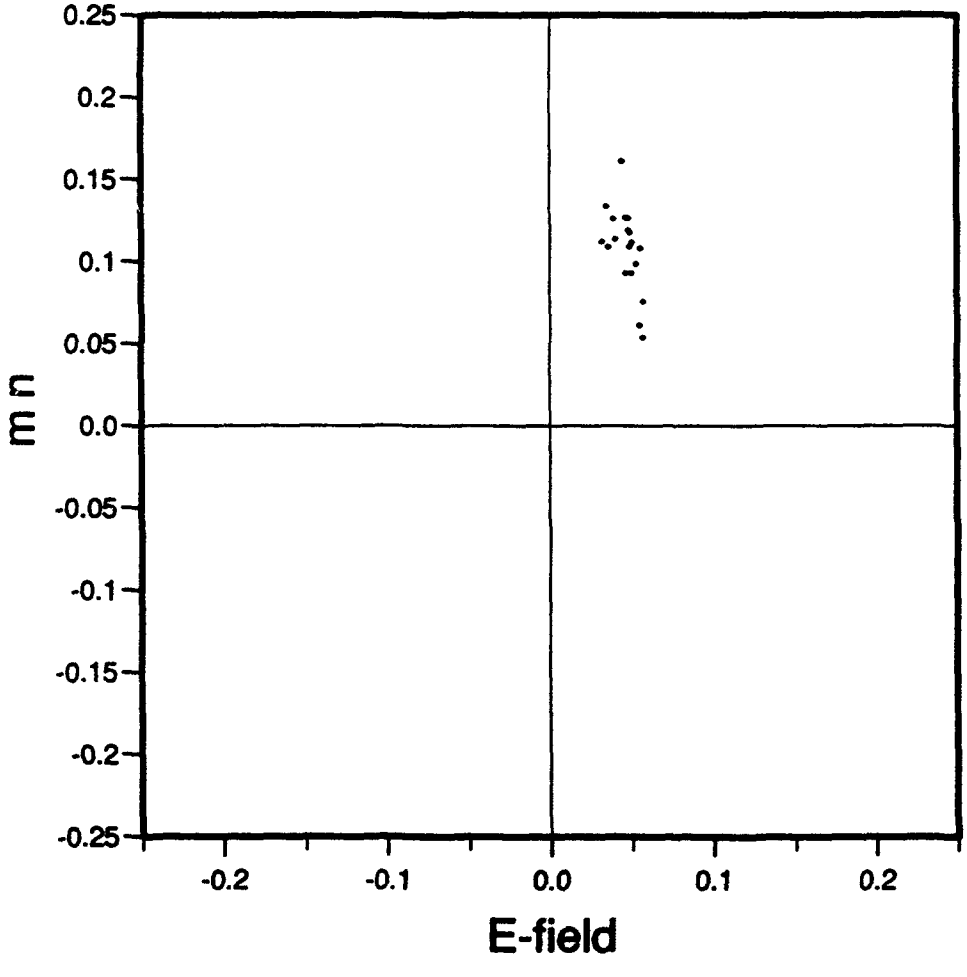

Fig. 15 e

ι =9. Tr=0.1

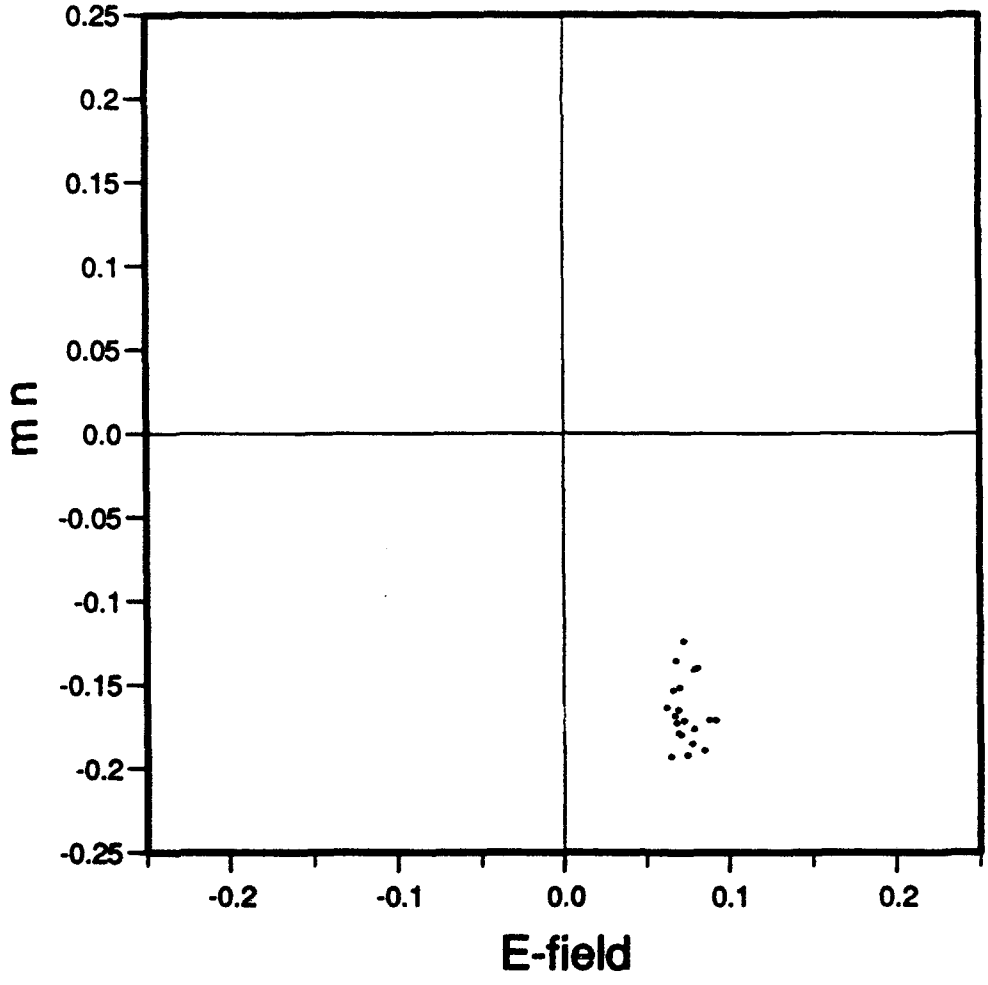

Fig. 15 f

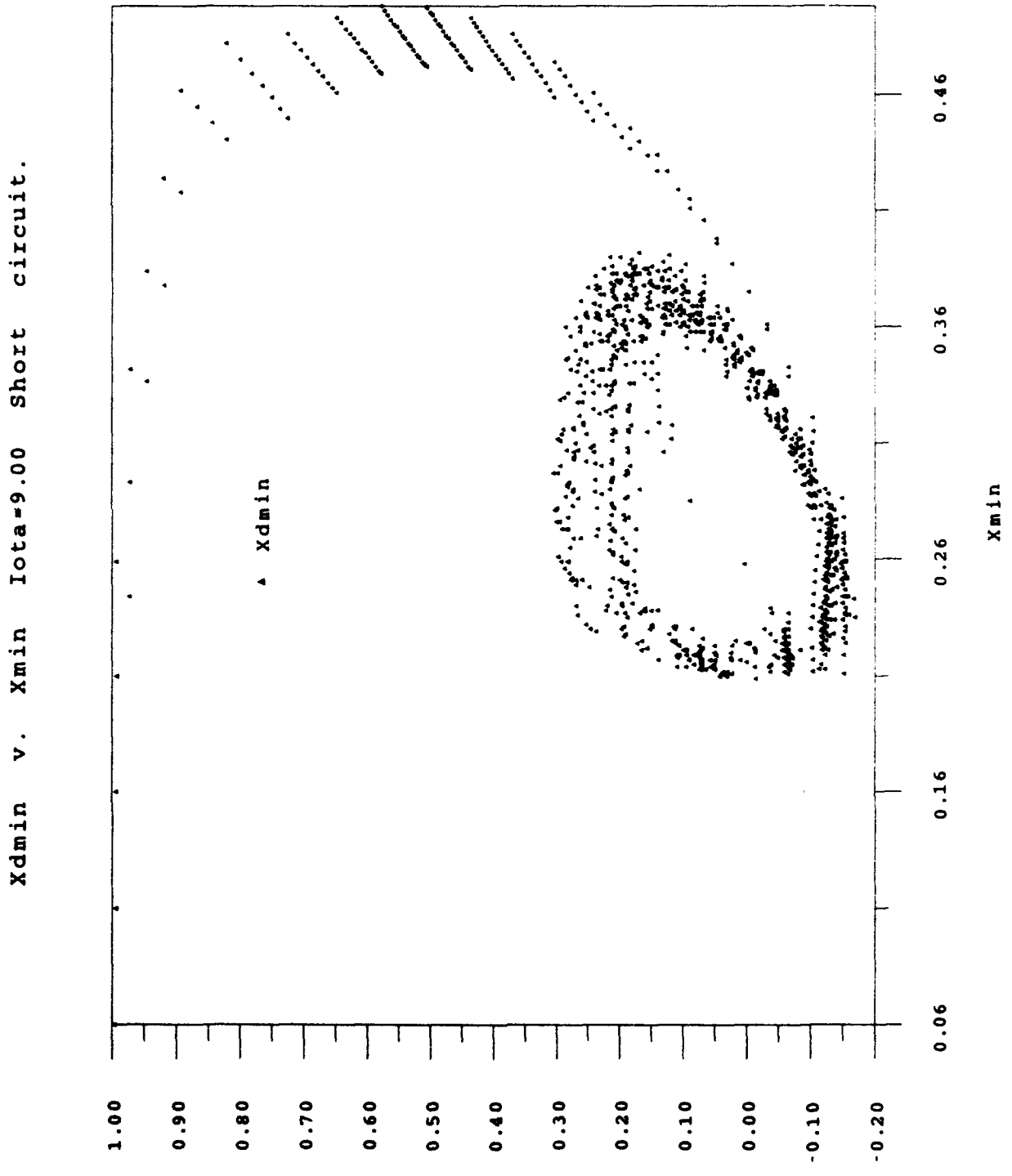
Xdmin v. Xmin Iota=9.00 Short circuit.
Xdmin
Xmin
1.00
0.90
0.80
0.70
0.60
0.50
0.40
0.30
0.20
0.10
0.00
-0.10
-0.20
0.06
0.16
0.26
0.36
0.46

Fig. 16 a

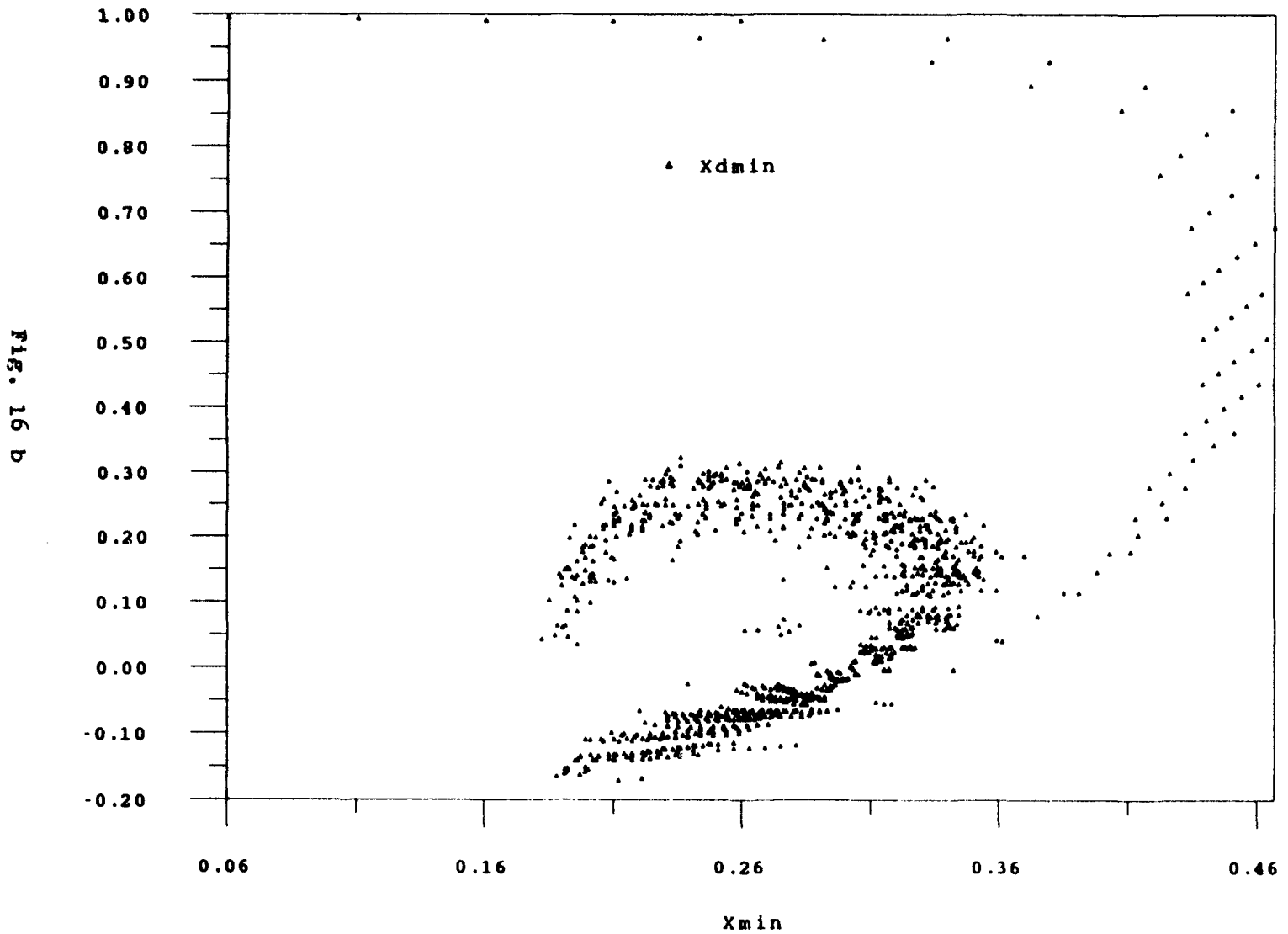
Xdmin v. Xmin Iota=12.0 Short circuit.
Xdmin
1.00
0.90
0.80
0.70
0.60
0.50
0.40
0.30
0.20
0.10
0.00
-0.10
-0.20
0.06
0.16
0.26
0.36
0.46
Xmin

Fig. 16 b

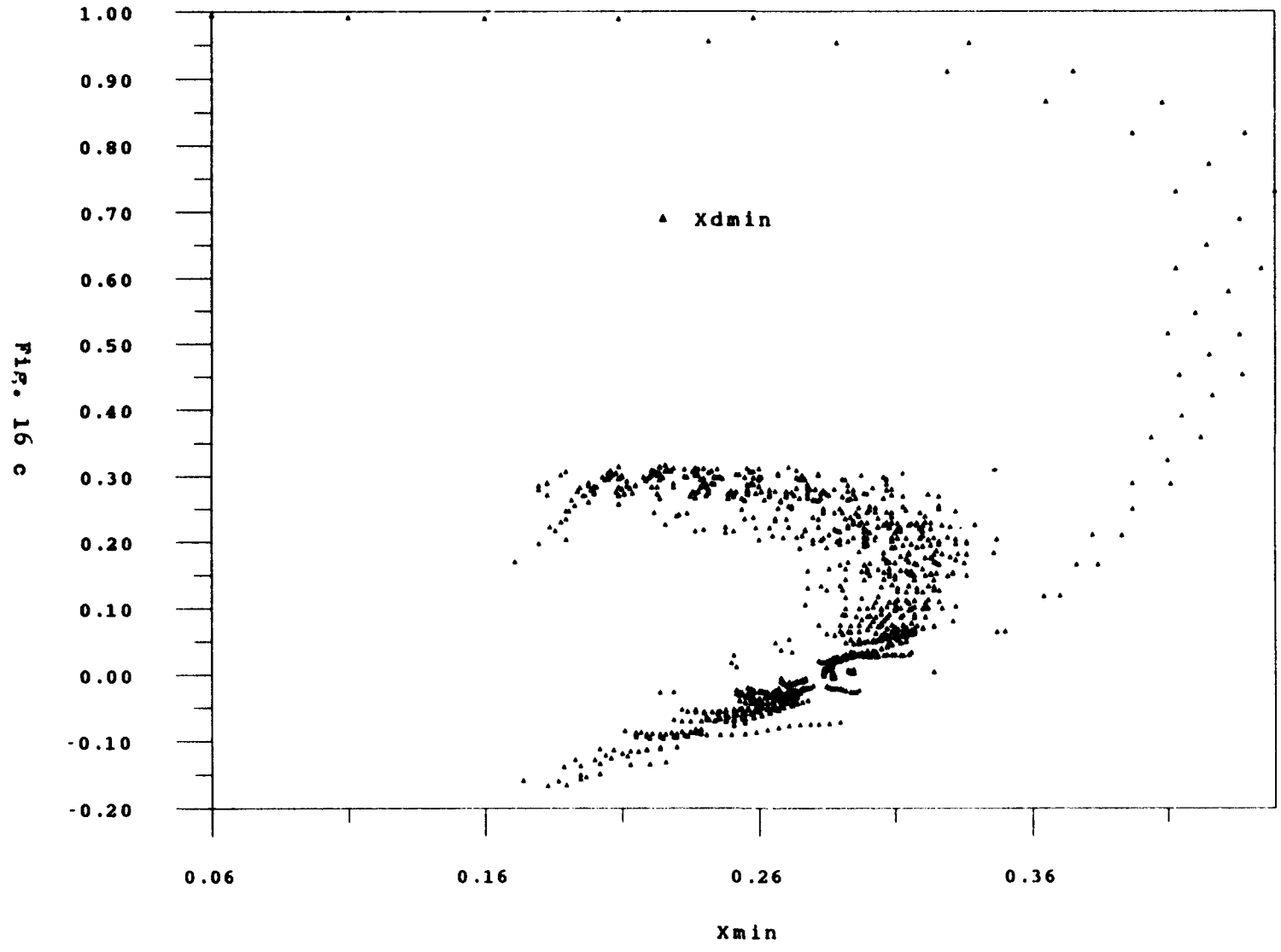
Xdmin v. Xmin Iota=15.0 Short circuit.
1.00
0.90
0.80
0.70
0.60
0.50
0.40
0.30
0.20
0.10
0.00
-0.10
-0.20
Fig. 16 c
Xdmin
0.06
0.16
0.26
0.36
Xmin

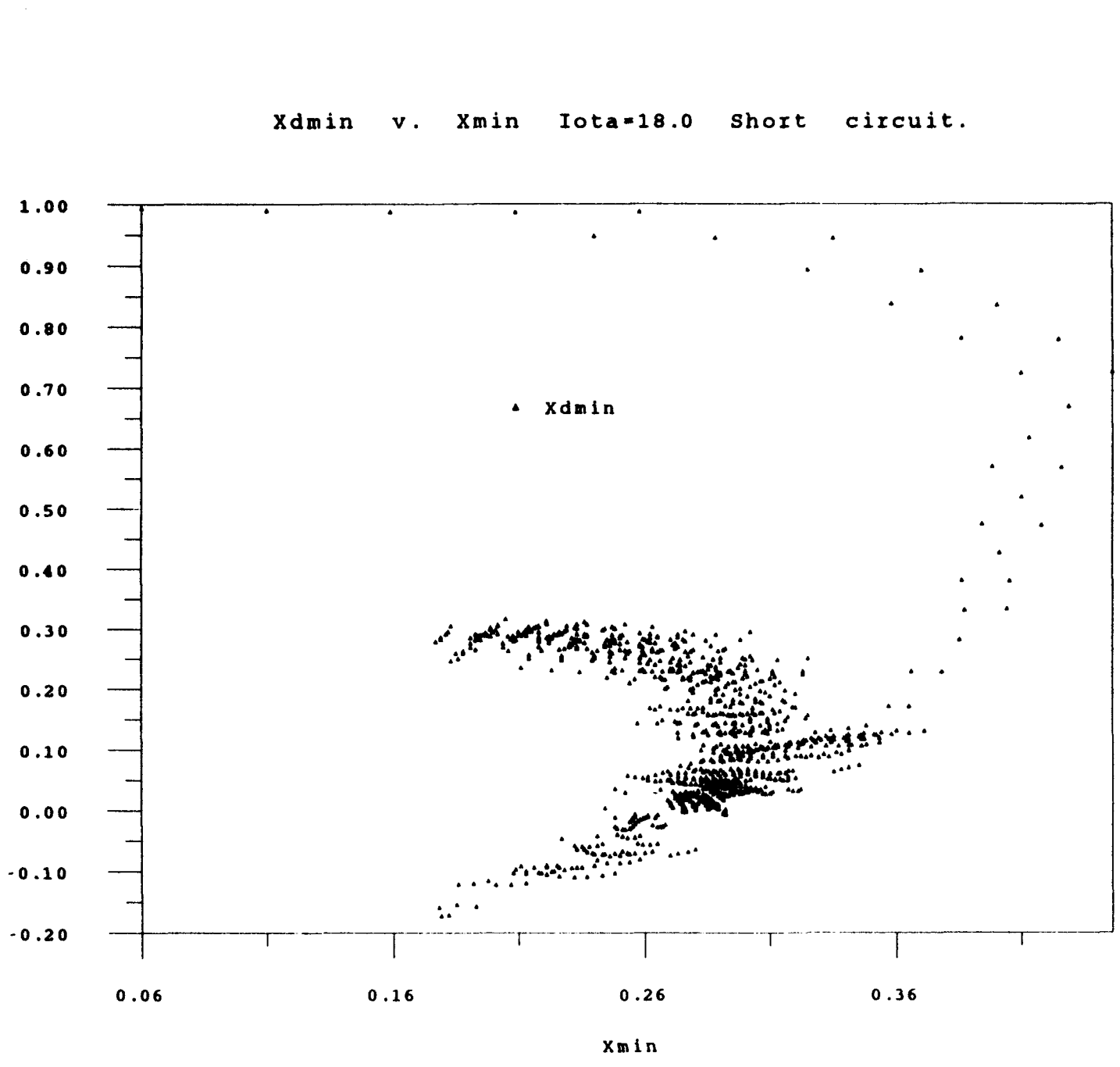
Xdmin v. Xmin Iota=18.0 Short circuit.
1.00
0.90
0.80
0.70
0.60
0.50
0.40
0.30
0.20
0.10
0.00
-0.10
-0.20
Xdmin
0.06
0.16
0.26
0.36
Xmin

Fig. 16 d

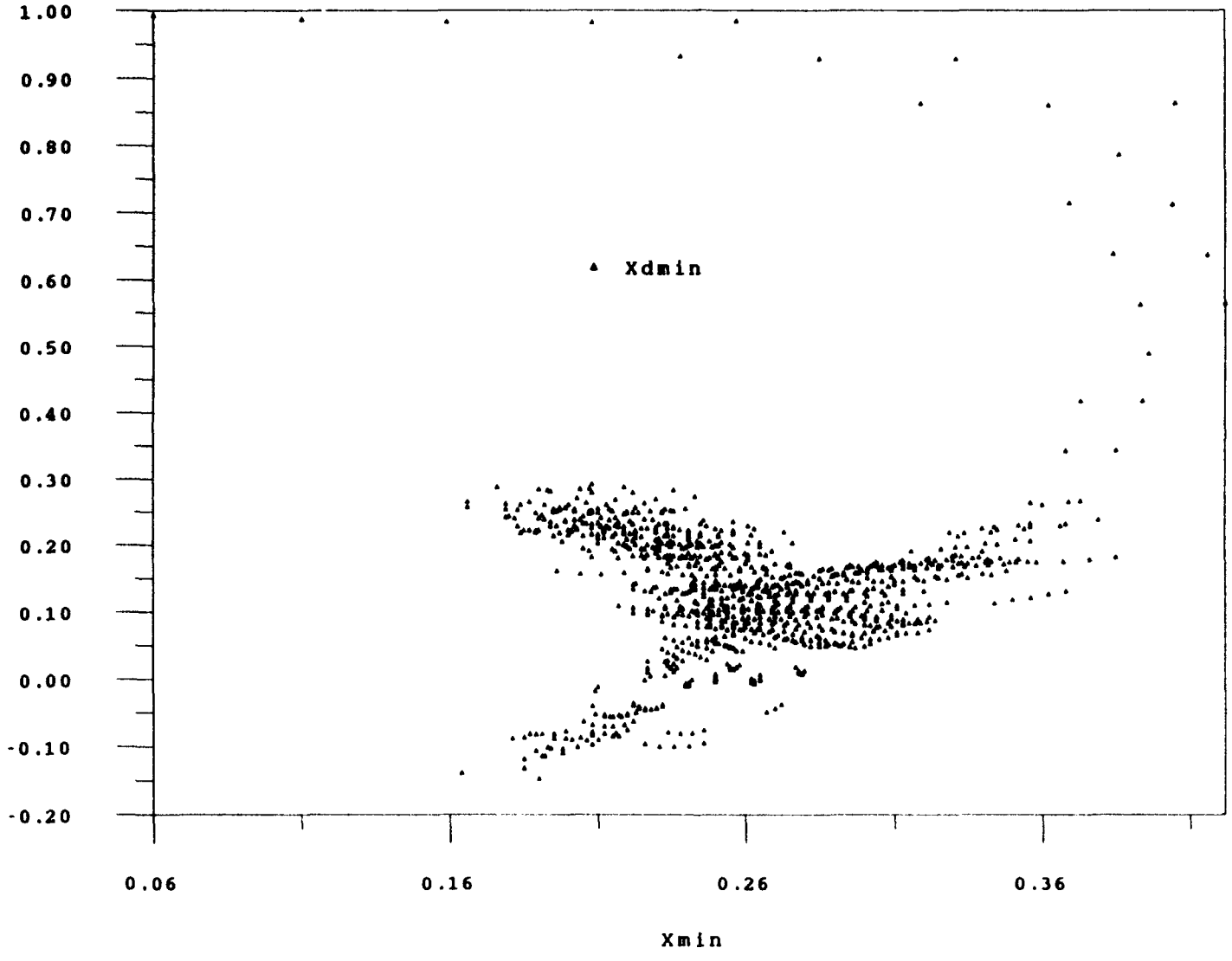
Xdmin v. Xmin Iota=23.0 Short circuit.
1.00
0.90
0.80
0.70
0.60
0.50
0.40
0.30
0.20
0.10
0.00
-0.10
-0.20
Xdmin
0.06
0.16
0.26
0.36
Xmin

Fig. 16 e

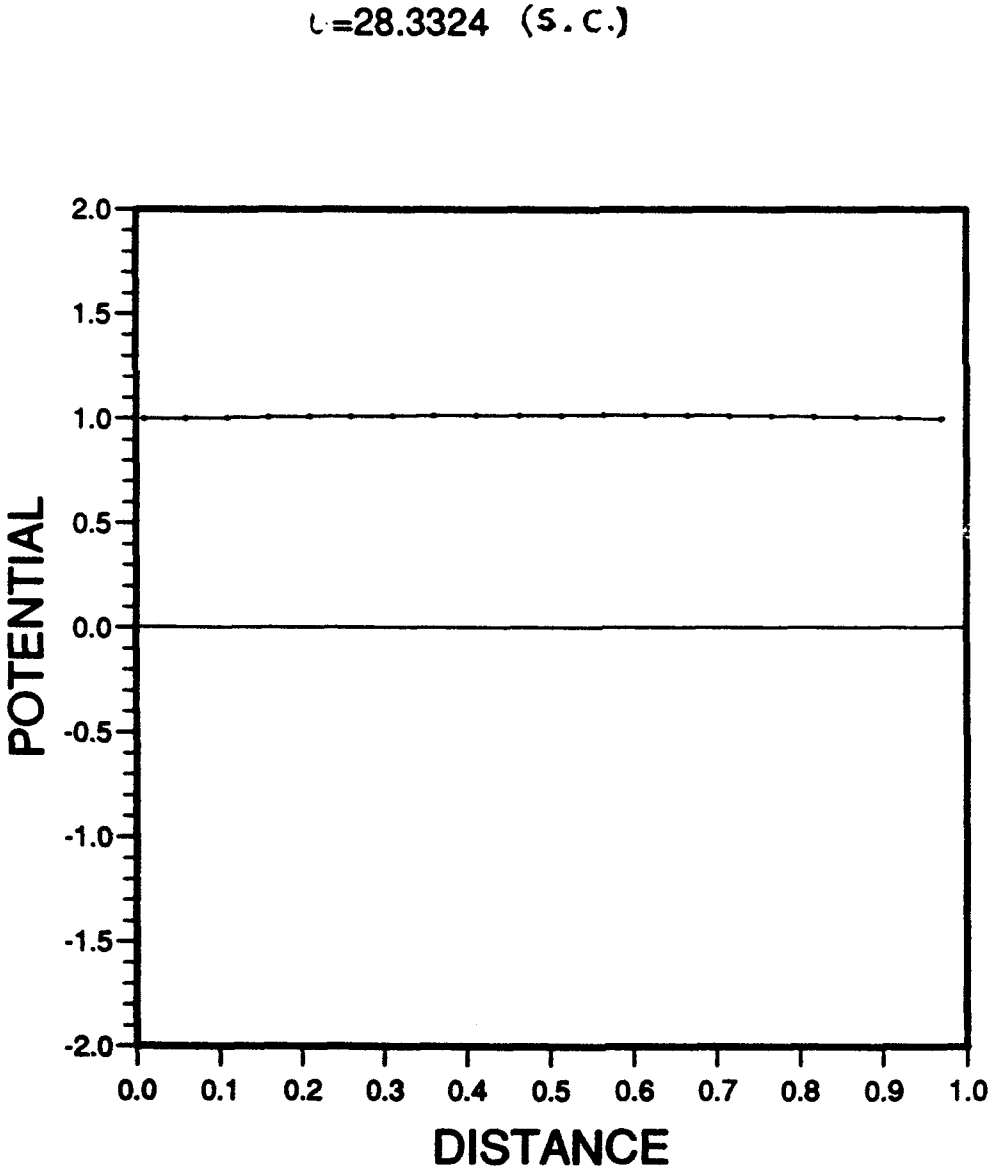
C=28.3324 (S.C.)
A=28.3324 PLAS
2.0
1.5
1.0
0.5
0.0
-0.5
-1.0
-1.5
-2.0
POTENTIAL
0.0
0.1
0.2
0.3
0.4
0.5
0.6
0.7
0.8
0.9
1.0
DISTANCE

Fig. 17 a